TEXAS Geosciences
The University of Texas at Austin
Jackson School of Geosciences

8th Annual
Jackson School of Geosciences
Student Research Symposium

February 2, 2019

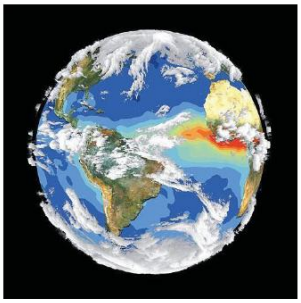


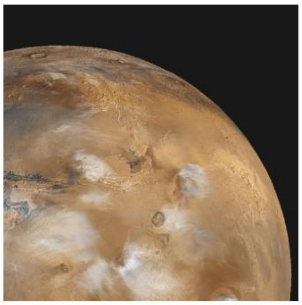

ConocoPhillips

GSEC
Graduate Student Executive Committee

Welcome to the 8th Annual Jackson School Research Symposium!

It is with great pleasure we welcome you all to the 8th Annual Jackson School Research Symposium at UT-Austin! This symposium would not have been possible without the hard work of student volunteers, the support of faculty/research scientists, and generous support from ConocoPhillips. Thank you for taking part in supporting our students and growing research program within the Jackson School. Enjoy the posters!

Schedule of Presentations and Events

Breakfast, A.M. session poster set-up.....8:30 a.m.

Early Career Graduate (ECG) posters.....9:00-11:30 a.m.

Late Career Masters (LCM) posters.....9:00-11:30 a.m.

Lunch, A.M. session poster take-down.....11:30 a.m.

P.M. session poster set-up.....12:30 p.m.

Undergraduate (U) posters.....1:00-3:30 p.m.

Late Career PhD (LCPhD) posters.....1:00-3:30 p.m.

Happy hour/judging.....3:30 p.m.

Awards/closing.....4:00 p.m.

8th Annual Jackson School Research Symposium

Texas Union, Shirley Bird Ballroom (3.202)

Saturday, February 2, 2019

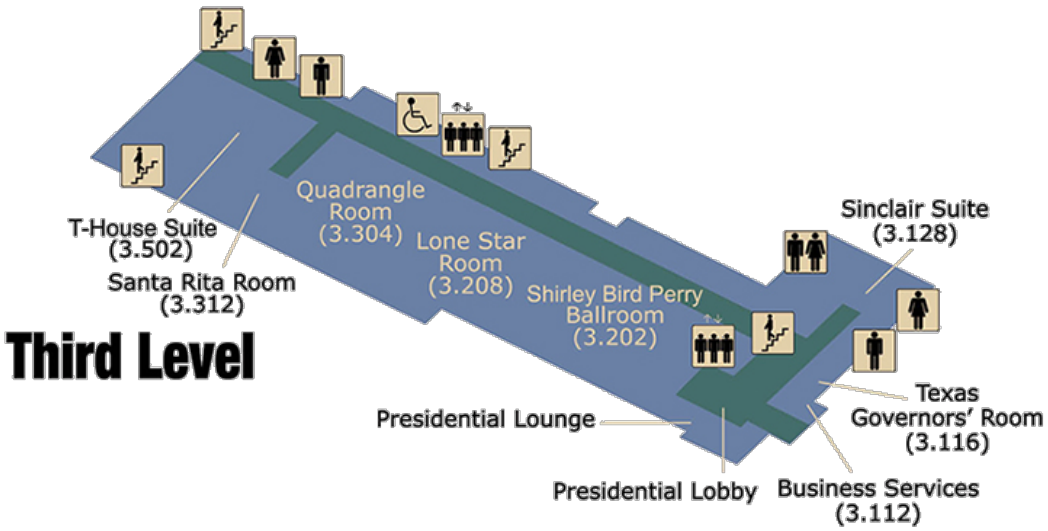

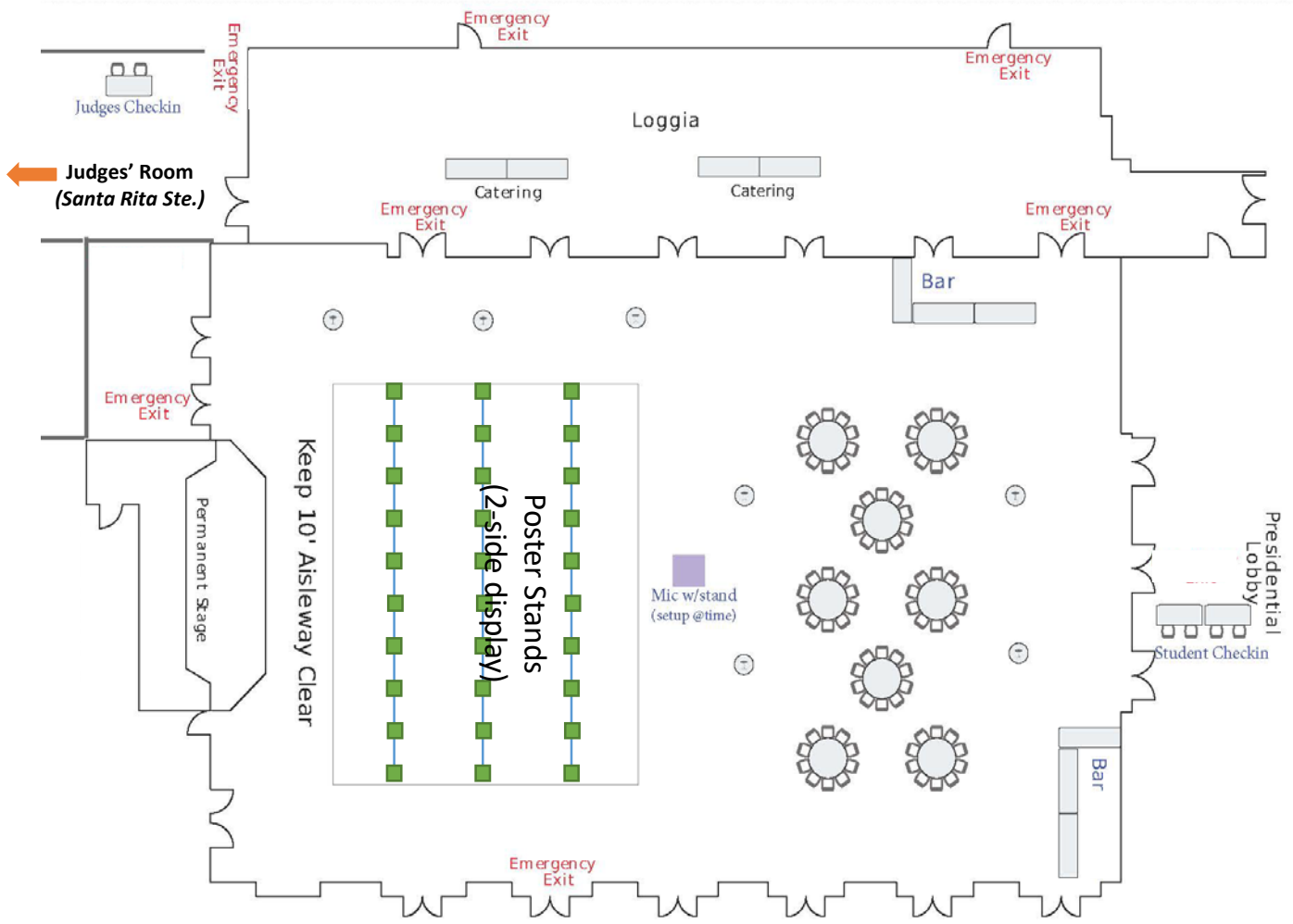

Student Abstracts

Themes:

Climate, Carbon, and Geobiology (CCG)

Energy Geosciences (EG)

Marine Geosciences (MG)

Planetary Sciences (PS)

Solid Earth and Tectonic Processes (SETP)

Surface Processes and Hydrology (SPH)

Early Career Graduate Student (ECG)

Poster ID	First Name	Last Name	Theme	Poster Title
ECG-1	Natchanan	Doungkaew	Other	Study of Fracture Growth in Chemically Reactive Geologic Systems Using Constrained Sintering
ECG-2	Estefania	Salgado Jauregui	Other	Multicriteria assessment of paleontological zones, in a context of integral management of geodiversity. Case study: Villa de Leyva, Boyacá, Colombia
ECG-3	Julia	Holland	CCG	Are urban bald cypress trees resilient to drought?
ECG-4	Wei	Wei	CCG	The bathymetric and subglacial hydrological context for basal melting of the Getz Ice Shelf, West Antarctica
ECG-5	Omar	Alamoudi	EG	A New MicroCT Enabled Triaxial Pressure Vessel for Rock Deformation Studies
ECG-6	Harpreet	Kaur	EG	Estimating inverse of Hessian for amplitude correction of migrated images using deep learning
ECG-7	Son	Phan	EG	Improved Horizon Delineation with High-Resolution Pre-stack Seismic Inversion using Boltzmann Machine
ECG-8	Andrew	Roberts	EG	Stratigraphic architecture and facies distribution in the Pennsylvanian Strawn Formation, Fort Worth Basin

ECG-9	Robert	Domeyko	MG	Influence of past changes in atmospheric CO2 on B/Ca of planktic fossil foraminifera
ECG-10	Zachary	Murphy	MG	Three-Phase Relative Permeability of Hydrate-Bearing Sediments
ECG-11	Kristian	Chan	PS	Mobilization of Near-surface Brine on Europa
ECG-12	Natalie	Wolfenbarger	PS	Can radar attenuation serve as a signal of ice shell salinity on Europa?
ECG-13	William	Dufresne	SETP	Raman spectroscopy of the eight natural calcite-group minerals
ECG-14	Scott	Eckley	SETP	Isotopically light carbon (?13C -31 to -24 ‰) in the mantle by at least 3.2 Ga: insights from carbonado diamond
ECG-15	Megan	Flansburg	SETP	Thermal-Tectonic Evolution of a South Cycladic Metamorphic Core Complex, Ios and Sikinos Islands, Greece
ECG-16	Stephanie	Forstner	SETP	Evolution of deformation in the Buck Mountain Fault damage zone, Cambrian Flathead Sandstone, Teton Range, WY
ECG-17	Andrew	Gase	SETP	Crustal structure of the northern Hikurangi margin from marine seismic reflection imaging and onshore-offshore seismic tomography: implications for megathrust heterogeneity and overpressure in a region of shallow slow earthquakes
ECG-18	Nicole	Guinn	SETP	Evolving Dynamic Pressures in Pyroclastic Density Currents: Evidence from the 18 May 1980 Blast Surge of Mount St. Helens
ECG-19	Evelin	Gutiérrez	SETP	The Gulf Coast stratigraphic response to Pleistocene-Holocene climate change.
ECG-20	Xin	Liu	SETP	Perfectly matched layer boundary conditions for frequency-domain acoustic wave simulation in the mesh-free discretization
ECG-21	Nicholas	Meszaros	SETP	Processes of Change in Magma Storage Conditions Beneath Valles Caldera
ECG-22	Eirini	Poulaki	SETP	Tectonic evolution of the Cycladic Blueschist Unit and Cycladic Basement with multiple geo-thermo chronometers, Sikinos and Ios Greece
ECG-23	Simone	Puel	SETP	Benchmarks and resolution analysis for visco-elastic subduction zone models
ECG-24	Samantha	Robbins	SETP	Thermal evolution of a distal hyperextended margin – A case study of Zabargad Island, Red Sea
ECG-25	Daniel	Ruiz Arriaga	SETP	Structural inheritance from metamorphic basements in inverted basins of southeast Mexico

ECG-26	Rachel	Ruthven	SETP	NEW CONSTRAINTS ON THE GEOMETRY, KINEMATICS, AND TIMING OF DEFORMATION ALONG THE SOUTHERN SEGMENT OF THE PAPOSO FAULT ZONE, ATACAMA FAULT SYSTEM, NORTHERN CHILE
ECG-27	Scott	Staniewicz	SETP	Automatic Detection of InSAR Deformation Signals Associated with Wastewater Injection and Induced Seismic Events
ECG-28	Cansu	Demir	SHP	Understanding the Hydraulic Behavior of the Güzelyurt Alluvial Coastal Aquifer via Numerical Modeling Approach
ECG-29	Kwun Yip	Fung	SHP	Evaluating the anthropogenic heat and global warming impacts on extreme precipitation in Pearl River Delta megacity based on dynamical downscaling
ECG-30	Emily	Pease	SHP	Evaluation of machine learning applications for springflow estimation and forecasting at Comal Springs, New Braunfels, Texas.
ECG-31	Esben	Pedersen	SHP	Carbonate Factory Recovery Following Oceanic Anoxic Events: a Closer Look at the Cow Creek Member of the Pearsall Formation in South Texas
ECG-32	Michelle	Pedrazas	SHP	Field Characterization of Hillslope Weathering Profiles in the Great Valley Sequence, Northern CA
ECG-33	Micaela	Pedrazas Hinojos	SHP	Missing ice or faulty eyes? Mapping supra-permafrost environments along the Arctic coast using electrical geophysics
ECG-34	Austin	Rechner	SHP	Juniperus Ashe Effects on West Texas Water Balance
ECG-35	Ana Maria	Restrepo Acevedo	SHP	Changes in the Hysteresis Between VPD and Sap-Flux Velocity in Different Tree Species in Northern Michigan Forests'
ECG-36	Cole	Speed	SHP	Anatomy of a Fluvial Avulsion: Linking Geomorphology and Stratigraphy using 3-D Outcrops of Exhumed Channel-Belt Deposits
ECG-37	Yue	Wu	SHP	Determining the link between hydraulic properties of arctic tundra soils and Interferometric Synthetic Aperture Radar deformation measurements

Late Career Master's Student (LCMS)

Poster ID	First Name	Last Name	Theme	Poster Title
LCMS-1	Fernando	Apango	EG	Top Seal Evaluation of Miocene Deep-Water Reservoirs, Southern Gulf of Mexico
LCMS-2	Cody	Draper	EG	Wolfcampian Shelf-to-Basin Stratigraphic Framework of the Central Basin Platform and Midland Basin, Andrews County, Texas
LCMS-3	Ben	Gremillion	EG	Seismic data interpolation to a regular grid
LCMS-4	Michael	McCann	EG	Low-Frequency Attenuation Measurements of Fluids
LCMS-5	Nam	Pham	EG	Missing well-log prediction using recurrent neural network
LCMS-6	Omar	Ramirez Garcia	EG	Geologic Characterization and CO2 Storage Resource Assessment of Two Depleted Hydrocarbon Fields in the Texas State Waters, Gulf of Mexico
LCMS-7	Tiannong	Dong	MG	Pore-scale methane hydrate formation under pressure and temperature conditions of natural reservoirs
LCMS-8	Gabriel	Giacomone	MG	Paleogeographic reconstruction and characteristic trends of a basin floor fan in Los Molles Fm, Neuquén Basin, Argentina
LCMS-9	Clara	Brennan	SETP	Achieving quantitative understanding of radiogenic He behavior in zircon using 4He/3He thermochronometry
LCMS-10	Jacob	Makis	SETP	Petrology, Geochemistry and Zircon U/Pb Geochronology of the Ertsberg Pluton, Ertsberg-Grasberg Mining District, Papua, Indonesia: Magma Chamber Recharge and Mixing
LCMS-11	Lakin	Beal	SHP	Tracking the sources and processes of urban development effects on stream water evolution in Austin, TX
LCMS-12	Kendra	Bunnell	SHP	An Investigation into the Applicability and Implications of Central Texas Speleothems in Paleotempestology
LCMS-13	Paul	Southard	SHP	Spring-associated riparian vegetation and its impact on morphology in dryland channels:Henry Mountains, UT, USA

Late Career Ph.D. Student (LPHD)

Poster ID	First Name	Last Name	Theme	Poster Title
LCPHD-1	Seungwon	Chung	CCG	Human-induced nitrogen exports to rivers in San Antonio and Guadalupe river basins
LCPHD-2	Lingcheng	Li	CCG	Developing plant hydrodynamics in the Noah-MP land surface model
LCPHD-3	Anna	Weiss	CCG	Extinction selectivity of Scleractinian corals during the Paleocene-Eocene Thermal Maximum
LCPHD-4	Wen-Ying	Wu	CCG	The Role of Multi-sensor Land Data Assimilation in Runoff and Streamflow Estimation
LCPHD-5	Eric	Goldfarb	EG	Estimating Properties from Millimetric Sized Rock Cuttings Using Micro Computed Tomography (CT)
LCPHD-6	Ken	Ikeda	EG	Numerical and Laboratory Study of Low-frequency Elastic Properties of Limestone
LCPHD-7	Ziqi	Jin	EG	Frequency-Dependent Q Estimation Method Based on Laboratory Experiments
LCPHD-8	Fnu	Prasanna Ganesan Krishnamurthy	EG	Mimicking Rock Heterogeneity in the Laboratory for Studying Buoyancy Driven Fluid Migration in Porous Media
LCPHD-9	Sebastian	Ramiro Ramirez	EG	Porosity and Permeability in Wolfcamp Lithofacies at Delaware Basin, West Texas
LCPHD-10	Yunzhi	Shi	EG	Deep learning for seismic interpretation
LCPHD-11	David	Tang	EG	Segmentation of Thin Sections with Machine Learning
LCPHD-12	Janaki	Vamaraju	EG	UNSUPERVISED PHYSICS BASED NEURAL NETWORKS FOR SEISMIC MIGRATION
LCPHD-13	Jennifer	Harding	MG	Nature and variation of oceanic crust at a global endmember, the Mid-Cayman Spreading Center
LCPHD-14	Patrick	Meazell	MG	Extraordinary preservation of a deepwater channel-levee system in Green Canyon 955, Northern Gulf of Mexico
LCPHD-15	Kelly	Olsen	MG	Heterogeneous Upper Plate Extension in South Central Chile and Implications for Megathrust Fault Development
LCPHD-16	Naoma	McCall	PS	Fracture orientations of granitoid peak ring rocks in the Chicxulub impact crater
LCPHD-17	Catherine	Ross	PS	Helium Diffusion Kinetics of Shocked Zircon from the Chicxulub Impact Crater
LCPHD-18	Tomas	Capaldi	SETP	Cordillera evolution along the southern Central Andean margin recorded by detrital zircon U-Pb and Hf isotopes

LCPHD-19	Thomas	Etzel	SETP	Tectonometamorphic evolution of the Southern and Central Menderes Massif, western Turkey
LCPHD-20	Zachary	Foster-Baril	SETP	Triassic and Jurassic Rift Basin Records of Continental Breakup along the Eastern North American Margin, U.S.A.
LCPHD-21	Sarah	George	SETP	Drainage networks in the early-northern Andes Mountains: Paleogene depositional and paleo-environmental record of the Quingeo Basin, Ecuador
LCPHD-22	Cullen	Kortyna	SETP	Provenance and Pathways of the Cretaceous-Paleogene Paleo-Rio Grande River: Deciphering Signals from Complex Source Terranes Using Detrital Zircon Geo-Thermochronology
LCPHD-23	Chelsea	Mackaman-Lofland	SETP	Andean deformation and foreland basin evolution during Neogene changes in subduction zone geometry (32-33°S)
LCPHD-24	Peter	Nelson	SETP	Inner core hemispherical differences inferred from waveform modeling of stacked dense array data
LCPHD-25	Margaret	Odlum	SETP	Reconstructing middle to lower crustal thermal and tectonic histories from apatite U-Pb thermochronometry by laser-ablation depth-profile ICP-MS analysis
LCPHD-26	Brandon	Shuck	SETP	From Rifting to Subduction: Evidence for the Role of Past Tectonics Influencing Subduction Initiation at the Puysegur Trench, New Zealand
LCPHD-27	Wanying	Wang	SETP	Upper Mantle Seismic Anisotropy as a Constraint for Mantle Flow and Continental Dynamics of the North American Plate
LCPHD-28	Benjamin	Cardenas	SHP	Anatomy of an exhumed river-channel belt
LCPHD-29	Max	Daniller-Varghese	SHP	Detrital Zircon Transport Lag in Fluvial Bedload
LCPHD-30	Yuqian	Gan	SHP	Linear-sourced slope channel systems in high sediment supply basin margin clinoforms
LCPHD-31	Evan	Ramos	SHP	Toward a mechanistic understanding of Li isotope transfer within landscapes

Undergraduate Student (U)

Poster ID	First Name	Last Name	Theme	Poster Title
U-1	Brooke	Bogan	CCG	A new description and analysis of the extinct lobster genus *Uncina*.
U-2	Michael	Christoffersen	CCG	A new long wavelength airborne sounding radar for temperate glacier thickness measurement with a case study on the Hubbard Glacier, Alaska, USA
U-3	Sean	Kacur	CCG	Strontium Isotope Profile from a Lower Jurassic Shallow Water Carbonate Platform in the Dinarides, Slovenia: A High-Resolution Picture of the Toarcian Oceanic Anoxic Event
U-4	Brooke	Kopecky	CCG	Reconstructing paleo-ENSO variability during the Holocene using geochemical proxies from corals
U-5	Preston	Fussee-Durham	EG	Modeling Episodic Fluid Migration in Salt Basins
U-6	David	Wiggs	EG	Quantitative Uncertainty Assessment of Reservoir Facies Estimates from Inverted Impedances and Rock-Physics Modeling
U-7	Patricia	Standring	MG	Benthic Foraminiferal Paleoenvironmental Analysis of the Trinity River Paleovalley on Cores Collected Offshore Galveston Bay, Gulf of Mexico
U-8	Mauricio	Exiga	PS	Semi-Automatic Glacier Terminus Recognition Through Landsat Image Processing
U-9	Hannah	Anderson	SETP	Insights to copper porphyry deposits from magmatic apatites in the Grasberg-Ertsberg mining district of Papua, Indonesia
U-10	Eytan	Bos Orent	SETP	Stockwork vein zone in the Grasberg porphyry Cu-Au deposit, Papua, Indonesia: Structural and chemical implications
U-11	Jesse	Gu	SETP	The Effect of H2O on the Anomalous Velocities and Compressibilities of Rhyolitic Glasses up to 3 GPa
U-12	Thomas	Quintero	SETP	Origin of Cockade Textures in the Multi-Stage Vein System of the Rozália Mine, Banská Hodruša, Slovakia
U-13	John	Franey	SHP	Effects of Grain Interlocking on the Threshold of Motion in Gravel-Bed Rivers
U-14	James	Gearon	SHP	Geomorphic Influence on Canopy Structure in Eldorado Valley, Nevada
U-15	Kate	Grobowsky	SHP	Refining Sediment Transport Models
U-16	Ryan	Herring	SHP	The Fate of the Mississippi River Sediment During the Last Glacio-eustatic Cycle: A Volumetric Quantification
U-17	Jaime	Hirtz	SHP	Sediment mixing in modern eolian environments with detrital zircon U-Pb geochronology and detrital feldspar REE geochemistry: Example from the Andean broken foreland basin of Argentina

U-18	Matthew	Nix	SHP	Controls on the sedimentation and morphology of an oxbow lake along the Trinity River, Texas, USA
U-19	Arisa	Ruangsirikulchai	SHP	EVOLUTION OF RETURN-FLOW CHANNELS CUT INTO SAN JOSE ISLAND, TEXAS, CAUSED BY HURRICANE HARVEY
U-20	Nicholas	Soto-Kerans	SHP	Stratigraphic Evaluation of Trinity Aquifers in Hays and Western Travis County and Implications for Groundwater Availability
U-21	Xiafei	Zhao	SHP	Grainflow Thickness: Surface Process to Subsurface Record

GeoFORCE and STEMFORCE 12th Grade Academy Central Texas Field Experiences

Authors: GeoFORCE and STEMFORCE Students, High School Class of 2019

During the summer of 2018, GeoFORCE and STEMFORCE students worked in groups to complete projects associated with one of two hypothetical geoscience tasks or "challenges." Over the course of a week, students collected data at field sites, synthesized observations in the classroom through research and hands-on activities and visited JSG labs engaged in research related to concepts explored. They presented their findings in the form of technical talks and a poster accompanied by a 5-min "lightning talk." The two challenges are described below. GeoFORCE and STEMFORCE students will be on hand to present their group posters created during their academy.

1. Site Investigations for Scenic Connectors of a High-Speed Railway through Central Texas

The Texas Department of Transportation (TXDOT) has announced a plan to build a high speed rail line connecting Austin, Dallas, San Antonio, and Houston. The line will have "scenic connectors" that transport tourists to locations in the Hill Country of Central Texas. Specific rail corridors have not been decided; site investigations need to occur first. You and your team of colleagues work for a geological engineering firm and will conduct site investigations for the project. It is your responsibility to decide if the region is suitable for such a project. The department would like to answer the following questions: (1) Is the region stable from faults, earthquakes, and volcanism? What other potential hazards are associated with building across the geological regimes of Texas? (2) Are there cultural or conservational issues (human or ecosystem) that may impact a large engineering project? (3) What are the primary geological regimes of Texas as you travel along the rail? How are the lithologies going to impact the feasibility of building the rail?

2. Communicating the Geologic History of Central Texas through Snapchat (Snap Inc.) Filters

Texas Parks and Wildlife Department (TPWD) has noticed a significant decline in 18-30 year olds at State Parks. In an effort to target this age group, TWPD has commissioned your new company with its team of expert geological consultants to make seven geologically relevant Snapchat filters (one for each field stop). These Snapchat filters will allow park visitors, as well as anyone in close proximity, to travel "back to the past" through geological time, learning about the past environment, climate, and flora and fauna. Your series of seven filters should communicate to the public the answers to the following questions: (1) When and where in geologic time and space (paleogeographic reconstruction and UTM coordinates) is the setting of the filter? (2) What types of rocks are present and what is the geologic setting? (3) What was Earth's climate like at the time? (4) What geologic processes are recoded here and how is the landscape continuing to change?

ECG

Study of Fracture Growth in Chemically Reactive Geologic Systems Using Constrained Sintering

Natchanan Doungkaew
Doungkaew, N., Bureau of Economic Geology, The University of Texas at Austin, Austin, TX
Eichhubl, P., Bureau of Economic Geology, The University of Texas at Austin, Austin, TX

Fractures control the mechanical properties of the brittle crust and fluid flow in the subsurface. Fractures pose many engineering problems such as structural stability and engineering challenges; these can be found in such areas as reservoir exploration and waste containment. Geologic settings where subsurface fractures are present can be considered chemically reactive environments. The main goal of this research is to replicate fracture formation due to solution-precipitation creep in chemically reactive environments using constrained sintering. We hypothesize that: 1) Fractures developed in a heterogeneous material differ from those formed in a homogeneous material due to reactions between the material composites; and 2) Duration of sintering affects the fracture characteristics because it allows longer time for chemical reaction and densification of materials to occur. To test these hypothesis, we sintered different mixtures of calcite and quartz powders of different ratios (C:Q of 1:1, 1:2, and 2:1) for 0.5 hour and 1 hour under 1100°C. The mixtures of powders were attached to a mullite brick substrate that undergoes no chemical change during heating. Using XRD analysis, we observed solid-solid net reactions between the two minerals that produced wollastonite and larnite. Combustion of calcite also produced lime. In all experimental settings, all calcite was consumed while quartz was still present after sintering. Wollastonite peaks also became more prominent with increasing sintering duration under 1100°C. We were also able to document in-situ fractures initiation at temperatures of 900°C; and observed fracture grew as temperature increased to 1100°C. With increasing temperatures, lengths and widths of fractures increased. These observations suggest that the extent of solid-solid net reactions coupling with stress can result in different fracture characteristics including fracture shapes and lengths. Future research includes calculating rates of fracture length growth during sintering of materials of various ratios of quartz and calcite. Sintering may prove to be a new method to replicate fractures growth in subsurface condition. The information on characteristics of natural fractures formed under chemically reactive conditions such as their shapes, sizes, and distributions; may be used as input parameters for numerical fracture growth simulations and may also be used to improve existing fracture growth models.

Keywords: Fracture,Sintering, Experiment,Constrained sintering

ECG

Multicriteria assessment of paleontological zones, in a context of integral management of geodiversity. Case study: Villa de Leyva, Boyacá, Colombia

Estefania Salgado Jauregui
Salgado-Jauregui, E., University of Texas at Austin
Garzon-Gomez, C., National University of Colombia

Multicriteria analysis has been implemented broadly in the field of environmental sciences, as a tool for decision making about the study and management of the territory. In geosciences it could be an alternative which enhance the appropriate management of geological features scientifically relevant. A prototype of Multicriteria assessment in areas of geological and paleontological interest is proposed, aimed to its integral management.

This research presents methodological strategies for the Multicriteria assessment of the Colombian territory, from its geological diversity. The prototype was built following the Analytic Hierarchy Process (AHP) methodology, based on decomposing the decision problem in a hierarchy of related elements, including an objective, criteria and subcriteria which influence the decision and the alternatives of solution.

A case study is presented in the Villa de Leyva municipality of Boyacá, due to the scientific national and international relevance of its geological and paleontological features, in a context of vulnerability given the economic, social and cultural conditions of the region, where the local population has perceived the fossils as natural resources with a monetary value.

The valuation prototype was applied to the *Kronosaurus boyacensis*, Hampe 1992 paleontological outcrop, located in Monquira, Villa de Leyva. The criteria and subcriteria include geological, environmental, sociocultural and economic components. Three management alternatives were taken into account, *in situ* conservation, *ex situ* conservation and fossils sale. The results obtained with the methodology and the experimental prototype demonstrate that the best alternative for this specific site is *in situ* conservation (44,5%). If the scientific relevance, reflected in the geological component of the model, were the unique criteria contemplated the more desirable alternative would be *ex situ* conservation (56,5%). The same if the vulnerability, reflected in the environmental component were the only considered (with a 38,5%). However, including criteria from the sociocultural and economic components such as progress generation, community-government-academy trust, between others, the best alternative turns to be *in situ* conservation.

This research is a methodological contribution to the assessment of the geodiversity that has been historically valuated with an economic-neoclassic focus, considering just its economic value. The study and application of the Multicriteria analysis in the field of geosciences will enhance the conservation of geological features of scientific relevance and will bring a more holistic vision of nature, promoting its sustainable management.

Keywords: Geodiversity, geological heritage, paleontological, Multicriteria assessment, Analytic Hierarchy Process-AHP, Villa de Leyva, Boyacá, Colombia

CCG
ECG

Are urban bald cypress trees resilient to drought?

Julia Holland
Holland, J., Jackson School of Geosciences, The University of Texas at Austin, Austin, TX
Banner, J., Jackson School of Geosciences, The University of Texas at Austin, Austin, TX
Black, B., Laboratory of Tree-Ring Research, The University of Arizona, Tucson, AZ
Burkhalter-Castro, R., Eckerd College, St. Petersburg, FL
Beal, L., Jackson School of Geosciences, The University of Texas at Austin, Austin, TX

Trees are well know to be good proxies for their environment of growth. Considering the input of municipal water into natural stream systems, it is plausible that trees in environments where there is significant municipal water input may not suffer the effects of drought on tree growth. For this study, 40 cores were collected from 20 bald cypress (*Taxodium distichum*) trees in Waller Creek of Austin, Texas for tree ring analysis to understand their growth response to the 2011 drought. Linear regression analysis was performed to understand the relationship between tree ring growth and variables that are assumed to control tree growth including annual precipitation and discharge averages. Results show a very weak linear correlation between tree ring growth and precipitation ($R^2 = 0.0005$) and a strong linear correlation between tree ring growth and discharge ($R^2 = 0.669$). This implies that the growth of these trees is predominantly controlled by discharge rather than precipitation. Far-reaching conclusions may be drawn that this information supports the hypothesis that urban trees are resilient to drought due to urban water leakage.

Keywords: dendrochronology, hydrology, statistics

CCG
ECG

The bathymetric and subglacial hydrological context for basal melting of the Getz Ice Shelf, West Antarctica

Wei Wei
Wei, W., Institute for Geophysics and Department of Geological Sciences, Jackson School of Geosciences, University of Texas at Austin, Austin, TX, United States
Blankenship, D., Institute for Geophysics and Department of Geological Sciences, Jackson School of Geosciences, University of Texas at Austin, Austin, TX, United States
Greenbaum, J., Institute for Geophysics and Department of Geological Sciences, Jackson School of Geosciences, University of Texas at Austin, Austin, TX, United States
Goumelen, N., School of Geosciences, University of Edinburgh, Edinburgh, United Kingdom
Dow, C., Department of Geography and Environmental Management, University of Waterloo, Waterloo, Ontario, Canada
Richter, T., Institute for Geophysics and Department of Geological Sciences, Jackson School of Geosciences, University of Texas at Austin, Austin, TX, United States
Young, D., Institute for Geophysics and Department of Geological Sciences, Jackson School of Geosciences, University of Texas at Austin, Austin, TX, United States
Lee, S., South Korea Polar Sciences, Korea University of Science and Technology, Daejeon, South Korea
Lee, W., South Korea Polar Sciences, Korea University of Science and Technology, Daejeon, South Korea
Wa?hlin, A., Department of Earth Sciences, University of Gothenburg, Gothenburg, Sweden
Assmann, K., Department of Earth Sciences, University of Gothenburg, Gothenburg, Sweden

The ice shelves in the Amundsen Sea Embayment are thinning rapidly. Among them, the Getz Ice Shelf is the largest but remains poorly sampled. It is believed to supply the largest amount meltwater from Antarctica to the Southern Ocean. We present a new bathymetry of the Getz Ice Shelf. Our study demonstrates the practical use of high-resolution helicopter airborne gravity to fill critical gaps in seafloor bathymetry in Antarctica, especially over the deep troughs under the ice-shelf cavity that generally go undetected in more regional aerogeophysical surveys. These troughs are sometimes continuous from the continental shelf to the ice sheet grounding line and thus provide natural pathways for modified Circumpolar Deep Water (mCDW) to enter into the ice cavity, drive rapid basal melt, and channel subglacial discharge. We show discharge of subglacial freshwater from upstream is playing a role in regulating the basal melt rate of Western Getz. Our results confirm the importance of constraints on bathymetry and subglacial discharge for understanding ocean forcing on basal mass loss of Antarctic ice shelves. These new data will also be critical for guiding new airborne/ground-based surveys, interpreting recent and past ice-shelf changes, and assisting ocean circulation modeling of future impacts for this sector of West Antarctica.

Keywords: ice sheet ocean interaction

EG
ECG

A New MicroCT Enabled Triaxial Pressure Vessel for Rock Deformation Studies

Omar Alamoudi
Alamoudi, O., Jackson School of Geosciences, The University of Texas at Austin, Austin, TX
Tisato, N., Jackson School of Geosciences, The University of Texas at Austin, Austin, TX
Grasselli, G., Department of Civil & Mineral Engineering, University of Toronto
Goldfarb, E., Jackson School of Geosciences, The University of Texas at Austin, Austin, TX

Rocks are heterogeneous composite materials with complex physical, and chemical properties. In order to predict the rheology of rocks, two modeling procedures are usually considered. First, material behavior models, commonly referred to as constitutive laws, are used to describe how materials behave under well-defined boundary conditions. Second, material property complexities are replaced by material property models.

On one hand, constitutive laws permit the characterization of stress-strain behavior of rocks by comparing them to results obtained from laboratory experiments. On the other hand, material property models provide us the means to approximate the material properties used in the constitutive law of choice. Examples of constitutive laws that are used in describing solid material rheology are Elasticity, Visco-elasticity, Plasticity, Visco-plasticity, Hyper-elasticity, etc. The simplest material model is Elasticity, in particular Elasticity of homogeneous, isotropic materials. Under the constraints of such material model assumptions, namely homogeneous isotropic material, rheology of the lithology can be fully described by measuring only two elastic parameters the bulk, and shear moduli.

Although considering a rock sample as a homogeneous isotropic material provides sometimes a “good enough” insight about its rheology, such assumptions are too simplistic. An alternative, less constrained material model is to consider the material to be homogeneous, and vertically transverse isotropic (VTI). This configuration is more applicable to sedimentary rocks, especially that it depicts the visible horizontal lamination observed in sedimentary rocks. Often, rheology cannot be properly described from laboratory experiments because the deformation under elevated pressure and temperature cannot be observed, or it can observed only post-mortem. Thus, in the last decade, with the advent of new analytical technologies, such as X-ray Micro Computed Tomography (MicroCT), scientists have started observing in-situ in-operando rock deformation.

With this in mind, we are presenting a design of an X-ray transparent tri-axial pressure vessel that allows us to subject a cylindrical rock sample to different stress configurations and pore pressure. Such apparatus is ubiquitous in engineering and geo-sciences. What is unique about this apparatus however, is that the enclosure within which the sample and the fluid that provides the confining pressure is made out ofAluminum, and the entire apparatus is made to fit within a MicroCT scanning machines. Such setup, allows us, in addition to measuring the effective properties of a sample under well-defined boundary conditions, to image our sample over time. Our hope is that the MicroCT data will help us in understanding how different rock types behave under different physical, and possibly chemical, scenarios.

Keywords: Rock Physics, deformation, triaxial, MicroCT

EG
ECG

Estimating inverse of Hessian for amplitude correction of migrated images using deep learning

Harpreet Kaur
Kaur, H., Graduate research assistant
Pham, N., Graduate research assistant
Fomel, S., Professor

Seismic imaging algorithms often use adjoint of forward modeling operator to estimate subsurface model. Although adjoint operation is more robust yet it is less accurate than inverse operation because most of the operators used in seismic processing are non unitary which makes it difficult to obtain migrated images with true amplitudes. One possible solution to this problem is incorporating depth migration algorithms such as reverse time migration (RTM) into an iterative inversion framework, known as least-squares RTM (LSRTM), to improve the quality of images. Since inversion is an expensive process, we propose to estimate migrated images with meaningful amplitudes similar to least-squares inverse images by approximating inverse of Hessian using generative adversarial networks (GANs) in a conditional setting. We use the framework of CycleGAN and extend it to conditional CycleGAN such that mapping from migrated image to true reflectivity is subjected to attribute condition of velocity. This approach gives results similar to iterative inversion by approximating inverse of Hessian at much reduced cost. This algorithm is applied after migration and is computationally efficient. Proposed method shows noticable improvements in image resolution, noise attenuation, migration artifact reduction and enhancement of reflection amplitudes. We train our network with two different data sets and for testing we use two other data sets which are not a part of training. Test on validation data sets verify the effectiveness of the proposed approach.

Keywords: LSRTM, GAN

EG
ECG

Improved Horizon Delineation with High-Resolution Pre-stack Seismic Inversion using Boltzmann Machine

Son Phan
Phan, S., Institute for Geophysics
Sen, M., Institute for Geophysics

Seismic inversion is one popular approach that aims at predicting some indicative properties to support the geological interpretation process. The existing inversion techniques show weaknesses when dealing with complex geological area, where the uncertainties arise from the guiding model, which are input by the interpreters. In this study, we employ the Boltzmann machine, a stochastic neural network, to perform automatic pre-stack inversion for some elastic properties. Unlike the common inversion approaches, this method does not require a starting model at the beginning of the process to guide the solution; however low frequency models are required to convert the inversion-derived reflectivity terms to the absolute elastic P- and S- impedance as well as density. The process incorporates a single layer Hopfield neural network whose neurons can be treated as the desired reflectivity terms. The optimization process seeks the global minimum solution by combining the network with a stochastic model update from the Mean Field Annealing algorithm. Also, to improve the lateral continuity of the results and to stabilize the inversion process, we employ a “Z” shaped sample sorting scheme and the first order Tikhonov regularization. We applied this method to a field 2D dataset to invert for high resolution indicative P- and S-impedance sections to better capture some features away from the reservoir zone. The resulting models are strongly supported by the well results and suggested realistic features that were not displayed from the model-based deterministic inversion approach. In combination with well log analyses, we conclude those features might be potential targets for exploration purposes.

Keywords: Machine Learning, Pre-stack Seismic Inversion, High Resolution, Horizon Delineation

EG
ECG

Stratigraphic architecture and facies distribution in the Pennsylvanian Strawn Formation, Fort Worth Basin

Andrew Roberts
Ambrose, W., Bureau of Economic Geology, The University of Texas at Austin, Austin, TX

Within the Pennsylvanian Strawn Formation in the Fort Worth Basin, a variety of lithofacies have been identified, which include, but are not limited to, low-energy mudstone, rippled sandstone-mudstone, and planar, cross-bedded sandstones. Given the heightened scrutiny required for finding conventional reserves in mature plays and basins, this study provides an in-depth technique for stratigraphic analysis and description of reservoir units. Delineation of distinct siliciclastic units was accomplished by describing whole cores for facies interpretations and correlating wireline logs as the basis for constructing lithofacies maps. These facies are interpreted to represent a variety of depositional environments in the Pennsylvanian Perrin Delta system including, but not limited to, distributary channels, tide-influenced shallow marine, and distal marine. Their provenance and distribution reflect tectonic control by major structural elements including the Bend Arch to the west and Ouachita fold belt to the east. Mapping of regional stratigraphic surfaces such as flooding surfaces reveal the extent and distribution of these siliciclastic units, as well as the frequency of the repetitive stratigraphic successions of marine and nonmarine strata, known as cyclothems. Additionally, thickness maps will demonstrate the influence of the Bend Arch on sediment distribution and provide a model for how this dispersal varies along trend. Determination of sandstone quality and distribution within the Strawn Formation will be made possible by this study and provide analogs for similar deltaic environments in the subsurface.

Keywords: Stratigraphy, Facies Analysis, Petroleum Geology

MG
ECG

Influence of past changes in atmospheric CO2 on B/Ca of planktic fossil foraminifera

Robert Domeyko
Domeyko, R., Institute for Geophysics, University of Texas at Austin
Allen, K., University of Maine at Orono
deMenocal, P., Lamont-Doherty Earth Observatory, Columbia University

Influence of Past Changes in Atmospheric CO_2 on B/Ca of Planktic Fossil Foraminifera

Culture experiments have revealed that B/Ca of shells grown by the foraminiferal species *Globigerinoides ruber* increase with increasing seawater pH. Specifically, B/Ca responds to changes in the relative abundance of pH-sensitive dissolved carbon and boron species. Here, we present a high-resolution study on fossilized *G. ruber* from two sites in North Atlantic subtropical gyres (VM25-21 and ODP 1055B) through 20 ka BP to evaluate how B/Ca responds to past changes in atmospheric CO_2. Forams were picked and crushed gently, then cleaned and dissolved using a variation of the Boyle and Keigwin (1985) and Barker et al. (2003) cleaning protocols prior to analysis. ODP 1055B (from Carolina Slope, West Atlantic) produced a high-resolution record with lower B/Ca values during the glacial period followed by a rapid shift to higher B/Ca values in the early deglaciation, with values remaining high through the Holocene. These results were not predicted by culture calibrations, but they are consistent with B/Ca records from the Caribbean (ODP 999), suggesting this pattern is characteristic of surface waters in the greater North Atlantic region.

Keywords: foraminifera, B/Ca, CO2, pH, Holocene, Atlantic Ocean, climate change

MG
ECG

Three-Phase Relative Permeability of Hydrate-Bearing Sediments

Zachary Murphy
Murphy, Z., Department of Geological Sciences, Jackson School of Geosciences, The University of Texas at Austin, ,Austin, TX
Fukuyama, D., Hildebrand Department of Petroleum and Geological Engineering, The University of Texas at Austin, Austin, TX
Daigle, H., Hildebrand Department of Petroleum and Geological Engineering, The University of Texas at Austin, Austin, TX
DiCarlo, D., Hildebrand Department of Petroleum and Geological Engineering, The University of Texas at Austin, Austin, TX
Flemings, P., Department of Geological Sciences, Jackson School of Geosciences, The University of Texas at Austin, Austin, TX

We formed methane hydrate in a brine-saturated Berea Sandstone core by injecting methane and cooling the sample to hydrate-stable pressure and temperature conditions. Hydrate formation continued until the pore water reaches three-phase stability and the increased salinity buffers hydrate formation. After hydrate saturation is determined by mass balance, the remaining free gas is purged from the system, and the sample is saturated with the three-phase brine. Steady-state relative permeability measurements are then made by flowing one or two phases through the sample and measuring the pressure drop across 5 sections of the 24-inch core. First only brine is injected then increasing amounts of methane gas relative to the brine are injected until only gas is injected. At each injection ratio, steady-state is reached when the pressure does not change with respect to time. The phase saturation(s) are measured at each step. Using Darcy's Law, the relative permeability for gas and water can be calculated at each saturation. Relative permeability is the effective permeability of a single phase divided by the intrinsic permeability and is the key parameter affecting flow in porous media. We have measured complete drainage relative permeability curves for various hydrate saturations. These relative permeability curves illustrate how fluid(s) interact and flow through hydrate-bearing samples in production or emplacement scenarios. These results are then compared to currently used models of relative permeability to determine how to best model multi-phase flow in hydrate-bearing sediment.

Keywords: Hydrate, permeability

PS
ECG

Mobilization of Near-surface Brine on Europa

Kristian Chan
Chan, K., University of Texas Institute for Geophysics, The University of Texas at Austin, Austin, TX
Grima, C., University of Texas Institute for Geophysics, The University of Texas at Austin, Austin, TX
Blankenship, D., University of Texas Institute for Geophysics, The University of Texas at Austin, Austin, TX
Young, D., University of Texas Institute for Geophysics, The University of Texas at Austin, Austin, TX
Soderlund, K., University of Texas Institute for Geophysics, The University of Texas at Austin, Austin, TX

Europa is assumed to have an ice regolith layer ranging from hundreds of meters to kilometers thick. In addition, recently developed models for some of Europa's characteristic geologic features – chaos terrains, lenticulae, and ridges – have attributed the formation of such features to the existence of shallow subsurface water. These models provide implications for brine transport through the porous ice regolith in the near surface, i.e., depths of tens of meters, by delivering pressurized brine as a result of fracture and disruption of the local ice shell. The brine would most likely exist in the vicinity of their geological counterparts. Its evolution in the near surface depends on a combination of factors, such as porosity, grain size, brine composition, salinity, and temperature. This brine can play a significant role in the ice cycling process occurring on Europa, and pores and cracks may also serve as habitats for microbial life.

Future ice-penetrating radars on the upcoming Jupiter Icy Moons Explorer and Europa Clipper missions have the capability to detect near-surface brines, while their depth is potentially within range of in-situ sampling from a future lander mission. Here, we discuss recent hypotheses for near-surface brine mobilization at Europa and their terrestrial analog counterparts.

Keywords: Brine, Flow through porous media, Europa, Ice-penetrating radar

PS
ECG

Can radar attenuation serve as a signal of ice shell salinity on Europa?

Natalie Wolfenbarger
Wolfenbarger, N., Institute of Geophysics, The University of Texas at Austin, Austin TX
Steinbrugge, G., Institute of Geophysics, The University of Texas at Austin, Austin TX
Soderlund, K., Institute of Geophysics, The University of Texas at Austin, Austin TX
Young, D., Institute of Geophysics, The University of Texas at Austin, Austin TX
Grima, C., Institute of Geophysics, The University of Texas at Austin, Austin TX
Blankenship, D., Institute of Geophysics, The University of Texas at Austin, Austin TX

Ice-penetrating radar has served as an invaluable tool in the field of glaciology. Radar reflections, referred to as echoes, are produced when the transmitted electromagnetic wave encounters a change in the dielectric properties of the medium. Classically, these radar echoes are used to derive ice thickness and bed geometry, both of which play an important role in ice dynamics. However, properties of the radar echoes, including their amplitude and distribution, can be used to infer additional properties of the medium. Leveraging these signal characteristics to constrain properties of interest can be valuable for planetary science applications, where ground truth is sparse or nonexistent.

The spacecraft for the upcoming Europa Clipper and JUICE missions are both equipped with ice-penetrating radar instruments, tasked with peering through the thick, icy shells of the Galilean moons to uncover the processes occurring beneath the surface. The ice-penetrating radar instrument on Europa Clipper, Radar for Europa Assessment and Sounding: Ocean to Near-surface (REASON), is in part designed to search for ice-ocean interfaces from 3-30 km depth.

Here, we discuss how radar attenuation might serve as a signature of column-averaged ice shell salinity on Europa. Radar attenuation is the decay in echo strength experienced by the signal as it propagates through a medium. Radar attenuation in ice is a function of the temperature and the concentration of conductivity-enhancing chemical impurities and is often modeled using an Arrhenius relationship. Where ice shell salinity contrasts are hypothesized to exist, such as at impact crater sites or between hemispheres, these could manifest as a locally enhanced or reduced region of attenuation. For example, the apparent attenuation rate associated with a region consisting of relatively pure ice should appear reduced relative to the higher-salinity surroundings.

Using radar attenuation as a signal of column-averaged ice shell salinity can yield ambiguous results. Typically, attenuation is far more sensitive to scattering and temperature than to chemical impurities. Decoupling the effects of scattering and temperature from the chemical contribution to attenuation is challenging and, in most cases, not possible. For this preliminary analysis, the effects of scattering on the radar signal are not considered. Scattering can affect echo amplitudes by reducing the apparent echo strength. In practice this can have the effect of overestimating the attenuation rate as modeled by the Arrhenius relationship. Existing methods, including specularity analysis and radar statistical reconnaissance, can be used to quantify the effects of scattering to aid in interpretation.

This work represents a preliminary feasibility study for the use of radar attenuation to help constrain the salinity of Europa's ice shell.

Keywords: radar, attenuation, europa, ice shell, salinity

SETP
ECG

Raman spectroscopy of the eight natural calcite-group minerals

William Dufresne
Dufresne, W., Department of Geology, University of Kansas, Lawrence, KS
Rufledt, C., Department of Geology, University of Kansas, Lawrence, KS
Marshall, C., Department of Geology, University of Kansas, Lawrence, KS

To date, only five natural carbonate minerals of calcite structure have been studied by Raman spectroscopy. These include calcite ($CaCO_3$), magnesite ($MgCO_3$), siderite ($FeCO_3$), smithsonite ($ZnCO_3$), and rhodochrosite ($MnCO_3$). Thus far, only synthetic compounds of otavite ($CdCO_3$), spherocobaltite ($CoCO_3$), and gaspeite ($NiCO_3$) have been investigated by Raman spectroscopy. However, the Raman spectra of natural otavite, spherocobaltite, and gaspeite have yet to be interpreted and compared with the Raman spectra of the other five natural carbonate minerals of calcite structure. This work has been undertaken to fill this gap and provide a comparison and interpretation of Raman spectra representative of all the eight natural carbonate minerals of calcite structure. The data here show that the carbonate *Eg* (*T*) phonon shifts are due to influences from the nearest neighbor distance; that is, M?O, and different ionic radii of the divalent metal cation, as shown graphically by a strong correlation ($r2 = 0.88$ and 0.91, respectively). Using this graphical approach, we have developed a Raman spectroscopic model based on the equation, $y = -2.067x + 356.2$ (±5 pm) to calculate the ionic radii of the divalent metal cation present within the mineral and hence affording the identification and discrimination of calcite?group minerals based on the band position of the *Eg* (*T*) mode.

Keywords: Raman spectroscopy, calcite-group, carbonate minerals

SETP
ECG

Isotopically light carbon (?13C -31 to -24 ‰) in the mantle by at least 3.2 Ga: insights from carbonado diamond

Scott Eckley
Eckley, S., Department of Geological Sciences, The University of Austin, Austin, TX
Ketcham, R., Department of Geological Sciences, The University of Austin, Austin, TX
Galster, F., Department of Geological Sciences, The University of Austin, Austin, TX

Diamonds passively record the evolution of mantle carbon. Their average carbon isotopic composition mirrors the average value for the mantle (~ -5 ‰), but excursions down to -41‰ and up to +5‰ have been measured. This variability has been attributed to a likely combination of primordial heterogeneities, fractionation processes, and recycling of crustal carbon. The latter process, by introducing organic carbon, is the leading hypothesis for the origin of light carbon in the mantle.

Carbonado is an unusual variety of highly porous, polycrystalline diamond that has a narrow range of isotopically light carbon ($\delta^{13}C$ -31 to -24 ‰) and a loosely constrained age between 2.6 and 3.8 Ga. However, their enigmatic nature and lack of conclusive evidence for a mantle origin has excluded them from being used to make interpretations about carbon in the Archean mantle.

During the first multi-sample X-ray CT study on carbonado, we identified two varieties of carbonado based on inclusion material. Acid-leaching and solution ICP-MS on the first variety, which contains a mineral suite reflecting crustal P-T conditions filling > 99% of pores, revealed REE enrichments (avg. ΣREE = 2.3 wt. %) and patterns similar to carbonatites, kimberlites, and high-density fluids in fibrous diamonds. The second variety is characterized by isolated phases sparsely distributed throughout the pore network, including abundant rutile. LA-ICP-MS trace element analysis revealed high chromium concentrations, 2.01 to 4.10 wt. % (avg. 2.93 wt. %) which, combined with Zr-in-rutile temperatures > 800°C, are unequivocal evidence for rutile formation in an ultramafic environment and, by association, a mantle origin for carbonado. Furthermore, U-Pb ages of 3.2 Ga ± 300 Ma fall within the accepted age range of carbonado (2.6 to 3.8 Ga), but provide further constrained values.

These data confirm carbonado's mantle origin and require a mechanism for introducing isotopically light carbon into the diamond stability window by 3.2 Ga. Since typical isotopic fractionation usually only leads to a change of a few per mil, then either primordial heterogeneities or recycling of organic carbon by 3.2 Ga are the most likely sources of carbonado's carbon.

Keywords: Diamond, Mantle, Rutile, Inclusion

SETP
ECG

Thermal-Tectonic Evolution of a South Cycladic Metamorphic Core Complex, Ios and Sikinos Islands, Greece

Megan Flansburg
Flansburg, M., Department of Geological Sciences, The University of Texas at Austin, Austin, TX
Poulaki, E., Department of Geological Sciences, The University of Texas at Austin, Austin, TX
Stockli, D., Department of Geological Sciences, The University of Texas at Austin, Austin, TX
Soukis, K., Department of Geology and Geoenvironment, National and Kapodistrian University of Athens, Athens, Greece

The Cycladic archipelago in the Aegean Sea exposes the subducted and metamorphosed equivalents of allochthonous terranes sequentially accreted to the southern margin of Eurasia during the Paleogene. Subsequent large-magnitude extension in the backarc of the retreating Hellenic subduction zone resulted in the formation of Oligo-Miocene metamorphic core complexes (MCCs) and the exhumation of the HP-LT Cycladic Blueschist Unit (CBU) and Cycladic Basement (CB). In the southern Cyclades, the contact between the CBU and the CB on Ios and Sikinos islands has been interpreted as a top-to-the-N low-angle normal fault associated with Miocene MCC-formation. Associated mylonitic fabrics in the CB have subsequently been attributed to Miocene extensional shear. Contrastingly, the contact has also been interpreted as a S-directed subduction-related thrust fault later reactivated by Miocene detachment faulting.

Considering limited published thermochronometric data that constrain the Miocene MCC-formation, the formation of mylonitic fabrics is believed to be related to Miocene crustal thinning. We present new apatite U-Pb ages ($T_C \approx 450°C$), constraining the timing of HT mylonitization in the crystalline CB, and zircon (ZHe, $T_C \approx 180°C$) and apatite (AHe, $T_C \approx 50°C$) (U-Th)/He ages elucidating the exhumation of the CB and CBU in the footwall of the Ios-Sikinos MCC. Surprisingly, apatite U-Pb analyses for the crystalline CB on Ios and Sikinos yielded ages ~295-275 Ma, strongly suggesting a Permian rather than Paleocene subduction-related or Miocene exhumation-related initial mylonitization and that temperatures did not exceed 450-550°C after the Paleozoic. These ages imply that at least part of the pure-shear mylonitic fabrics are unrelated to Miocene MCC-formation but are related to significant early to mid-Permian crustal extension immediately following plutonic emplacement of the crystalline CB (~330-305 Ma). Quartz microstructures within mylonitic crystalline CB are dominated by grain boundary migration and feldspar microstructures are dominated by cataclasis and bulging, corroborating initial fabric formation at T>450°C. In contrast, ZHe ages (~14-10 Ma) and AHe ages (~13-8 Ma) record the rapid Miocene exhumation of the CB and the CBU through the middle and upper crust and the formation of the Ios-Sikinos MCC. ZHe and AHe ages do not exhibit any differential cooling across the CB/CBU contact, suggesting that the two units were exhumed as one coherent unit in the footwall of a top-to-the-N low-angle normal fault with timing and kinematics similar to neighboring Naxos and Paros islands. ZHe and AHe ages from the southern part of Ios island may also weakly suggest a bivergent detachment, with top-to-the-S movement similar to neighboring Thira (Santorini). These results illustrate that the combination of high- and low-T thermochronometry can differentiate and attribute tectonic fabrics that have previously been attributed to a single event and suggests the potential for applying these methods to other MCC belts around the globe.

Keywords: detachment faulting, mylonitization, metamorphic core complex, Cyclades, Aegean Sea, Hellenic Subduction Zone, apatite U-Pb thermochronometry, low-temperature thermochronometry

SETP
ECG

Evolution of deformation in the Buck Mountain Fault damage zone, Cambrian Flathead Sandstone, Teton Range, WY

Stephanie Forstner
Forstner, S., Bureau of Economic Geology, The University of Texas at Austin, Austin, TX
Laubach, S., Bureau of Economic Geology, The University of Texas at Austin, Austin, TX
Fall, A., Bureau of Economic Geology, The University of Texas at Austin, Austin, TX

The Teton Range is a normal fault block that contains older reverse faults. Although generally considered to be Late Cretaceous to early Tertiary structures, the timing, kinematic style, and history of faulting remains conjectural. The Buck Mountain Reverse Fault (BMRF) is rooted in Precambrian crystalline rocks and dips steeply to the east about 60°. The fractured Cambrian Flathead sandstone, an orthoquartzite (90%+ quartz), is an ideal horizon to study spatial patterns of brittle deformation. The unit rests nonconformably on the Precambrian basement, is relatively homogeneous in composition, and outcrops drape across various types of structures.

Oriented Flathead hand samples have been collected from the footwall of the BMRF along a partially overturned syncline. Continuous SEM-Cathodoluminescence (SEM-CL) scanlines of these samples allow for a systematic kinematic analysis of the cemented opening-mode fractures. Attributes such as fracture geometry, spacing, and orientation can be quantified. In isotropic rock, mode-I fractures primarily propagate along the plane perpendicular to S_{hmin}. Therefore, microfractures can be used to indicate paleostress trajectories, strain, and relative fracture timing. Since fracture cements appear synkinematic, we've determined the temperatures and fluid compositions present during fracturing by conducting a high-resolution fluid inclusion assemblage (FIA) petrographic and microthermometric analysis. Our kinematic and geochemical analysis of diagenetic damage zone features provides spatial and temporal constraints on the conditions present during fracture development, the evolution of the local tectonics, and paleohydrology.

Steeply dipping fractures strike NE, NW, and WNW. Fractures have opening displacements ranging from ~0.5 μm to 3 mm. In general, opening-mode fracture strain increases towards the fault and is highest near the fold axis. SEM-CL images of diagenetic cements reveal alternating light and dark luminescing textures; overgrowths are syntaxial and zoned whereas fractures contain wall-parallel crack-seal and wall-perpendicular fibrous textures, an indication of synkinematic cementation. Fracture cements luminesce different colors under Color-SEM-CL, suggesting variation in fluid source and composition. Quartz overgrowths are crosscut by fractures and, therefore, formed early. The relative evolution of each brittle deformation period is supported by cross-cutting relationships and FIAs which reveal; NE fractures formed first, followed by NW fractures, and lastly WNW fractures.

The fluids present during overgrowth and fracture cementation are preserved in primary two-phase aqueous FIAs. Initial ice melting temperatures suggest cements precipitated from a H_2O-NaCl-$CaCl_2$-(±$MgCl_2$)-type fluid; however, only T_{mICE} was observed. Therefore, we calculated salinity (expressed as wt% NaCl equivalent) assuming a H_2O-NaCl fluid model. Within petrographic context, minimum trapping temperatures (T_h) and salinity provide temporal geochemical trends of deformation. Quartz overgrowths; T_h: 135-209°C and salinity: 4 to 7.5 wt.%. NE fractures; T_h: 110-191°C and salinity: 4.8-5.1 wt.%. NW fractures; T_h: 136-160°C and salinity: 11.7-13.5 wt.%. WNW-fractures; T_h: 140-170°C and salinity: 2.0-6.9 wt.%. On average, T_h ranges by 16.5°C within a single FIA.

Diagenetic cements precipitated from a wide range of fluid conditions. However, we have begun to temporally constrain fracture kinematics and fluid conditions present during diagenesis. Temperatures in quartz overgrowths show a heating trend which is compatible with progressive burial to maximum burial conditions. Cross-cutting relations and temperatures in fractures show a general cooling trend and suggest brittle deformation occurred after maximum burial, probably during uplift. Assuming fractures formed during tectonic shortening, orientations and cross-cutting relations suggest S_{Hmax} rotated from NE to NW and finally to WNW.

Keywords: Microfracture, fluid inclusion assemblages, sandstone, SEM-CL, diagnesis

SETP
ECG

Crustal structure of the northern Hikurangi margin from marine seismic reflection imaging and onshore-offshore seismic tomography: implications for megathrust heterogeneity and overpressure in a region of shallow slow earthquakes

Andrew Gase
Gase, A., Department of Geosciences, University of Texas at Austin, Austin, TX
Van Avendonk, H., University of Texas Institute for Geophysics, University of Texas at Austin, Austin, TX
Bangs, N., University of Texas Institute for Geophysics, University of Texas at Austin, Austin, TX
Arnulf, A., University of Texas Institute for Geophysics, University of Texas at Austin, Austin, TX
Okaya, D., University of Southern California, Los Angeles, CA
Henrys, S., GNS Science, Lower Hutt, New Zealand
Barker, D., GNS Science, Lower Hutt, New Zealand
Jacobs, K., GNS Science, Lower Hutt, New Zealand
Kodaira, S., Japan Agency for Marine-Earth Science and Technology (JAMSTEC), Yokohama, Japan
Fujie, G., Japan Agency for Marine-Earth Science and Technology (JAMSTEC), Yokohama, Japan

The northern Hikurangi margin is the site of recurring shallow slow slip events and historic tsunami earthquakes. We present results of a trench perpendicular multichannel seismic and onshore-offshore wide-angle seismic transect in northern Hikurangi margin, acquired during the Seismogenesis at Hikurangi Integrated Research Experiment (SHIRE). We invert wide-angle P-wave (Vp) traveltime arrivals recorded on 18 ocean-bottom seismometers and 13 IRIS/PASSCAL seismometers to estimate VP structure to depths up to ~25 km. A zone of elevated Vp below a major out-of-sequence thrust at Tuaheni Ridge is interpreted as a subducted seamount. Ocean-bottom and onshore receivers down-dip of the subducted seamount show low Vp in the prism (~2-3.5 km/s) and a shadow zone. The shadow zone (i.e. velocity inversion) coincides with the landward appearance of a reflective zone near the subduction interface. Wide-angle reflections after the shadow zone are attributed to the subduction interface, subducted basement, and the subducted Moho. The shadow zone may result from elevated pore pressures in the lower prism and/or deep under-consolidated, basally accreted sediments down-dip of a subducting seamount. These features coincide with the source regions of shallow slow-slip events and tectonic tremor, implying that megathrust heterogeneity and elevated pore pressures promote slow earthquake nucleation.

Keywords: Subduction zone structure, slow earthquakes, marine seismic imaging

SETP
ECG

Evolving Dynamic Pressures in Pyroclastic Density Currents: Evidence from the 18 May 1980 Blast Surge of Mount St. Helens

Nicole Guinn
Guinn, N., Jackson School of Geoscience, The University of Texas at Austin, Austin, TX
Gardner, J., Jackson School of Geoscience, The University of Texas at Austin, Austin, TX

On 18 May 1980, Mount St. Helens erupted a lateral, topography influenced pyroclastic density current (PDC) to the north, which decimated ~600km^2 of conifer forest. Most trees were uprooted or broken and stripped of vegetation, leaving only the tree trunks lying on the ground. In this blowdown zone, there are 51 patches of standing trees, some of which vegetation remains, situated on the lee sides of hills near the end of the PDC runout. As a PDC travels over a ridge, it entrains and heats air leading to expansion within the current. This expansion is directed downward in the proximal part of the current due to its relatively high velocity and density, toppling every tree. In the distal part of the current, the PDC density and/or velocity has decreased and allowed for temporary liftoff at the crests of hills, creating patches of standing trees on the lee sides. The purpose of this study is to use uprooted verses standing trees to characterize the changes of dynamic pressure of the Mount St. Helens PDC. Dynamic pressure is a function of the density and velocity of the PDC, and is typically highest at the front of the current. The maximum dynamic pressure can be used to distinguish the most destructive path of the PDC. Analysis of aerial photography taken 1 month after the eruption and a 30-meter Data Elevation Model (DEM) was used to determine the heights and number of trees. The trees are treated as cylinders because they were stripped of all limbs and foliage. The heights of trees in the patches will determine the projectile heights of a localized maximum dynamic pressure as the PDC was temporarily lifted. Trees with foliage in the patches will demonstrate where the maximum dynamic pressure within the PDC was lifted above the patch, instead of shearing off the tops of the trees. The lengths of isolated downed and heights of standing trees outside of the patches will be used to constrain a lower limit of approximate dynamic pressure which will be contoured in ArcMap to indicate how dynamic pressure varied for the PDC near its runout. Understanding the deadly phenomenon of the Mount St. Helen's PDC will impact volcanic hazard mapping.

Keywords: dynamic pressure, pyroclastic density current, Mount St. Helens, liftoff, patch, trees, ArcMap, runout

SETP
ECG

The Gulf Coast stratigraphic response to Pleistocene-Holocene climate change.

Evelin Gutiérrez
Gutierrez, G., Department of Geological Sciences, Jackson School Geosciences, University of Texas at Austin, Austin, Texas 78712, USA
Covault, J., Bureau of Economic Geology, University of Texas at Austin, Austin, Texas 78713, USA
Stockli, D., Department of Geological Sciences, Jackson School of Geosciences, University of Texas at Austin, Austin, Texas 78712, USA

Climate change related to the latest Pleistocene-Holocene glacial-interglacial transition can influence eustasy and rainfall erosivity patterns, with consequences for sediment transport and deposition. In particular, variability in sediment transport as a result of transient storage and release of sediment can modify signals of climate change in a sediment-routing system. Pleistocene-Holocene of the Gulf of Mexico is characterized by high-frequency climate changes and coupled eustatic shifts without the interference of long-term hinterland tectonic variations, offering the opportunity to investigate the time-transgressive stratigraphic record as a function of coupled eustasy and varying precipitation.

Pleistocene-Holocene glaciation may have played a role in varying climate and sedimentation that can potentially be distinguished in the sedimentary record in the Gulf of Mexico. Sedimentation patterns in the Gulf of Mexico were very different during the latest Pleistocene glaciation compared to the present day. During the latest Pleistocene, ~20 ka, glaciers stored water on the continent and, as a result, global sea level was lower. As glaciers melted, sea level rose and the shoreline transgressed. This change is sea level relocated space for sediment deposition from the deep sea to the submerged continental shelf. There is an additional wrinkle to this general model of the Gulf of Mexico and other continental margins that have glaciated upstream fluvial reaches; as glaciers melt due to climate change, significantly increased discharge of water and sediment can deliver enormous volumes of terrigenous sediment to the coast and offshore. We hypothesize that glacial-eustatic changes influenced sedimentation patterns in the Gulf of Mexico, especially the location and three-dimensional architecture of depocenters. Target areas in this study include rivers of Central Texas like the Brazos and Trinity, representing catchment areas with no glaciers in their upstream reaches. Initial results will be compared to existing information of the Mississippi River, representing a changing watershed with the presence of glaciers in their upstream reaches and the Rio Grande River deposits, representing a drainage basin with varying precipitation, where glaciers may or may not be present in the upper areas of the watershed. Our initial approach to characterize depositional systems across the shoreline and shelf margin of the Gulf of Mexico consists of detailed mapping of deposits formed during glacial and interglacial times using seismic reflection datasets, and sampling key rock formations for age control and proxies of environmental change, namely drainage reorganization and climate.

Keywords: GOM, climate change, stratigraphic architecture

SETP
ECG

Perfectly matched layer boundary conditions for frequency-domain acoustic wave simulation in the mesh-free discretization

Xin Liu
Liu, X., University of Texas Institute for Geophysics, The University of Texas at Austin, Austin, TX
Sen, M., University of Texas Institute for Geophysics, The University of Texas at Austin, Austin, TX
Liu, Y., State Key Laboratory of Petroleum Resources and Prospecting, China University of Petroleum, Beijing, China.

Mesh-free discretization, flexibly distributing nodes without computationally expensive meshing process, is able to deal with staircase problem, oversampling and undersampling problems and saves plenty of nodes thorough distributing nodes suitably with respect to irregular boundaries and model parameters. However, the time-domain mesh-free discretization usually exhibits poorer stability than the in regular grids discretization. In order to reach unconditional stability and easy implementation in parallel computing, we develop the frequency-domain finite-difference method in a mesh-free discretization, incorporated with two perfectly matched layer boundary conditions. Furthermore, to maintain the flexibility of mesh-free discretization, the nodes are still irregularly distributed in the absorbing zone, which complicates the situation of artificial boundary reflections. In this paper, we implement frequency-domain acoustic wave modeling in a mesh-free system. First, we present the perfectly matched layer boundary condition to suppress spurious reflections. Moreover, we develop the complex-frequency shifted-perfectly matched layer boundary condition to improve the attenuation of grazing waves. In addition, we employ the radial-basis-function-generated finite difference method in the mesh-free discretization to calculate spatial derivatives. The numerical experiment on a rectangle homogeneous model shows the effectiveness of the perfectly matched layer boundary condition and the complex-frequency shifted-perfectly matched layer boundary condition, and the latter one is better than the former one when absorbing large angle incident waves. The experiment on the Marmousi model suggests that the complex-frequency shifted-perfectly matched layer boundary condition works well for the complicated model.

Keywords: Mesh free, Frequency domain, acoustic wave modeling, absorbing boundary condition.

SETP
ECG

Processes of Change in Magma Storage Conditions Beneath Valles Caldera

Nicholas Meszaros
Meszaros, N., Jackson School of Geosciences, The University of Texas at Austin, Austin, TX

The catastrophic volcanic eruption that formed Valles Caldera marks a departure from relatively minor volcanism that persisted for the previous 360 ka. During this cataclysmic eruption the voluminous Tshirege Member of the Bandelier Tuff was deposited with a mineral assemblage of quartz + sanidine + orthopyroxene + clinopyroxene + fayalite (referred to here as T-type), which contrasts with the quartz + sanidine +/- biotite +/- hornblende mineral assemblage of pre and post-caldera lavas and tephras (referred to here as CT-type). These shifts in mineralogy suggest that magma storage conditions must have changed significantly prior to the caldera-forming eruption, and potentially returned to pre-caldera conditions afterwards. Furthermore, the nearly identical ages of the oldest pre-caldera lava dome (1.26 +/- 0.1 Ma) and the Tshirege Tuff (1.25 +/- 0.1 Ma) imply that the initial change in storage conditions must have occurred over a relatively short timescale. This project aims to constrain the change in the Valles magmatic system that occurred prior to catastrophic volcanism, the process driving such change, and whether post-caldera mineralogy signifies that the system returned to pre-caldera storage conditions. These objectives will be met by characterizing the similarities and differences of storage conditions between CT and T-type magmas, as well as between pre and post-caldera CT-type magmas. In particular, changes in storage conditions such as temperature, pressure, oxygen fugacity, and fluid saturation state or composition may be responsible for the observed shifts in mineral assemblage; however, temporal changes in magma composition may also influence mineralogy. These potential variations in storage conditions or magma composition may be driven by changes in magma sources, mixing, degassing, or fractional crystallization. Presented here are data that characterize the mineralogy and composition of CT and T-type magmas, as well as offer a first glance into how the Valles magmatic system varied temporally in terms of water content and magma sources. Additional planned work includes constraining crystallization temperature, pressure, and fluid saturation conditions through experiments on both CT and T-type magma compositions, as well as measurement of $Ce^{4+}/Ce^{3+}$and U/Pr in zircon grains from field samples to gain insight into the temporal variation and cause of change in oxygen fugacity. Isotopic characterization of CT and T-type magmas in terms of ????^{7}Li, ????^{18}O, $^{87}Sr/^{86}Sr$, and ????^{56}Fe will serve as evidence to characterize how processes such as degassing, magma mixing, and fractional crystallization changed over both short and long timescales. Additional data pertaining to the timescale of the initial shift from CT to T-type mineralogy will be obtained by examination of Mg zonation in pyroxenes,thus enabling determination of magma residence times through Mg-Fe diffusion modelling. Collectively these data will characterize temporal evolutionary trends and identify processes of change in the Valles magmatic system on both short and long timescales. Knowing this information is critical in understanding how and if volcanic activity could resume in the Valles magmatic system in the future.

Keywords: Caldera magmatism, eruption processes, New Mexico

SETP
ECG

Tectonic evolution of the Cycladic Blueschist Unit and Cycladic Basement with multiple geo-thermo chronometers, Sikinos and Ios Greece

Eirini Poulaki
Poulaki, E., The University of Texas at Austin, Austin, TX
Flansburg, M., The University of Texas at Austin, Austin, TX
Stockli, D., The University of Texas at Austin, Austin, TX
Soukis, K., National and Kapodistrian University of Athens

The Cycladic islands of Greece expose an assemblage of HP/LT metamorphic rocks that record processes related to both Paleogene subduction along the Hellenic Trench and Neogene backarc extension and metamorphic core complex formation. Sikinos and Ios islands are located in the southern Cyclades and contain the Cycladic Blueschist Unit (CBU), consisting of metapelite, metabasite and marble and the tectonically underlying Cycladic Basement (CB) composed of Late Paleozoic felsic plutonic rocks and Early Paleozoic metasedimentary country rock. The contact between the two units has previously been described as an extensional shear zone, as a subduction-related thrust fault that was reactivated as an extensional top-to-the-N detachment, or as a depositional contact prior to subduction. This study presents geo and thermo-chronometers to elucidate the tectonic evolution of the CBU and CB and the role of the contact between the two units during backarc extension. (1) Zircon and apatite depth profile U-Pb and trace elements LA-ICP-MS analyses were used to understand timing and tectonic processes of subduction related deformation, metamorphism and metasomatism. (2) Zircon and apatite (U-Th)/He provide insight into the cooling and exhumation history of the CBU and CB, and the role of the contact between the two units during Cenozoic backarc extension. The depth-profile LA-ICP-MS analyses reveal two distinct generations of metamorphic zircon rims with ages of 50 and 26 Ma. In addition to previously published provenance similarities, metamorphic zircon rims at 50 Ma in the CBU and apatite U-Pb rim ages at 50 Ma in the CB support the scenario in which the two units either juxtaposed during or were in a depositional contact prior to subduction. Samples with 26 Ma metamorphic zircon rims occur in both CBU-CB restricted to a zone along the contact, and likely related to garnet break down during Oligocene metasomatism, possibly related to the High-Temperature metamorphism in the Cyclades. Zircon (U-Th)/He ages from CB and CBU are statistically indistinguishable (9 to 12 Ma) and record rapid exhumation in response to top-to-the-N detachment faulting. Apatite (U-Th)/He ages from the CB (9 to 4 Ma) record the final tectonic exhumation along NE-SW striking high angle normal faults linked to Anatolian extrusion.

Keywords: Geochronology, Thermochronology, Metamorphic core complexes, Subduction zone, Sikinos, Ios, Greece,

SETP
ECG

Benchmarks and resolution analysis for visco-elastic subduction zone models

Simone Puel
Puel, S., Department of Geological Sciences, Jackson School of Geosciences, The University of Texas at Austin
Becker, T., Department of Geological Sciences, Jackson School of Geosciences, The University of Texas at Austin; Institute for Geophysics, Jackson School of Geosciences, The University of Texas at Austin

Subduction zones represent an important piece of the well established plate tectonic theory. Although there are many models which describe the processes occurring in this complex system, many uncertainties still remain, for instance in the explanation of postseismic deformation. It is still unclear which between afterslip, visco-elastic relaxation and poro-elastic rebound is the dominant mechanism, what the interactions between them are, and how their evolution in time affects surface displacements and stresses. In order to better constrain these three processes, we build visco-elastic models of the earthquake cycle using PyLith, an open-source finite element software for crustal deformation. Here, we present some benchmarks of a simple model in PyLith exploring variable resolutions in order to better fit the analytical surface displacement and decrease the error between the numerical and the exact solutions. In particular, we compare these two solutions both for an elastic isotropic homogeneous half-space (Okada, 1985 and 1992), which simulates the rheology of the crust, and for a visco elastic homogeneous and isotropic half-space (Matsu'ura and Tanimoto, 1980; Piombo et al., 2007), which mimics the rheology of the mantle. We explore numerical resolution, accuracy, robustness and efficiency and highlights how different contributions of the mechanical processes are detectable at the surface with application to the Tohoku-oki 2011 M9 event.

Keywords: deformation, dislocation, rheology, elasticity, visco-elasticity

SETP
ECG

Thermal evolution of a distal hyperextended margin – A case study of Zabargad Island, Red Sea

Samantha Robbins
Robbins, S., Dept. of Geological Sciences, Jackson School of Geosciences, University of Texas at Austin
Stockli, D., Dept. of Geological Sciences, Jackson School of Geosciences, University of Texas at Austin

Dramatic advances in our understanding in how to break-up continents in the absence of a hot spot or abundant magmatism have taken place over the past decades. Geophysical data have elucidated the structural and stratigraphic evolution of these magma-poor hyperextended continental rifted margins. These magma-poor margins share overall geometric and evolutionary similarities, which have been used to define general architectural characteristics for these types of margins. The broad architectural zones commonly interpreted in magma-poor rift margins, through geophysical data and geological observations, are the proximal margin, preserving normal faulting associated with diffuse initial extension and stretching, a necking domain, a highly attenuated or hyperextended distal margin, and an exhumed mantle. However, beyond fossil continental margins caught up in orogenic systems, such as in the Alps, only few exposed examples of hyperextended distal margins exist in rift systems in the world. One of these examples is Zabargad Island, Egypt, in the central Red Sea – a section of the distal rifted margin uplifted and subaerially exposed along an oceanic fracture zone. Zabargad Island exposes a hyperextended slice of lower continental crusts, sandwiched between exhumed subcontinental mantle peridodite and syn- and post-rift sedimentary strata. The subcontinental mantle consists of three bodies of peridotite and a highly deformed lower crustal basement complex consisting of granulites, gneisses interlayed with amphibolites, gabbros, and pyroxenites. Studies in the past have focused on the tectonothermal and geochemical history of the island, but the timing and magnitude of exhumation during hyperextension within the context of the Red Sea distal rift margin is still poorly understood. This study employs multiple U-Pb and (U-Th)/He thermochronometric techniques to investigate the thermal and tectonic evolution of the lower crust during hyperextension and lithospheric break-up. In particular, we are looking to determine whether the lower crust experienced any reheating in response to juxtaposition with the mantle during exhumation and the structural kinematics of the lower crust during rifting. Preliminary data show that the basement material is a fragment of the Nubian Shield with zircon U-Pb ages ranging from 559 +/- 12 Ma to 588 +/- 14 Ma. The granulites/peridotites also appear to have been cross-cut by 8.1 +/- 0.2 Ma felsic dikes that likely formed during rifting. Apatite (~450°C) and rutile (550°C) U-Pb thermochronometry will be applied to constrain the thermal evolution in the lower crust during rifting. Finally, (U-Th)/He low-temperature thermochronometry will constrain the thermal evolution during final exhumation. Overall, this project aims to reconstruct the continuous time-temperature history of the distal magma-poor Red Sea hyperextended margin exposed on Zabargad Island, which will allow for a better understanding of the structural, thermal, and hydrothermal processes operating during continental break-up. These new results will also provide new constraints for the timing of extreme crustal thinning during Red Sea rifting and help better understand the mechanisms of lower crustal/mantle exhumation during hyperextension.

Keywords: geochronology, thermochronology, rifting, extension tectonics

SETP
ECG

Structural inheritance from metamorphic basements in inverted basins of southeast Mexico

Daniel Ruiz Arriaga
Ruiz, D., Jackson School of Geosciences, The University of Texas at Austin
Stockli, D., Jackson School of Geosciences, The University of Texas at Austin
Fitz-Díaz, E., Instituto de Geología, Universidad Nacional Autónoma de México

The tectonic history of Mexico has been influenced by several major events that have been recorded in the country's physiographic features and rock assortment. In the southern and eastern portion of Mexico, the exposure of Paleozoic and Precambrian basement rocks and the deformed sedimentary cover have been interpreted as a sequence of tectonic events that include the opening of the Gulf of Mexico and the formation of the Mexican Fold and Thrust Belt. Such events have dictated the formation and later exposure of the metamorphic basements of Mexico, and are also responsible for the formation and inversion of basins. This study focuses on the metamorphic rocks of the Acatlán Complex, the Huiznopala Gneiss and their Jurassic sedimentary covers, which show a close spatial dependency with the basement's history of exhumation.
This work will emphasize in the reconstruction of the post-Paleozoic basement exhumation history and the thermal history of the Jurassic basins, in the western portion of the Acatlán Complex and in the Huiznopala Gneiss, through the use of low temperature thermochronology and geochronology dating. The expected results will give insight into the structural-sedimentary relationship between basins and ancient major structures, by documenting the rock source of such basins. Additionally, these new data will allow the constraining of the basement's exposure evolution since the Jurassic; which has not been documented in southeast Mexico. The approach for deciphering the thermal history of the rocks is planned along transects that have basement exposure, and it consist of: 1) registration of major structures with multi-scale observations; 2) (U-Th)/He dating of zircon and apatite bearing blocks displaced by faults, and apatite fission track dating of basement rocks; 3) U-Pb and (U-Th)/He (double dating) provenance studies of the basin's zircon grains; 4) comparison of the structural inheritance between the basements, and later results comparison with an external similar structural scenario.
The development and findings from this project will provide time contains and insights in the crustal scale burial-uplift history of southern and eastern Mexico. Such results will allow a more accurate perception of fault generated basin formation and fault reactivation during major tectonic processes. And the understanding of such processes will lead to a better comprehension of sediment sources and basin formation, which will improve the planning of oil and gas reservoir prospecting in deformed tectonic environments.

Keywords: Acatlán, Huiznopala, Basin inversion, Provenance, Structural inheritance

SETP
ECG

NEW CONSTRAINTS ON THE GEOMETRY, KINEMATICS, AND TIMING OF DEFORMATION ALONG THE SOUTHERN SEGMENT OF THE PAPOSO FAULT ZONE, ATACAMA FAULT SYSTEM, NORTHERN CHILE

Rachel Ruthven
Ruthven, R., The University of Texas at Austin, Austin, TX
Singleton, J., Colorado State University, Fort Collins, CO
Seymour, N., Colorado State University, Fort Collins, CO
Magloughlin, J., Colorado State University, Fort Collins, CO
Gomila, R., Pontificia Universidad Católica de Chile, Santiago, Chile
Arancibia, G., Pontificia Universidad Católica de Chile, Santiago, Chile
Stockli, D., The University of Texas at Austin, Austin, TX

The Paposo fault zone is a major brittle-ductile strand of the Atacama Fault System (AFS), which records sinistral shear associated with Mesozoic oblique subduction beneath northern Chile. The southern portion of the Paposo fault juxtaposes mylonitized granites against Jurassic volcanic and sedimentary rocks. Geologic mapping along a 1.25 km-long transect across the ductile root of the Paposo fault documents a strain progression towards the core of the fault. Moving from E to W, Early Cretaceous and Late Jurassic granites grade from unstrained to a 350 m-thick zone containing discrete mylonitic bands. This zone of variably strained granite transitions to a 650-1100 m-thick pervasive high strain zone which contains a 200-550 m-thick band of hydrothermally-altered ultramylonite and locally mylonitized cataclasite, indicating that fluids played an important role in brittle-ductile deformation. This mylonitized cataclasite contains oblate clasts and S>L tectonite fabrics, suggesting transpressional flattening. Across the transect, mylonitic foliations and lineations have a mean orientation of 043/62 SE and 18/211, respectively. Most SE-dipping mylonitic fabrics record sinistral-reverse shear, but in several areas, symmetric microstructures suggest a component of pure shear. Near the core of the fault, a 250 m-thick protomylonite zone is overprinted by a 50 m-thick illite-rich, subvertical gouge zone that strikes 018 and records sinistral S-C fabrics.

The upper age limit of deformation is constrained by zircon U-Pb ages on the mylonitized granites (138.8 ± 1.6 Ma and 151.1 ± 1.8 Ma) and a mylonitized aplite dike with ages ranging from ~137-148 Ma. A zircon (U-Th)/He cooling age of 116.6 ± 5.4 Ma from the ~151 Ma granite provides a lower age limit for mylonitic deformation. Together these data constrain deformation to the Early Cretaceous, similar to the age of deformation along other segments of the AFS. Regionally, the Paposo fault is arcuate, trending NNW-SSE in the north and NNE-SSW in the south. Previous studies have observed sinistral transtension in the north, whereas we observe sinistral transpression in the south. We propose that transtension and transpression along the AFS are controlled by the arcuate geometry, and both are compatible with sinistral simple shear along the N-S-trending magmatic arc.

Keywords: Paposo, Intra-arc, Strike-slip fault, fault, Chile, Kinematics, Deformation, Atacama

SETP
ECG

Automatic Detection of InSAR Deformation Signals Associated with Wastewater Injection and Induced Seismic Events

Scott Staniewicz
Staniewicz, S., The University of Texas at Austin, Austin, TX
Chen, J., The University of Texas at Austin, Austin, TX
Rathje, E., The University of Texas at Austin, Austin, TX
Olson, J., The University of Texas at Austin, Austin, TX
Lemons, C., Bureau of Economic Geology, The University of Texas at Austin, Austin, TX
Hesse, M., The University of Texas at Austin, Austin, TX

Since 2008, the rate of seismic events within the Central United States has dramatically increased, which is likely associated with wastewater injection from nearby oil and gas operations. Surface deformation measurements derived from spaceborne interferometric synthetic aperture radar (InSAR) data can be used to quantify the magnitude and spatial extent of the injection-related stress perturbation, which are critical for understanding the complex interaction between the injected fluid and the earth's subsurface.
In this study, we processed Sentinel-1 InSAR data over Central and West Texas using a recently developed processing framework that performs topography/geometry phase corrections prior to the interferogram formation (Zebker 2017). We streamlined the creation of upsampled digital elevation maps (DEMs) from NASA Shuttle Radar Topographic Mission (SRTM) data, as well as the collection of Sentinel-1 precise orbit data. We developed a tool for InSAR time-series analysis and data visualization.
To detect unknown deformation signatures from large volumes of InSAR data, we employed computer vision ideas for feature detection independent of scale, well known through their success in the Scale Invariant Feature Transform (SIFT). We used multi-scale Laplacian-of-Gaussian (LoG) filters to find local maxima and minima in a coarse deformation solution, corresponding to "bowls" of uplift and subsidence, respectively. This allowed us to drastically cut down processing time of high-resolution InSAR products. As a validation, our method successfully detected all sinkhole locations, injection-related uplift signals and production-related subsidence signals as reported in Kim and Lu (2017) over a 100 km x 100km search area without the need for manual inspection. We begin to quantify the uncertainty from common noise sources to produce more confident time-series results.

Keywords: InSAR, Remote Sensing, Induced Seismicity, Computer Vision

SHP
ECG

Understanding the Hydraulic Behavior of the Güzelyurt Alluvial Coastal Aquifer via Numerical Modeling Approach

Cansu Demir
Demir, C., Jackson School of Geosciences, The University of Texas at Austin, Austin, TX
Akintug, B., Civil Engineering Department, Middle East Technical University North Cyprus Campus, Kalkanl?, Güzelyurt, Mersin 10, Turkey
Unlu, K., Environmental Engineering Department, Middle East Technical University, Ankara, Turkey

Güzelyurt, a coastal and unconfined aquifer, is the most important, and at the same time, the largest drinking, municipal, and irrigational water resource of the Turkish Republic of Northern Cyprus (TRNC). Yet, the aquifer has exceeded its safe yield capacity due to excessive and uncontrolled pumping over the years, and the water quality has been seriously deteriorated due to seawater intrusion. With the implementation of "TRNC Water Supply Project" in June 2016 by Turkish Government, annually about 75 MCM of water was started to be transferred from Turkey to TRNC, by a submerged pipeline system in the Mediterranean Sea, to solve the water shortage problem of Northern Cyprus. About 38 MCM/year of the total water transferred has been allocated to domestic water demand. The remaining 37 MCM/year planned to be used for irrigation can potentially be utilized to artificially recharge the aquifer, and in turn, the deteriorated water budget of the aquifer can be reestablished in the mid- and long-term. The objective of this study is to predict the hydraulic behavior of the aquifer under predefined stress and recharge scenarios regarding water usage. For this purpose, the 3-D detailed conceptual and numerical simulation models of Güzelyurt Aquifer have been developed using system modeling approach integrated with today's modern technologies of Geographical Information Systems (GIS) and numerical simulation techniques. The available geologic, hydrologic and hydrogeological data provided by Geology and Mining Department (G&MD) of TRNC, and collected from previously published field reports were used in the model development process. The developed numerical model was first calibrated under steady-state and transient conditions. Then, the calibrated model was run for simulations of three different scenarios involving rehabilitation of the deteriorated water balance of the aquifer. In the initial scenario, the aquifer was simulated by excluding the pumping for irrigation. In the last two scenarios, in addition to the conditions of the first one, 28 MCM/year of the water coming from the project was artificially fed to the aquifer via the Güzelyurt Dam and/or the injection wells. In all three scenario simulations, the depression zone has been observed to be disappeared, and the "zero" head contour has approximated to the coast after an average of 12 years. Moreover, it has been found that at least 76% of the water allocated for irrigation should be used for artificial recharge in order to obtain an effective aquifer recovery. However, the model has shown that although more than half of the water transferred for irrigation was used for this purpose, the aquifer could not return to its natural conditions in the near simulated future. The earliest natural state was achieved in 48 years by the artificial water recharge through the combination of injection wells and the dam. Thus, this option was found to be the most effective method.

Keywords: Numerical model, Aquifer, Groundwater modeling, Güzelyurt, Coastal

SHP
ECG

Evaluating the anthropogenic heat and global warming impacts on extreme precipitation in Pearl River Delta megacity based on dynamical downscaling

Kwun Yip Fung
Fung, K., Department of Geological Sciences, Jackson School of Geosciences, The University of Texas at Austin, Austin, TX
Tam, C., Earth System Science Programme, The Chinese University of Hong Kong, Hong Kong
Wang, Z., School of Atmospheric Sciences, Sun Yat-sen University, China
Yang, Z., Department of Geological Sciences, Jackson School of Geosciences, The University of Texas at Austin, Austin, TX

In recent decades, a substantial increase (~5-10%) of extreme rainfall intensity was observed over the Southeastern China. It is plausible that both global warming and rapid urbanization in Pearl River Delta (PRD) in southern China are contributing to the increment. In this poster, global warming and anthropogenic heat impacts on non-tropical cyclone induced extreme rainfall were evaluated. The extreme rainfall cases were identified in GFDL-ESM2M present and RCP8.5 climate scenarios and dynamically downscaled by Weather Research and Forecasting (WRF) model coupled with a single-layer urban canopy model (SLUCM). The extreme events were dynamically downscaled into two parallel experiments, (1) without anthropogenic heat (AH) emission and (2) with diurnal peak AH = 300 Wm^{-2} (significant AH effect) over the urban region in the SLUCM. The WRF model was integrated at a resolution of 2km x 2km over the PRD megacity, with 72 hours before and after the peak of the rainfall intensity. Results show that, AH enhanced the accumulated rainfall as well as the probability of extreme rain rate (> 10mm/hr) in the urban domain. The presence of AH raises the near-surface temperature and hence the Convective Available Potential Energy (CAPE) while suppress Convective Inhibition (CIN) in the urban area at the same time. The urban atmosphere is energized and destabilized which provide a more favorable condition for convections to occur. Hence, more intense rainfall was formed in the urban area. The atmospheric warming signals due to global warming were observed in the whole troposphere which enhance CAPE and reduce CIN over the whole PRD area. The global warming effect also enhance the extreme rain rate significantly in the PRD region, with a comparable magnitude to that due to AH effect.

Keywords: Anthropogenic heat, urbanization, global warming, extreme rainfall

SHP
ECG

Evaluation of machine learning applications for springflow estimation and forecasting at Comal Springs, New Braunfels, Texas.

Emily Pease
Pease, E., University of Texas at Austin
Kushnereit, R., Intera
Pierce, S., Texas Advanced Computing Center

Quantifying springflow is essential in regulating groundwater resources in the Edwards Aquifer, especially during drought conditions. The Edwards Aquifer in central Texas is one of the largest karst aquifer systems in the United States and serves as the primary water supply for over 1.5 million Texans in Bexar, Comal, Hays, Medina, and Uvalde counties. The Edwards Aquifer Authority (EAA) and other stakeholders rely on estimations of springflow from Comal Springs to make daily decisions to balance multiple water needs. The discharge from the Edwards Aquifer through Comal Springs provides water for recreational activities, businesses, and downstream users. Additionally, these waters serve as a home to many aquatic species, eight of which are endangered or threatened. The current method of springflow estimation through baseflow separation has been used since the 1990s but contains a manual component that can vary through time due to variations in interpretation. Here, machine learning and regression models are implemented to calculate springflow at Comal Springs as an automated method of estimating springflow discharge and modeling future conditions. The hydrologic factors that correlate with springflow discharge are presented and their extents quantified. Additionally, preliminary models of machine learning algorithms are explored with their model scores calculated (model performance evaluation). This new automated system of springflow estimation will serve to further integrate computational methods and hydrology. No single springflow estimation method will be applicable nationwide due to differences in regional precipitation, recharge rates, and aquifer type (confined vs. unconfined, sandy vs. karst). This case study is a first step towards a reproducible workflow that any region's water management could follow to create springflow estimations.

Keywords: hydrology, data science

SHP
ECG

Carbonate Factory Recovery Following Oceanic Anoxic Events: a Closer Look at the Cow Creek Member of the Pearsall Formation in South Texas

Esben Pedersen
Pedersen, E., Jackson School of Geosciences, The University of Texas at Austin, Austin, TX
Kerans, C., Jackson School of Geosciences, The University of Texas at Austin, Austin, TX
Larson, T., Bureau of Economic Geology, The University of Texas at Austin, Austin, TX

Ocean anoxic events (OAEs) are major carbon cycle perturbations that occurred multiple times in the Mesozoic. These events are most commonly associated with the shutdown of precursor benthic carbonate factories and followed by deposition of black shales, some of which are known economic source rocks. In central Texas, OAE?related source intervals include the Pearsall and into the Glen Rose Formations (OAE?1a through OAE?1b), the Eagle Ford Formation (OAE?2), and the Austin Chalk (OAE?3). Recovery of the benthic carbonate factory following OAEs sets up the potential for encapsulated source?reservoir play systems. Post?OAE Gulf of Mexico reservoirs are known to occur in shelf interior grainstone belts (James Limestone Member of the Pearsall Formation) and in association with patch reefs (e.g., James Limestone, Bexar Shale, and lower Glen Rose Formations). While significant academic research has focused on identifying mechanisms that are responsible for the onset of OAEs, less research has focused on understanding how carbonate factories recover from these perturbations and return to an environment that fosters a healthy carbonate platform.

This study seeks to investigate the Early Cretaceous (Aptian) OAE?1a that is recorded by the Pine Island Member of the Pearsall Formation in South Texas, with a particular focus on shelf sequences preserved in a transect from the San Marcos Arch to the Pearsall Arch. To accomplish this, selected cores of interest will be scanned using pXRF at 5 cm spacing to build upon available XRF datasets. When linked to detailed study of ichnofossils and macrofossils, stratigraphy, and organic carbon chemistry, this coupling of core characterization with field observations may yield understanding of the evolution of carbonate facies along this transitional interface during carbonate recovery. This work aims to clarify the stratal architecture of the Pearsall Formation and to refine our understanding of the relative timing of events from the peak of biotic crisis preserved in the Pine Island Member during OAE?1a, through the partial recovery phase recorded in the deposition of the Cow Creek Formation, and into the second major biotic perturbation marked by OAE?1b in the Lower Glen Rose Formation.

Considering post?OAE recovery mechanisms, the transformation from anoxic to oxygenated conditions will vary along the carbonate platform depending on depth, proximity to shoreline, and basin restriction. Unlike the onset of OAEs which appear to be sharp, recovery mechanisms from OAEs may be more gradual. Depending on shelf position and basin restrictions, carbonate deposition and fossil fauna may evolve differently. For example, slow recovery from anoxic conditions would be expected in more restricted basins, resulting in longer persistence of stressed fauna including dense oyster assemblages and burrowed mixed siliciclastic carbonate deposits. In contrast, carbonate systems in unrestricted basins may more quickly reach a condition to sustain reef structures with the potential to develop into steep?walled carbonate platforms indicative of full carbonate recovery.

Ultimately, identifying the dominant mechanisms driving recovery and transition from stressed OAE environments to sustained carbonate deposition will allow for better characterization of both conventional and resource plays by predicting spatial variability of source and reservoir rocks.

Keywords: Pearsall, Cow Creek, OAE, Cretaceous, Carbonate

SHP
ECG

Field Characterization of Hillslope Weathering Profiles in the Great Valley Sequence, Northern CA

Michelle Pedrazas
Pedrazas, M., The University of Texas at Austin, Austin, TX
Rempe, D., The University of Texas at Austin, Austin, TX

In many montane environments, the partitioning of infiltrating water between (i) evapotranspiration, (ii) runoff, and (iii) groundwater recharge is controlled by weathered and fractured bedrock beneath the soil layer. As bedrock weathers, mineral transformations alter the hydraulic properties of the bedrock, however little data exist to establish relationships between weathering and water retention. This study investigates the distribution of clay minerals in shale weathering profiles and their impact on water retention through field characterization of weathering profiles and hydrologic monitoring. Geophysical well logging and core sampling was carried out at three field sites in Northern California associated with the Coastal Belt and Central Belt of the Franciscan Formation, and the Great Valley Sequence. We characterized elemental and mineralogical compositions in core samples via x-ray diffraction and x-ray fluorescence spectroscopy, and conducted cross-correlation of geophysical well-logs, including nuclear magnetic resonance, neutron density, and spectral gamma, to directly link in-situ moisture dynamics to clay mineralogy. Through this cross-site characterization effort, we seek to develop understanding of how bedrock weathering transforms water storage and transport such that we can develop more accurate models for groundwater recharge in montane environments.

Keywords: clay mineralogy, water dynamics, x-ray diffraction, well-logging, vadose zone

SHP
ECG

Missing ice or faulty eyes? Mapping supra-permafrost environments along the Arctic coast using electrical geophysics

Micaela Pedrazas Hinojos
Pedrazas, M., Department of Geological Sciences, The University of Texas at Austin, Austin, TX
Cardenas, B., Department of Geological Sciences, The University of Texas at Austin, Austin, TX
Watson, J., Hays Trinity Groundwater Conservation District
Connolly, C., Department of Marine Sciences, The University of Texas at Austin, Austin, TX
McClelland, J., Department of Marine Sciences, The University of Texas at Austin, Austin, TX

The Arctic is undergoing profound changes due to amplification of global warming in northern latitudes. Subsea permafrost is an understudied but critical component of the Arctic system. Changes to subsea permafrost impacts coastal and shelf erosion, subsea methane and carbon dioxide release, and water and nutrient fluxes. All of these are vital to communities and ecosystems. More importantly, these changes represent a positive feedback to the global climate system. However, subsea permafrost is poorly mapped and hence any changes remain untracked. There is a recently growing number of scientists conducting marine electrical resistivity (ER) surveys to map submarine permafrost, but there is lack of studies assessing the feasibility and performance of the ER geophysical method in Arctic coastal environments.

To our knowledge, there has not been a study that validates the performance, limitations or reliability of using marine ER as the primary geophysical method to map supra-permafrost along the Arctic coast. The Arctic coastline is characterized by a salty, conductive sea layer which can easily let current flow through it and a very resistive low lying permafrost layer in the subsurface which may result in the current focusing in the more conductive sea layer, also known as current channeling. Thus, while it seems promising, it is unclear whether ER is a feasible technique for application in subsea permafrost mapping particularly in the absence of corroborating and complementary information. Here, we address the following research questions to advance the current understanding of ER application in supra-permafrost coastal environments:

1. Will ER surveys be able to distinguish seawater, saturated thawed coastal sediment, and frozen coastal sediment?
2. What are the environmental conditions that limit or enhance the applicability of ER surveying?
3. What survey designs are optimal for a given environmental condition?

These questions will be addressed within a forward modelling framework based on a petrophysical model and the interpretation of a 2D boat-towed multi-electrode ER survey in a shallow estuarine lagoon in the Arctic coastline (Kaktovik, Alaska). This study confirms that interpreting marine ER surveys in coastal environments must be guided by prior modeling and sensitivity analysis, and is susceptible to electrical current channeling to a significant degree. We demonstrate a methodology to determine whether ER is a reliable geophysical method to capture permafrost in the subsurface beneath a conductive sea layer, what limitations exist and how can an ER survey be optimized when used in an Arctic coastal environment to map the distribution, thickness and degradation rates of permafrost.

Keywords: electrical resistivity, geophysics, marine, permafrost, subsea, target, alaska, arctic, global warming,

SHP
ECG

Juniperus Ashe Effects on West Texas Water Balance

Austin Rechner
Rechner, A., Department of Geosciences, The University of Texas at Austin, Austin, TX
Restrepo Acevedo, A., Department of Geosciences, The University of Texas at Austin, Austin, TX

A common held belief among many West Texans is that cedar trees (Juniperus ashe) extract and utilize a large amount of water causing streams and springs in the areas they inhabit to go dry. However, there is not scientific consensus supporting the belief that cedars consume water at this disproportionate rate compared to other species. This study aims to analyze water used by cedars in comparison to the co-occurring species on a ranch near Rock Springs, Texas. We use Granier-style sap flux sensors to quantify the rates at which transpiration is occurring in three species of trees *Pinus remota* (pinyon pine), *Quercus virginiana* (live oak), and *Juniperus ashe* (cedar). We compare water rates between the cedars with the oaks and pines in response to varying environmental conditions. The data analyzed at 30-minute and twenty-four hour time steps. In March, more than half of the cedar trees on the ranch will be cleared allowing analysis of any changes in species performance and site water balance to be observed. In addition to sap flux data, we also monitor meteorological conditions onsite including temperature, precipitation, humidity, radiation, and soil moisture. These will continue after cedar clearing in order to determine if cedar removal will significantly increase water availability.

Keywords: sap flux, water balance, Juniperus ashe, land management, ecohydrology

SHP
ECG

Changes in the Hysteresis Between VPD and Sap-Flux Velocity in Different Tree Species in Northern Michigan Forests'

Ana Maria Restrepo Acevedo
Restrepo Acevedo, A., Jackson School of Geosciences The University of Texas at Austin Austin TX
Matheny, A., Jackson School of Geosciences The University of Texas at Austin Austin TX

Xylem sap flow measurements are commonly applied to monitor plants water use and transpiration in response to environmental variables such as soil water availability, radiation, temperature, and vapor pressure deficit (VPD). Understanding the response of sap flux to these variables is crucial for predicting how plants' water use changes under daily and seasonally varying conditions; in addition, VPD, which varies substantially over daily and seasonal timescales, is an important driver of plant transpiration. However, a particular VPD often does not produce the same results in sap velocity depending on the time of day. This causes hysteresis in the daily relationship between sap velocity and VPD. It has been observed that for a given VPD that occurs in both the morning and the evening, sap velocity is higher in the morning producing a clockwise rotation in the hysteresis curve. Recent studies in Northern Michigan have shown that red oak, a ring porous anisohydric species, demonstrated the largest mean relative hysteresis, while red maple, bigtooth aspen, and paper birch, all diffuse porous species, have the lowest relative hysteresis. Similarly, another pattern of hysteresis has been observed. On some days, the plot of sap velocity versus VPD has shown a figure-8 pattern of hysteresis.

This study makes the argument that this unusual pattern can be related to the behavior of the daily cycles of the environmental drivers supported by the asymmetry between its behavior and sap flux cycle. In addition, the relationship between the type of specie and the patron will be discussed as a response to the influence of other factors, such as antecedent weather conditions, that can affect the magnitude and pattern of sap flow hysteresis and how this species response to varying changes in sap velocities.

Keywords: Sap-Flux, VPD, hysteresis, anisohydric species, diffuse porous species

SHP
ECG

Anatomy of a Fluvial Avulsion: Linking Geomorphology and Stratigraphy using 3-D Outcrops of Exhumed Channel-Belt Deposits

Cole Speed
Speed, C., Department of Geological Sciences, Jackson School of Geosciences, The University of Texas at Austin, Austin, TX
Sylvester, Z., Bureau of Economic Geology, The University of Texas at Austin, Austin, TX
Flaig, P., Bureau of Economic Geology, The University of Texas at Austin, Austin, TX
Goudge, T., Department of Geological Sciences, Jackson School of Geosciences, The University of Texas at Austin, Austin, TX
Mohrig, D., Department of Geological Sciences, Jackson School of Geosciences, The University of Texas at Austin, Austin, TX

Fluvial processes construct and shape landscapes on Earth and are inferred to have been active on the surface of early Mars. Establishing linkages between fluvial geomorphology and the stratigraphic record is key to accurately reconstruct past landscapes and environments on these planets. However, reconstructing geomorphic surfaces from stratigraphic elements, determining paleo-channel and channel-belt dimensions, and characterizing the planform evolution of channel-belts is difficult using 2-D outcrops or satellite imagery.

Topographically-inverted fluvial channel-belt deposits of the Cedar Mountain Formation in eastern Utah offer three-dimensional exposures of fluvial stratigraphy. This study will characterize the stratigraphic architecture of these deposits and relate it to the geomorphological and sedimentological processes (i.e., aggradation, lateral migration, avulsion, and reoccupation) involved in their deposition and preservation. Primary focus will be on two channel-belt segments that are likely to represent an avulsion event; this is a unique opportunity to characterize the stratigraphy of a fluvial avulsion in three dimensions. Although the processes of fluvial avulsion, abandonment, and reoccupation are often interpreted from the stratigraphic record, the third dimension and a well-defined context are often missing. Our analysis will rely on 3-D digital outcrop models developed from Unmanned Aerial Vehicle (UAV) photogrammetry and extensive field mapping. UAV-derived basemaps enable correlation of facies with key bounding surfaces and paleocurrent data. Channel-belt evolution will be studied using field observations, a simple numerical model for river meandering, and examples of fluvial avulsions in the modern.

Keywords: Geomorphology, Sedimentology, Stratigraphy

SHP
ECG

Determining the link between hydraulic properties of arctic tundra soils and Interferometric Synthetic Aperture Radar deformation measurements

Yue Wu
Wu, Y., University of Texas at Austin, Aerospace Engineering & Engineering Mechanics
Chen, J., University of Texas at Austin, Aerospace Engineering & Engineering Mechanics
O'Connor, M., University of Texas at Austin, Jackson School of Geosciences
Ferencz, S., University of Texas at Austin, Jackson School of Geosciences
Kling, G., University of Michigan, Ecology and Evolutionary Biology, Michigan
Cardenas, M., University of Texas at Austin, Jackson School of Geosciences

The North Slope of Alaska is covered with continuous permafrost. Permafrost thawing affects delivery of water and carbon from the landscape to surface waters, which has further influences on the global C cycle. Remotely sensed measurements are especially useful for studies of thaw processes over the Arctic region due to inaccessibility for ground-based measurements. In this study, we use spaceborne Interferometric Synthetic Aperture Radar (InSAR) data acquired from ALOS and Sentinel-1 missions to estimate Active Layer Thickness (ALT) near Toolik Lake, Alaska. We show the magnitude of land surface seasonal uplifting and subsidence when permafrost soil undergoes thaw-freeze processes, due to the density difference between liquid water and ice. Compared with ground-based techniques such as probing and thaw tubes, InSAR monitors the hydrologic state of the permafrost over larger areas at relatively high spatial resolution. To understand the link between hydraulic properties of the suprapermafrost zone and InSAR deformation signals, we analyzed soil samples and ALT data from Imnavait Creek. Based on field measurements of soil porosity and soil moisture content of different types of soils, we developed algorithms to translate InSAR deformation signals to soil moisture content and ALT. This is the first step toward our overall goal of regional, real-time estimation of hydrological C transport through overland and groundwater flow in the Arctic region and examine how it will affect Arctic climate.

Keywords: InSAR, surface deformation, arctic tundra soil, hydraulic properties

EG
LCMS

Top Seal Evaluation of Miocene Deep-Water Reservoirs, Southern Gulf of Mexico

Fernando Apango
Apango, F., Institute for Geophysics, The University of Texas at Austin, Austin, TX
Snedden, J., Institute for Geophysics, The University of Texas at Austin, Austin, TX

Integration of core, 3D seismic, and well data provided by the Mexican National Hydrocarbon Commission (CNH) was used to evaluate the top seals of Miocene deep-water reservoirs within the Veracruz Trough in the Southeastern Gulf of Mexico. Deep-water well discoveries in this region have often been a mix of oil, gas, or water, raising some questions about the quality of both the source and the seal rock. Nonetheless, traces of hydrocarbons in some water-bearing reservoirs suggest that hydrocarbons were effectively generated. Therefore, the lack of economically viable volumes of oil and gas in these reservoirs are probably a consequence of seal failure and/or traps that were filled to an unmapped shallow spill point.

XPT pressure data from the Pemex operated Kunah-1 and Yoka-1 wells for the Upper and Lower Miocene, were used to construct 'Excess Pressure' plots to evaluate both top and internal seals. Subtle but significant pressure contrasts over small depth intervals that suggest the presence of thin but effective seal rocks. To better assess the seal strength for each case, 'Mercury Injection Capillary Pressure' (MICP) lab measurements were performed on cuttings for those particular depths. Results from these measurements had a general concordance with our interpretations from pressure data, although in some cases the estimated 'entry capillary pressure' for some samples was lower than expected.

However, top seal capillary leakage does not necessarily equate to trap failure, as there could be a matched flowage into the base of the hydrocarbon column and leakage from the top of the column, with a commercial volume of hydrocarbons retained. In these cases, and in the presence of strong seals, spill points can be the controlling factor of fluid contacts. There are relatively few faults in the large folded anticlines tested by the Kunah-1 and Yoka-1 wells. Using 3D seismic mapping to define structural closures in both Kunah-1 and Yoka-1 wells we have identified the structural spill points for various Miocene reservoirs. Fluid contact elevations are much shallower the structural spill points suggesting another controlling mechanism.

Seal rocks' effectiveness was ultimately assessed and defined utilizing various conventional seal classifications (Sneider, Dawson and Almon, Sales, etc.), which are primarily based on the results of MICP measurements and/or the control of the spill points. We conclude that Miocene seal rocks are effective for the observed columns of oil and gas in the southern Mexico deepwater areas but some capillary leakage is probably occurring. Another factor being investigated is the evolution of the trap versus hydrocarbon charge timing. Late trap formation may explain why the Yoka structure is not filled to spill.

Keywords: Top seal, trap formation, gas reservoirs, Gulf of Mexico, deep-water reservoirs, Miocene, Veracruz Trough

EG
LCMS

Wolfcampian Shelf-to-Basin Stratigraphic Framework of the Central Basin Platform and Midland Basin, Andrews County, Texas

Cody Draper
Draper, C., Department of Geological Sciences, The University of Texas at Austin, Austin, TX
Kerans, C., Department of Geological Sciences, The University of Texas at Austin, Austin, TX
Wahlman, G., Wahlman Geological Services, LLC

Lower Permian (Wolfcampian) strata are important reservoirs and exploration targets on the Central Basin Platform, along its eastern slope, and in the adjacent Midland Basin. Controls on deepwater allochthonous carbonate reservoir facies development and stacking can be better understood through analyses of shelf-to-basin stratigraphic frameworks which identify the timing and mechanisms of sediment bypass and accumulation across the depositional profile. This study aims to provide context for the deepwater elements within the basinal Wolfcamp B and C by examining contemporaneous stratal architecture and sedimentation patterns along the shelf to basin depositional profile using 3D seismic, well-logs, and core lithofacies data with fusulinid biostratigraphic constraints from North Cowden, Midland Farms, and Mabee fields.
Cores from Midland Farms Deep field show the Hueco Fm. includes up to 116 ft of Lower Hueco strata dominated by phylloid algal-calcisponge-*Tubiphytes* reefal buildup complexes with crinoid-dominated flank packstone beds. The mid-Wolfcamp unconformity (Upper-Lower Hueco Boundary) is marked by a gamma ray spike expressed in core as a subaerial exposure surface overlain by a green grey clay-rich mudrock. Well-log suites suggest this unconformity is correlative throughout Southeast Andrews County. The Upper Hueco includes up to 172 ft of upward shallowing successions of skeletal-fusulinid packstones, peloidal packstones, and ooid grainstones intercalated with carbonaceous shales, interpreted as representing deposition during an overall transgression. Lower Hueco strata generally have more consistent and lower gamma ray values than the Upper Hueco, consistent with the fewer clay-rich mudrocks and shales in the Lower Hueco. The Wolfcampian-Leonardian unconformity represents the early Leonardian transgression and the backstep of Leonardian deepwater carbonaceous to siliciclastic shales and debris flows over the Upper Hueco. Seismic data illustrates the evolution of the depositional profile from the subtle Pennsylvanian-Wolfcampian contact, to the distally steepened Wolfcampian profile, to the better-defined Leonardian downlap onto the Hueco. Reconstructing the Wolfcampian platform-to-basin stratigraphic architecture assists in predicting the timing and style of deposition on the slope and basin and improves the ability to predict sweet spots for hydrocarbon exploration in the deeper water facies.

Keywords: Carbonate, Shelf, Slope, Basin, Wolfcamp, Permian Basin, Hueco

EG
LCMS

Seismic data interpolation to a regular grid

Ben Gremillion
Gremillion, B., Bureau of Economic Geology, The University of Texas at Austin, Austin, TX
Fomel, S., Bureau of Economic Geology, The University of Texas at Austin, Austin, TX

Seismic data are traditionally acquired in 2D lines or in 3D volumes, where traces can lie at irregular locations and at varying azimuths within gathers. The processing and analysis of these data often benefits from or even requires the data to be defined on a regular grid. We present a method to interpolate and regularize seismic data to a regularly sampled 3D volume. Our technique utilizes dynamic time warping and fast scattered data gridding to flatten reflection data at nonuniform locations, interpolate to a regular grid, and unflatten the interpolated data, yielding a regularly sampled 3D dataset. We test this method on a field dataset and obtain promising results.

Keywords: Interpolation, Regularization, Seismic Data Processing

EG
LCMS

Low-Frequency Attenuation Measurements of Fluids

Michael McCann
McCann, M., The University of Texas at Austin, Austin, TX
Tisato, N., The University of Texas at Austin, Austin, TX
Spikes, K., The University of Texas at Austin, Austin, TX

Pore fluids significantly affect the elastic responses of rocks. Rock physics models can be used to predict how pore fluids affect the elastic responses of rocks when rocks are fully or partially saturated. Thus, to identify fluids in the subsurface it is useful to know the elastic properties of such fluids. In addition, new technologies to assess and monitor hydrocarbon exploration rely on the precise determination of fracking fluid elastic properties. Moreover, the elastic properties of rocks depend on the frequency of the wave propagating through the rock. Methodologies to measure high-frequency elastic properties of fluids have been widely reported. What have not been established are methodologies to measure the low-frequency elastic properties of fluids in a laboratory setting. Using the low-frequency properties, rather than the already known high-frequency properties of pore fluids, will provide more accurate values when calculating the low-frequency elastic properties of rocks saturated with pore fluids from rock physics models.

A machine has been designed and built to measure the low-frequency attenuation and bulk modulus of fluids at frequencies from 0.1 to 10 Hz. Deionized water and aqueous guar gum solutions have been tested. Results for measurements of attenuation and bulk modulus of water are in agreeance with reported values for water. Measurements of guar gum solutions show attenuation is greater than 0.01 with higher concentration samples having higher attenuation. The machine used for these experiments is most reliable at frequencies less than 5 Hz.

Keywords: Experimental rock physics, Attenuation, Low frequency

EG
LCMS

Missing well-log prediction using recurrent neural network

Nam Pham
Pham, N., The University of Texas at Austin, Austin, TX

Missing well-log prediction using recurrent neural network
Nam Pham
Pham, N., Bureau of Economic Geology
Some common available well-log types in a well are Gamma-ray and density logs. Getting many types of well-logs are expensive and time-consuming. However, for some workflow such as seismic-well tie, we need both sonic and density logs. There are many available methods have been used for missing well-log prediction. I propose to use a recurrent neural network for missing well-log prediction from available input logs. The method can also produce the uncertainty of the prediction.

Keywords: missing logs prediction, deep learning, recurrent neural network

EG
LCMS

Geologic Characterization and CO2 Storage Resource Assessment of Two Depleted Hydrocarbon Fields in the Texas State Waters, Gulf of Mexico

Omar Ramirez Garcia
Ramirez, O., Jackson School of Geosciences, The University of Texas at Austin, TX
Ruiz, I., Jackson School of Geosciences, The University of Texas at Austin, TX
Meckel, T., Bureau of Economic Geology, The University of Texas at Austin, TX
Fifariz, R., Jackson School of Geosciences, The University of Texas at Austin, TX

ABSTRACT

Carbon dioxide capture, utilization and storage (CCUS) has been proposed as one of the main technologies that could help mitigate climate change by reducing CO_2 emissions to the atmosphere and instead inject such emissions into deep geologic formations. Storage is one of the key axes for CCUS technology and therefore one of the most important aspects of the technology that is addressed properly in this project. The principal targets for CO_2 storage need to have high pore volume and good permeability such that they provide appropriate capacity and injectivity, as well as a good-quality seal that prevents the CO_2 from migrating upwards to the upper geologic formations or to the surface. In addition, a geologic structure favorable for CO_2 accumulation (e.g. anticlines, fault closures, etc.) is also sought, such that it prevents CO_2 lateral migration. The previous and even current, vast hydrocarbon exploration in offshore Gulf of Mexico has proven that it fulfills the criteria mentioned above.

This study focuses on site-specific geologic characterizations and CO_2 storage resource assessments of two depleted oil and gas fields located on the inner continental shelf of the Gulf of Mexico. The High Island 10L and 24L fields serve as prime case studies for CCUS based solely on their hydrocarbon production. Lower Miocene sands in the Fleming Group beneath the regional transgressive *Amphistegina B* shale have great geologic properties and are therefore characterized utilizing 3-D seismic and well logs. Key surfaces between MFS-9 to MFS-10 demonstrate how marine regression and transgression impact the stacking pattern of the thick sands, influencing the overall potential for CO_2 storage. This study therefore includes a stratigraphic analysis of both fields, as well as their respective geologic models populated with porosity and permeability to estimate CO2 capacity. .

Estimating a range of CO2 capacity estimates for both these fields provides a better insight to how geological interpretations and parameters on a field scale can assess storage potential.

Keywords: Storage assessment, characterization, Miocene, offshore, Gulf of Mexico, capacity, CO2

MG
LCMS

Pore-scale methane hydrate formation under pressure and temperature conditions of natural reservoirs

Tiannong Dong
DONG, T., Institute for Geophysics and Department of Geological Sciences, Jackson School of Geosciences, The University of Texas at Austin
LIU, J., Department of Geological Sciences, Jackson School of Geosciences, The University of Texas at Austin
GU, J., Department of Geological Sciences, Jackson School of Geosciences, The University of Texas at Austin
LIN, J., Department of Geological Sciences, Jackson School of Geosciences, The University of Texas at Austin
FLEMINGS, P., Institute for Geophysics and Department of Geological Sciences, Jackson School of Geosciences, The University of Texas at Austin
POLITO, P., Department of Geological Sciences, Jackson School of Geosciences, The University of Texas at Austin
O'CONNELL, J., Institute for Geophysics, Jackson School of Geosciences, The University of Texas at Austin

μWe synthesized methane hydrates in glass beads (porous medium) and 3.5 wt% NaCl brine and probed micron-scale hydrate formation over 850 hours with a Raman spectrometer. Instead of forming the thermodynamically stable structure-I hydrate immediately, we formed metastable hydrates, which gradually converted to structure-I hydrate over time. Structure-I hydrate has a large- to small-cage molar ratio of 3:1, but the metastable hydrates initially show a chaotic distribution of cage configurations.
Methane hydrates were formed from gaseous methane and dissolved methane in spherical silica glass beads (210–297 μm in diameter) in a pressure chamber with a sapphire window. We injected methane vapor to the chamber and supplied 3.5 wt% NaCl brine to elevate the pressure to experimental conditions. We waited several days for gaseous methane to dissolve into the water. The temperature was gradually decreased to enter the hydrate stability zone. Methane hydrates formed at 17.58 MPa and 280.4 K (10.0 K of subcooling). We used Raman spectroscopy to map the methane hydrates in glass beads at 25 μm resolution over a 2-by-2 mm area. We deconvoluted Raman spectra to derive large- to small-cage ratios.
We observed small cages formed faster than large cages upon the initial hydrate formation. It took time to form large cages, which are necessary building blocks of structure-I hydrate. This observation is consistent with multiple molecular dynamics studies. After ~300 hours, enough small cages converted to large cages, and over 90% of the hydrates in the mapped region converted to structure-I hydrates. With our experimental observations, we show insights to the molecular-level mechanism of methane hydrate formation.

Keywords: Methane hydrate, Raman spectroscopy

MG
LCMS

Paleogeographic reconstruction and characteristic trends of a basin floor fan in Los Molles Fm, Neuquén Basin, Argentina

Gabriel Giacomone
Giacomone, G., Jackson School of Geosciences, The University of Texas at Austin, Austin, TX
Olariu, C., Jackson School of Geosciences, The University of Texas at Austin, Austin, TX
Steel, R., Jackson School of Geosciences, The University of Texas at Austin, Austin, TX
Shin, M., Jackson School of Geosciences, The University of Texas at Austin, Austin, TX

The Jurassic deep-water marine deposits of Los Molles Fm in Neuquén Basin, Argentina (La Jardinera area) have received much attention through the years; however, a detailed characterization of the basin floor fans that outcrop in the area was missing.
We made use of a high-resolution satellite image, drone imagery and 3500 m of logs with detailed measurements to build isopach and net/gross (NG) maps that with facies analysis helped reconstruct the evolution of the system. In addition, grain size, facies and bed thickness trends were useful to refine the interpretation at a lobe scale in unit LC3.
Lithofacies, NG ratios and sandstone bodies' geometries help defined six facies association; hemipelagic deposits, fringe lobes, off axis lobes, on axis lobes, distributary channels and debris flows. The facies associations define lobe elements that are grouped into lobes (<10 m thick) and these into lobe complexes (~20-40 m thick). The studied basin floor fan comprises five lobe complexes (LC1-5) separated by fine-grained intervals. Here, we evaluated only LC1-4, since LC5 is poorly exposed. LC1 shows different paleoflows trends, one towards the north and the other towards the east; it is composed of two lobes with high proportion of unconfined deposits. LC2 shows northeastward paleoflows, it is composed of three lobes that onlap and fill relative low areas left by LC1. LC3 exhibits paleoflows to the east and it is composed of six lobes, five of which show channels on their axis, evidencing the most proximal setting on the system. The lobes of LC3 aggrade and migrate laterally towards the NW. LC4 develops on top, with its axis shifting to the south and backstepping, exhibiting only unconfined lobe elements. Detailed study of lobes 2 and 3 in LC3 show interesting trends in axial sections. Proximal to lobe axis beds are thicker (>40 cm), grain size is greater (medium sand to granules) and main facies are conglomerates and structureless sandstones. Off axis, beds are thinner (<40 cm), grain size ranges from fine to medium sand and there is an increase on normally graded and laminated sands. These trends are associated with the confinement and density of the flow. From lobe axis to off-axis, channelized elements disappear and the facies vary from high density to low density turbidites.
The present work shows that Los Molles Fm has significant sandstone units that likely form good reservoirs when present in the subsurface and a good analog for coarse-grained fan deposits.

Keywords: Deep-water, basin floor fans, turbidites, hierarchy, geometry of depositional elements, Neuquen Basin

SETP
LCMS

Achieving quantitative understanding of radiogenic He behavior in zircon using 4He/3He thermochronometry

Clara Brennan
Brennan, C., The University of Texas at Austin, Austin, TX
Stockli, D., The University of Texas at Austin, Austin, TX
Patterson, D., The University of Texas at Austin, Austin, TX

Helium thermochronometry is a valuable tool used to constrain events that happen at very low temperatures. However, He closure does not occur at abrupt temperature boundaries but is characterized by a zone of partial accumulation due to thermally-activated diffusive loss. This is known as a Partial Retention Zone, or PRZ. For zircon, the closure temperature is ~180°C, while the HePRZ has been shown to span a 190-140°C temperature interval.

In this study, individual zircon crystals underwent systematic fractional loss step-heating experiments in order to create 4He/3He profiles. Parent element zonation was measured by LA-ICP-MS depth-profiling. The He fractional loss data and the 1-D U and Th zonation data were then inverted using Monte Carlo inverse modeling (HeFTy) to determine the time-temperature evolution of samples across the zircon HePRZ. Rapidly cooled Fish Canyon Tuff samples were analyzed as both reference material and procedural check.

Two case study locations were identified to test and benchmark the methodology. The German Continental Deep Drilling Project (KTB) recovered samples from ~9 km of crustal depth, while the Wassuk Range, an exhumed fault block in western Nevada, exposed an ~9 km thick crustal section. Both crustal sections have been studied extensively using a variety of thermochronometric methods and thus have thermal histories that are well understood.

The application of step-heating to zircon 4He/3He thermochronology allows for a detailed and quantitative understanding of the behavior of radiogenic He across the HePRZ. This knowledge is relevant to and has important implications for future He thermochronometry studies. The systematic procedures of combining both methods on well studied locations allow for (1) the recovery of continuous thermal history constraints, (2) determination of the resolution and accuracy of obtained thermal histories, and (3) observing the influence of radiation damage on resulting recovered thermal histories.

Keywords: thermochronology, geochronology, helium, 4He/3He, KTB, Wassuk Range, Fish Canyon Tuff, zircon

SETP
LCMS

Petrology, Geochemistry and Zircon U/Pb Geochronology of the Ertsberg Pluton, Ertsberg-Grasberg Mining District, Papua, Indonesia: Magma Chamber Recharge and Mixing

Jacob Makis
Makis, J., Department of Geological Sciences, The University of Texas at Austin

The Ertsberg Pluton is the largest (>10 km^3) and youngest (3.1-2.8 Ma) igneous body within the renowned Ertsberg-Grasberg mining district of Papua, Indonesia. It is associated with ore-grade Cu-Au mineralization in the form of three large skarns (Ertsberg/Gunung Bijih, Ertsberg East Skarn System: GBT/IOZ/DOZ/MLZ/DMLZ, and Dom) and a localized zone of classic porphyry style mineralization. Ertsberg rocks are clinopyroxene + titanite bearing and range in composition from quartz monzodiorite/monzodiorite to quartz monzonite/monzonite, but overall the intrusion is relatively homogeneous compared to others in the district. For this reason, it was thought that the bulk (>95% volume) of Ertsberg was emplaced as a single batch of magma that underwent fractionation (McMahon, 1994). In this study, major and trace element geochemistry was combined with LA-ICP-MS zircon U/Pb ages to constrain the emplacement and evolution of the pluton. A suite of 57 samples were analyzed. Twenty-four of these samples are from two NE-SW trending, near horizontal drillholes, that are up to 1200m long. Out of the entire suite, 34 samples have zircon U/Pb ages and 31 samples have ?Nd and $^{87}Sr/^{86}Sr$ isotopic measurements. When all samples are plotted on standard Harker diagrams for SiO_2 and MgO, apparent fractional crystallization trends are observed with SiO_2 ranging from 54-64 wt. % and MgO ranging from 1-3 wt. %. Samples with high SiO_2 or low MgO, have low Ca, Fe, Ti and P and high K. However, when major element geochemistry is compared with zircon U/Pb ages, the oldest samples are the most felsic and the youngest samples are the most mafic. Trace elements mimic this relationship with the youngest samples having high concentrations of Sc, V, Ni and Cr. Furthermore, the ?Nd and $^{87}Sr/^{86}Sr$ isotopic measurements follow this relationship. The sample suite defines a mixing curve and when the compositions are plotted against zircon U/Pb ages the ?Nd increased and $^{87}Sr/^{86}Sr$ decreased through time. These trends are opposite to those expected for a single batch of magma that underwent fractional crystallization. The geochemistry of the Ertsberg Pluton is explained by blending an original intermediate composition magma with increasing proportions of recharging mafic magma. Petrographic evidence from the two transects support the geochemical findings. Thin section billets stained for plagioclase, potassium feldspar and quartz reveal the presence of albitic cores surrounded by anorthitic rims, a consequence of mafic recharge. Embayed and corroded grain boundaries, sieve plagioclase cores, and other resorption features are common. These features are indicative of mixing magmas and thermal perturbations associated with incremental emplacement and construction of the Ertsberg Pluton.

Keywords: Magma Mixing, Magma Chamber Recharge, Pluton Emplacement, Porphyry Copper-Deposits, Indonesia,

LCMS-11

SHP
LCMS

Tracking the sources and processes of urban development effects on stream water evolution in Austin, TX

Lakin Beal
Beal, L., Jackson School of Geosciences, The University of Texas at Austin
Senison, J., Anadarko Petroleum Company, Houston, Texas
Yazbek, L., Department of Geology, Kent University
Banner, J., Jackson School of Geosciences, The University of Texas at Austin

Resilient fresh water resources are needed to facilitate rapid population growth projected for the 21st century, yet the associated urbanization of watersheds will increasingly impact the quality and quantity of these resources. Thus, it is critical to understand how water in the urban infrastructure interacts with natural watersheds and aquifers. We investigate sources and processes through which municipal (supply and waste) water impact stream composition in the Bull Creek watershed, which exhibits a pronounced spatial gradient in urban development. We investigate isotopic and elemental variations in stream water from 'urban' and 'rural' stream sites. Stream water compositions reflect increasing urban impact, wherein Sr isotopes ($^{87}Sr/^{86}Sr$) and ion concentrations are used to distinguish between municipal and natural sources of dissolved ions to streams. Water from urban sites show an increase over 15-years in waste water constituents (e.g. Na, Cl) and reflect the temporal increase in development of the watershed. A strong correlation between increased urbanization and $^{87}Sr/^{86}Sr$ values of stream water can be accounted for by two different processes: (1) municipal water leakage from failing urban infrastructure, or (2) ion exchange as precipitation infiltrates through soils. Significant increases in irrigated soil $^{87}Sr/^{86}Sr$ values relative to unirrigated soils indicate that municipal water resets soil compositions over time, and that process (1) is thus a dominant driver of stream water evolution at urban sites. This also indicates that soil compositions are a consequence of the elevated $^{87}Sr/^{86}Sr$ values of municipal water. Modeling supports a new geochemical evolution pathway, whereby leaking municipal water and irrigation water infiltrate through and interact with the carbonate bedrock as groundwater, which then discharges into streams. Continued urban development, and associated leakage and irrigation, may increase the susceptibility of surface and groundwater to this evolution pathway. This study demonstrates that municipal water can enter natural groundwater and surface water systems and result in significant geochemical evolution of municipal water and soil, and that municipal water evolved by these processes should be considered as a significant component of watersheds and aquifers.

Keywords: Urban Watershed, Geochemistry, Isotopes

SHP
LCMS

An Investigation into the Applicability and Implications of Central Texas Speleothems in Paleotempestology

Kendra Bunnell
Bunnell, K., Department of Geological Sciences, The University of Texas at Austin, Austin, TX
Banner, J., Department of Geological Sciences, The University of Texas at Austin, Austin, TX
Breecker, D., Department of Geological Sciences, The University of Texas at Austin, Austin, TX

The use of speleothems in paleoclimatological studies has increased dramatically in the past decade, and their use as paleotempest records is just starting to be explored. This project seeks to find the isotopic tracer precipitated by Hurricane Harvey in speleothem drip water from central Texas caves in order to i) understand and gain an estimate of the storage and mixing capacity of the soils and limestones overlying the cavern, ii) determine the extent to which a given drip site may preserve a hurricane event in the $\delta^{18}O$ values of calcite growing from that drip, and therefore determine the characteristics of sites with this preservation potential, and iii) investigate the extent to which the isotopic signature of Hurricane Harvey and other meteorological events may be preserved in speleothem calcite.

Hurricane Harvey hit the Gulf Coast region in August of 2017, depositing a large amount of isotopically light rainfall, with $\delta^{18}O$ values of approximately -12‰ vs. SMOW, as compared to the region's average rainfall value of approximately -4‰ vs. SMOW, which is also the drip water average. Given its high volume and distinct isotopic signature, the rainfall associated with Hurricane Harvey has the potential to serve as an isotopic tracer in groundwater and thus cave water. Central Texas caves are well suited for the study of this isotopic tracer and preservation potential for several reasons. Firstly, they are located in an area that felt the effects of the outermost edge of Hurricane Harvey towards the end of its lifespan, giving that rainfall an especially light $\delta^{18}O$ signature. Second, sites in several central Texas caves have continuous monitoring by Dr. Banner's research group at the University of Texas.

Drip water from sites in Inner Space Cavern (Georgetown, TX), Cave without a Name (Boerne, TX), Westcave Preserve (Round Mountain, TX), and Natural Bridge Caverns (San Antonio, TX) from before, during, and after Hurricane Harvey have been analyzed for stable oxygen isotopes to investigate the presence of a strong negative isotopic excursion. The presence or lack of this excursion was investigated in conjunction with site drip rate, calcite growth rate, and modeled/sampled calcite isotopic composition, as well as rainfall amount and isotopic composition, to determine if any response to Hurricane Harvey, and potentially hurricane events in general, would be preserved in the speleothem.

The results indicate that while most sites show a drip rate response to Hurricane Harvey, only a few sites show the expected negative isotopic excursion, and the modeled calcite shows little to no notable preserved response. Add in the lack of summer growth in many of the studied sites, and it is clear that the studied sites would not be reliable candidates for paleotempestology studies. From these findings, for a speleothem to be a viable candidate for paleotempestology studies it must i) have growth during the hurricane season and/or year round, ii) be moderately between diffuse and conduit-fed to allow for a longer period of time of hurricane-affected growth, and iii) be subjected to a relatively stable temperature.

Keywords: Speleothems, paleoclimatology, paleotempestology, stable oxygen isotopes

SHP
LCMS

Spring-associated riparian vegetation and its impact on morphology in dryland channels:Henry Mountains, UT, USA

Paul Southard
Southard, P., Department of Geological Sciences, The University of Texas at Austin, Austin, TX
Johnson, J., Department of Geological Sciences, The University of Texas at Austin, Austin, TX
Rempe, D., Department of Geological Sciences, The University of Texas at Austin, Austin, TX
Matheny, A., Department of Geological Sciences, The University of Texas at Austin, Austin, TX

Riparian zone vegetation on a channel's bed, banks and on bars or islands has well-documented effects on flow and sediment erosion, transport and deposition processes. The complexity of natural channel feedbacks, however, obscures exactly how alteration of sedimentation processes by vegetation and its effects on flow processes translate to a modification of long-term channel evolution and resulting channel morphology. In attempting to isolate the impact of vegetation on morphology, single channels with variable vegetation along their length are desirable for study because flow conditions and long-term sediment flux change minimally between major tributaries. Dryland channels in Henry Mountains, Utah, USA that are only densely vegetated downstream of springs provide an opportunity to test the hypotheses that 1) vegetated reaches experience different channel responses from unvegetated reaches during flood events, and 2) on the scale of multiple flood events, different channel responses accumulate to produce distinct channel morphologies in vegetated and unvegetated reaches. We quantitatively evaluate these hypotheses with field surveys, airborne LiDAR analysis and AnuGA flow modeling. Differencing airborne LiDAR datasets that bracket a major flood and modeling flood flow through parameterized vegetation in AnuGA indicate different flow characteristics and suggest more depositional sedimentation distributed across a greater cross-sectional span of channel in reaches with dense vegetation on a single-event timescale. Field observations and analyses of airborne and terrestrial LiDAR datasets also demonstrate distinct channel morphologies in vegetated reaches, characterized by incised thalwegs dotted with frequent root- and clast-supported knickpoints, less cross-sectional topographic variability and a prevalence of sand-sized particles on the channel bed. These results help to bridge the gap between disruptions to small-scale processes and disruptions to channel evolution that vegetation causes, and indicate how channels may adjust their morphology due to riparian succession caused by climate change and other natural or anthropogenic disturbance.

Keywords: geomorphology, riparian vegetation, morphology, sediment transport, change detection

CCG
LCPHD

Human-induced nitrogen exports to rivers in San Antonio and Guadalupe river basins

Seungwon Chung
Chung, S., Department of Geological Sciences, Jackson School of Geosciences, The University of Texas at Austin
Yang, Z., Department of Geological Sciences, Jackson School of Geosciences, The University of Texas at Austin
Tavakoly, A., U.S. Army Engineer Research and Development Center, Coastal and Hydraulics Laboratory

Nutrient transport and processes are significantly modified by human activities. Land use and land cover have impacts on nutrient inputs and pathways in the terrestrial ecosystems and on nutrient loading in rivers and other water bodies. The nutrient export to downstream plays a critical role in coastal water quality and is the primary condition for eutrophication.
This study presents a modeling framework for integrating terrestrial nitrogen inputs (Net Anthropogenic Nitrogen Inputs, NANI), a land surface model (The community Noah land surface model with multi-parameterization options, Noah-MP-CN) and a river routing model (Routing Application for Parallel computation of Discharge, RAPID) to simulate nitrogen transport in river networks. The Noah-MP-CN model was originally developed for weather and climate prediction, but recent modifications to the Noah-MP-CN model introduce large capabilities for nitrogen dynamics and hydrological simulations in river networks.
A six-year case study is conducted in the San Antonio and Guadalupe basins (2008 – 2013). The Noah-MP-CN model provides daily nitrogen loads to the river reaches through runoff. Nitrogen loadings are transported through streamflow to downstream of river basins under the impact of in-stream processes. The modeled nitrate concentrations are evaluated with the observed data at United States Geological Survey (USGS) gauge stations near the outlets of river basins.
In this study, we reflect anthropogenic nitrogen inputs on the nitrogen dynamics to represent regional nitrogen states/fluxes by replacing nitrogen input parameters of the model with NANI. The model employs atmospheric nitrogen deposition and fertilizer application rate from NANI. The NANI-implemented model simulates within Texas, one of the largest agriculture industries in the Nation. Regional differences of nitrogen inputs is expected to influence more on nitrogen state/flux variables simulation than annual differences.

Keywords: nitrogen transport, nitrogen dynamics, anthropogenic nitrogen inputs

CCG
LCPHD

Developing plant hydrodynamics in the Noah-MP land surface model

Lingcheng Li
Li, L., Jackson School of Geosciences, The University of Texas at Austin
Yang, Z., Jackson School of Geosciences, The University of Texas at Austin;
Matheny, A., Jackson School of Geosciences, The University of Texas at Austin;
Zheng, H., The Institute of Atmospheric Physics, Chinese Academy of Sciences
Yan, B., Jackson School of Geosciences, The University of Texas at Austin;

Vegetation plants with different hydraulic traits have different water use strategies, which could have different effects on the carbon-water cycle and land-atmosphere interaction. Few land surface models or dynamic vegetation models considered plant hydrodynamics at the large spatial scale. Potential problems include ET biases on diurnal scales and unrealistic ecosystem responses under water stress conditions. The goal of this study is to represent plant hydrodynamics in large-scale land surface modeling. Noah-MP land surface is chosen in this study because it is widely used in the NCAR WRF model, NASA's Land Information System, and the US National Water Model. We will compare the augmented Noah-MP with CLM5 to better understand the role of plant hydrodynamics in land surface modeling. Then We will use the augmented Noah-MP to better understand the forest hydraulic function at the ecosystem scale.

Keywords: Plant Hydrodynamics; Land surface modeling; Large scale

CCG
LCPHD

Extinction selectivity of Scleractinian corals during the Paleocene-Eocene Thermal Maximum

Anna Weiss
Weiss, A., Jackson School of Geosciences, The University of Texas at Austin, Austin, TX
Martindale, R., Jackson School of Geosciences, The University of Texas at Austin, Austin, TX

Coral reefs are particularly sensitive to environmental disturbances, such as rapid shifts in temperature or carbonate saturation. Work on modern reefs has suggested that some corals will fare better than others in times of stress and that their life history traits might correlate with species survival. These same traits can be applied to fossil taxa to assess whether life history traits correspond with coral survival through past intervals of stress similar to future climate predictions. This study aims to identify whether ecological selection (based on physiology, behavior, habitat, etc.) plays a role in the long-term survival of corals during the late Paleocene and early Eocene. The late Paleocene - early Eocene interval is associated with multiple hyperthermal events that correspond to rises in atmospheric pCO_2 and sea surface temperature, ocean acidification, and increases in weathering and turbidity. Coral reefs are rare during the late Paleocene and early Eocene, but despite the lack of reef habitat, corals do not experience an extinction at the generic level and there is little extinction at the species level. In fact, generic and species richness increases throughout the late Paleocene and early Eocene. We show that corals with certain traits (coloniality, carnivorous or suspension feeding diet, hermaphroditic brooding reproduction, living in clastic settings) are more likely to survive climate change in the early Eocene. These findings have important implications for modern coral ecology and allow us to make more nuanced predictions about which taxa will have higher extinction risk in present-day climate change.

Keywords: Extinction, Reef, Coral, Paleobiology, Paleophysiology, Paleoecology, Climate Change

CCG
LCPHD

The Role of Multi-sensor Land Data Assimilation in Runoff and Streamflow Estimation

Wen-Ying Wu
Wu, W., Jackson School of Geosciences, Department of Geological Sciences, The University of Texas at Austin, Austin, TX, USA
Yang, Z., Jackson School of Geosciences, Department of Geological Sciences, The University of Texas at Austin, Austin, TX, USA
Zhao, L., Chongqing Engineering Research Center for Remote Sensing Big Data Application, School of Geographical Sciences, Southwest University, Chongqing, China
Lin, P., The Department of Civil and Environmental Engineering, Princeton University

Runoff and streamflow are critical components of the water cycle and, reflecting integrated information on dominant hydrologic processes over the entire watersheds. Streamflow is precisely measured by gages, but the large-scale spatiotemporal variation in streamflow is poorly understood. We evaluate the impact of multi-sensor land data assimilation on intraseasonal-to-interannual availability of runoff. Eight experiments with assimilation of different combinations of satellites datasets are conducted using Community Land Model version 4 (CLM4) and Data Assimilation Research Testbed (DART). Different land states are updated upon the assimilated satellites observations (AMSR-E, MODIS, and GRACE) for 2003-2009. We compared the eight experiments to open loop. Assimilation of MODIS snow cover fraction affects simulated runoff in mid- and high-latitudes. Assimilation of lower frequencies AMSR-E brightness temperature plays an important role in soil moisture and therefore runoff in tropics. Generally, assimilating different satellite observations shows a spatially different impacts on runoff, and the combination of multiple satellite observations shows a largest spatial extend. We also quantify the impact of data assimilation by evaluating results with observation-based runoff and streamflow from GRDC. Our results suggest that land data assimilation of any of these datasets improve runoff estimation over the Arctic. This study indicates the limitation of modeling the large-scale hydrological cycle and shows how data assimilation can help improve streamflow estimation.

Keywords: data assimilation, climate model, streamflow, hydrology

EG
LCPHD

Estimating Properties from Millimetric Sized Rock Cuttings Using Micro Computed Tomography (CT)

Eric Goldfarb
Goldfarb, E., Jackson School of Geosciences, The University of Texas at Austin
Ikeda, K., Jackson School of Geosciences, The University of Texas at Austin
Ketcham, R., Jackson School of Geosciences, The University of Texas at Austin
Tisato, N., Jackson School of Geosciences, The University of Texas at Austin

Properties obtained from physical rock samples are necessary to calibrate accurate subsurface models. Models of rock type, porosity, density and elastic wave velocities are useful for civil, mining, and petrophysical engineers; hydrogeologists and municipal planners; and scientists (e.g. IODP). Cylindrical samples tens of centimeters in size are typically required to measure these properties in the laboratory. Collecting *in situ* samples such as drill cores is important to understand how rock properties change with depth; however, this is extremely expensive, and rarely done. Drilling is generally common, but rare for the purpose of collecting cores. Byproducts of all drilling activities include rock cuttings, which are millimetric sized pieces of the rock that break-off from the formation. Like cores, these cuttings come from *in situ* conditions. However, their unique sizes and shapes make them hard to test for elastic properties in the lab. Nevertheless, advances in micro-computed tomography offer new opportunities to digitally characterize regularly shaped but also small and irregularly shaped samples.

In the laboratory, we measured rock properties of a Berea sandstone core and then used micro-computed tomography to estimate rock properties on millimetric sized pieces of that core. These pieces are comparable to drill cuttings. To create our three-dimensional rock model we used the “targeted method” that does not involve segmentation. By scanning the sample along with phantoms of known density (air, two types of glass, and quartz), an empirical curve is created and used to convert X-ray attenuation to density for each voxel. Porosity is then estimated from its inverse relationship to density. An effective medium theory is used to translate the 3D distribution of porosity into elastic properties. Finally, we simulated on the numerical model the same tests that we performed on the laboratory core.

Elastic wave velocities, density, and porosity were estimated. Results from individual cuttings are accurate within 10% from the laboratory measured core. When averaging multiple cuttings, the results converge to within 5% of the laboratory core values. This suggests that at first order, scanning many cuttings can provide an analogue for an equivalent core.

Keywords: Velocity, Porosity, Computed Tomography (CT), Rock Physics, Numerical Simulation

EG
LCPHD

Numerical and Laboratory Study of Low-frequency Elastic Properties of Limestone

Ken Ikeda
Ikeda, K., Jackson School of Geoscience, The University of Texas at Austin, Austin, TX
Subramaniyan, S., Department of Earth Sciences, ETH Zurich, Zurich, Switzerland
Quintal, B., Institute of Earth Sciences, University of Lausanne, Lausanne, Switzerland
Saenger, E., GFZ German Research Centre for Geosciences, Helmholtz Centre Potsdam, Potsdam, Germany
Goldfarb, E., Jackson School of Geoscience, The University of Texas at Austin, Austin, TX
Tisato, N., Jackson School of Geoscience, The University of Texas at Austin, Austin, TX

To create accurate models of the subsurface geoscientists typically perform experiments and measure rock properties in centimetric sized samples. Another approach to obtaining rock properties is to perform numerical simulations by means of digital rock physics (DRP). Instead of measuring samples in the laboratory, DRP simulates common rock-physics experiments on digital samples that can be created by X-ray micro-computed tomography (micro-CT). The digital sample is stored in a three-dimensional array, representing the spatial distribution of X-ray attenuation, which is a function of material density. Often, the classic threshold-based DRP overestimates elastic properties. Instead, an alternative method, the segmentation-less approach, shows a significant improvement in estimating the elastic moduli of monomineralic rock samples. This study shows that a modified version of the segmentation-less approach can also efficiently predict low-frequency moduli of a multimineralic limestone sample.
Here, Low-frequency Young's modulus of the limestone sample was measured using the sub-resonance method and the Seismic Wave Attenuation Module (SWAM). The limestone sample was scanned with a micro-CT at the resolution of 10 micrometers per voxel. We applied a non-local mean filter and a statistical region merging algorithm to capture the spatial distribution of the dolomite phase, the calcite phase, and the pore space. Next, based on the previous step, the digital sample was partitioned into two monomineralic subsamples: the air-calcite subsample and the air-dolomite subsample. Then, each subsample was submitted to the target-less segmentation-less procedure. Following the segmentation-less procedure, each subsample CT-array was converted to density, porosity, and elastic moduli. We used a differential effective medium theory to estimate the elastic moduli of each voxel. Finally, we recombined the elastic moduli arrays of the subsamples and numerically evaluated quasi-static elastic moduli by means of the finite element code: MATelas3D. The algorithm solved for a stress tensor that minimized the elastic potential energy of the system. Then, the effective Young's modulus of the sample is approximated from the stress field. Numerical and laboratory results show good agreement. By using the segmentation-less approach we reduced the 118% modulus mismatch, which was calculated with the segmentation method, to only 13%. Further investigation is needed to improve the robustness of the method and the accuracy of the results.

Keywords: Digital rock physics, Experimental rock physics, Low-frequency moduli

EG
LCPHD

Frequency-Dependent Q Estimation Method Based on Laboratory Experiments

Ziqi Jin
Jin, Z., Department of Geological Sciences,The University of Texas at Austin, Austin, TX
Tisato, N., Department of Geological Sciences,The University of Texas at Austin, Austin, TX
McCann, M., Department of Geological Sciences,The University of Texas at Austin, Austin, TX
Ikeda, K., Department of Geological Sciences,The University of Texas at Austin, Austin, TX

Attenuation, the inverse of the quality factor (Q), describes how seismic waves lose energy while propagating in a material. In many attenuation (1/Q) estimation schemes, we generally assume that Q is frequency independent or described by a power-law. However, such assumption used, for instance in the Log Spectral Ratio, introduces a systematic bias in the estimation of Q. Instead, attenuation from field data should be considered frequency-dependent. One approach to consider frequency-dependent Q is the knowledge of attenuation mechanisms for different saturation-lithology scenarios.
Here, we measured and modeled the frequency-dependent Q of a saturated rock by means of laboratory experiments and the attenuation mechanism named wave-induced gas exsolution dissolution (WIGED), respectively. Further, to estimate the impact of Q on real seismic data, we simulate field-scale seismic reflection surveys with a numerical solver (Sofi3D). In Sofi3D, the frequency-dependent attenuation behavior is approximated by the general standard linear solid (GSLS) model. Attenuation in the GSLS model is controlled by three parameters: relaxation time (τ), relaxation frequency (f_C), and the number of relaxation mechanism (L). We fit the GSLS model to the results from laboratory measurements in a least-squares sense. Then, we implement the model in the numerical simulation. Modified Log Spectral Ratio method is applied to synthetic seismic gathers to estimate τ value. Thus Frequency-dependent Q is finally calculated using τ, L and f_C. We show that Q, approximated from the synthetic reflection events, could not be modeled with a constant or a power law Q model.
Further work will focus on performing experiments on rocks saturated with fluids containing bubbles, and to estimate frequency-dependent Q by designing a modified Log Spectral Ratio method for τ value estimation. This frequency-dependent Q estimation workflow will be applied to other attenuation mechanisms such as the wave-induced-fluid-flow.

Keywords: frequent-dependent Q estimation; wave-induced gas exsolution dissolution; laboratory experiments

EG
LCPHD

Mimicking Rock Heterogeneity in the Laboratory for Studying Buoyancy Driven Fluid Migration in Porous Media

Fnu Prasanna Ganesan Krishnamurthy
Krishnamurthy, P., Petroleum and Geosystems Engineering; Bureau of Economic Geology, The University of Texas at Austin
Meckel, T., Bureau of Economic Geology, The University of Texas at Austin
Dicarlo, D., Petroleum and Geosystems Engineering, The University of Texas at Austin

In this work, we present a novel technique for generating two dimensional beadpacks with reproducible natural geologic bedform like features in the laboratory. The heterogeneous bead-packs are constructed in a 0.6m x 0.6m x 0.01m Hele Shaw cell using an apparatus consisting of a programmable two-axis linear actuator. The mixture of glass beads are deposited into the glass cell using a feed tube attached to the actuator arm. As they fall through the tube and the chamber, and along the slope of the previously formed pile of beads, the grain mixture undergoes stratification and segregation. We utilize these mechanical sorting processes to our advantage, along with the ability to program the motion of the arm, to build crossbeds and ripple laminae in a facile manner. By using a mixture of grains, fabrics with multi-scale heterogeneity (sub mm to sub m) could be generated. Reproducibility tests showed very high correlation between different realizations of packed structures.

We use this capability to study migration of buoyant CO_2 in complex nature mimicking fabrics at scales larger than that of rock cores, during geologic carbon sequestration,. Light transmission method is used for visualization, and to calibrate and quantify saturation of the trapped non-wetting fluid during the experiments. With the ability to generate different types of heterogeneous structures in a reproducible manner, a systematic investigation of the effect of heterogeneity on trapping and migration behavior of CO_2 becomes possible

Keywords: Heterogeneity, Capillary Pressure, CO2 Sequestration, Bedforms

EG
LCPHD

Porosity and Permeability in Wolfcamp Lithofacies at Delaware Basin, West Texas

Sebastian Ramiro Ramirez
Ramiro-Ramirez, S., Institute for Geophysics, The University of Texas at Austin, TX
Bhandari, A., Institute for Geophysics, The University of Texas at Austin, TX
Reed, R., Bureau of Economic Geology, The University of Texas at Austin, TX
Flemings, P., Institute for Geophysics, The University of Texas at Austin, TX
Polito, P., Department of Geological Sciences, The University of Texas at Austin, TX

Porosity and permeability measurements in Wolfcamp Formation samples, when combined with a simple flow model, demonstrate that most fluid volume is stored in non-laminated mudstones, while most production occurs in mud- to grain-supported carbonates and laminated mudstones. Our samples correspond to four different lithofacies from the lower interval of the Wolfcamp Formation and were tested at 'as-received' conditions. The argillaceous and siliceous mudstones lithofacies have effective permeabilities ranging from 9.9×10^{-21} m^2 to 3.1×10^{-20} m^2 (10 nD to 30 nD) and total porosity between 13.5% and 16.5%. In contrast, effective permeabilities in laminated mudstone and siliceous wackestone/packstone lithofacies range from 4.9×10^{-19} m^2 to 9.9×10^{-19} m^2 (500 nD to 1000 nD) and the total porosity is ~5.5%. These lithofacies are heterogeneously distributed in the stratigraphic section. The argillaceous and siliceous mudstones occupy ~70% of the thickness and thus house ~90% of the total pore volume; the laminated mudstone and siliceous wackestone/packstone lithofacies occupy only ~7% of the thickness but are 12 to 25 times more permeable. This suggests that most of the oil and water in the Wolfcamp formation is stored or 'trapped' in low-permeability, high-porosity mudstones, while high-permeability, low-porosity carbonates and laminated mudstones act as preferential flow pathways during production. Our experimental approach to estimate total porosity included a combination of helium porosimetry and nuclear magnetic resonance measurements. We determined the in-situ effective permeability using the steady-state liquid (dodecane) method at varying confining pressures and Darcy's law. Our findings will help to understand the origin of the high water cut in the Wolfcamp formation by identifying which lithofacies can store most of the oil and water and which ones are responsible for transmitting these fluids during production.

Keywords: Shale, Petrophysics, Permian Basin, Permeability, Porosity, Drainage

EG
LCPHD

Deep learning for seismic interpretation

Yunzhi Shi
Wu, X., Bureau of Economic Geology
Shi, Y., The University of Texas at Austin
Fomel, S., The University of Texas at Austin

Seismic interpretation often involves tasks of extracting structural features including horizons, faults and salt bodies from 3D seismic images. Manually interpreting such seismic structural features can be highly time-consuming and labor-intensive. Although the seismic structural interpretation have been automated to some extent by others, fault and salt body interpretation today typically requires significant manual effort. We propose to improve the automatic seismic fault and salt body interpretation by using the convolutional neural network (CNN), which is powerful in image classification and segmentation. In our CNN methods, we consider the fault and salt body interpretation as problems of image classification and segmentation, respectively. Specifically, in our CNN method for fault interpretation, we construct a 7-layer CNN to first estimate local fault orientations (dips and strikes) from seismic image patches. With the estimated fault orientations, we then construct anisotropic Gaussian functions that mainly extend along the estimated fault dips and strikes. We finally stack all the fault-oriented Gaussians to generate a fault probability image. Although trained by using only synthetic seismic images, the CNN model can accurately estimate fault orientations within real seismic images acquired at different surveys. The fault probability image, computed from the estimated fault orientations, displays cleaner, more accurate, and more continuous fault features than those in the conventional fault attribute images. In our CNN method for salt body interpretation, we propose to adopt an alternative network architecture, inspired by Segnet and U-Net, to detect salt bodies from seismic images. This architecture is composed of a stack of encoders followed by a corresponding decoder stack which feeds into a softmax classification layer. Both encoder and decoder are fully convolutional layers. In order to test the proposed architecture, we generate salt body labels interactively with the aid of automatic tools. We first train the network on the selected 2D slices, then validate the model by predicting salt body location on other unseen slices. By using the proposed CNN methods, we are able to obtain more accurate results of fault and salt body interpretation than the conventional automatic methods.

Keywords: Deep learning, seismic interpretation, fault, salt

EG
LCPHD

Segmentation of Thin Sections with Machine Learning

David Tang
Tang, D., Department of Geological Sciences, The University of Texas at Austin, Austin, TX
Spikes, K., Department of Geological Sciences, The University of Texas at Austin, Austin, TX
Milliken, K., Bureau of Economic Geology, The University of Texas at Austin, Austin, TX

Thin sections provide geoscientists with a wealth of information about a rock's makeup and diagenetic history. For example, the amount of clay minerals or percentage of porosity can play a large role in the quality of a reservoir. However, the analysis of thin sections often requires many hours of manual labor, limiting the amount of analysis a single person can accomplish in a reasonable time frame.

Supervised machine learning brings the promise of automating time-consuming tasks, such as point counting and segmentation (i.e., identifying each pixel in a micrograph), to thin section analysis. In supervised machine learning, labeled examples are provided for the machine to learn from. Previous attempts using machine learning required an expert to hand design "features" to serve as inputs into a machine learning algorithm. These features could be mathematical representations of a grain's characteristics such as cleavage, color, or twinning. The design of such features can be quite arbitrary, and features that work in one thin section may not work for others. Here we apply a recent development in machine learning that only requires traced grains as the input. The traced grains form a six-dimensional image (RGB color channels for both plane- and cross-polarized light images), and the resulting output is a fully segmented image.

Keywords: Machine Learning, Thin Sections, Segmentation, Point Counting

EG
LCPHD

UNSUPERVISED PHYSICS BASED NEURAL NETWORKS FOR SEISMIC MIGRATION

Janaki Vamaraju
Vamaraju, J., University of Texas Institute for Geophysics
Sen, M., University of Texas Institute for Geophysics

This work introduces a novel framework for combining physics based forward models and neural networks to advance seismic processing and inversion algorithms. Migration is an effective tool in seismic data processing and imaging. Over the years the scope of these algorithms has broadened and today, migration is a central step in the seismic data processing workflow. However, no single migration technique is suitable for all kinds of data and all styles of acquisition. There is always a compromise on the accuracy, cost and flexibility of these algorithms. On the other hand, machine learning algorithms and artificial intelligence methods have been found immensely successful in applications where internet-scale data is available. The applicability of these algorithms is being extensively investigated in scientific disciplines such as exploration geophysics with the goal of reducing exploration and development costs. In this context, we propose to use a special kind of unsupervised recurrent neural network and its variant, Hopfield neural networks and Boltzmann machine to solve the problems of Kirchhoff and Reverse time migrations. We employ a Hopfield neural network to migrate seismic data and use simulated annealing to globally optimize the cost function of the neural network. The weights and biases of the neural network are derived from the physics based forward models that are used to generate seismic data. The optimal configuration of the neural network after training corresponds to the minimum energy of the network and thus gives the reflectivity, solution of the migration problem. Using synthetic examples, we demonstrate that 1) Hopfield neural networks are fast and efficient, and 2) provide high resolution reflectivity images with mitigated migration artifacts and improved spatial resolution. In specific, the presented approach minimizes the artifacts that arise from limited aperture, low subsurface illumination, coarse sampling and gaps in the data.

Keywords: Seismic Imaging, Neural Networks, Inverse Problems, Seismic migration

MG
LCPHD

Nature and variation of oceanic crust at a global endmember, the Mid-Cayman Spreading Center

Jennifer Harding
Harding, J., University of Texas at Austin, Austin, TX
Van Avendonk, H., University of Texas Institute for Geophysics, The University of Texas at Austin, Austin, TX
Hayman, N., University of Texas Institute for Geophysics, The University of Texas at Austin, Austin, TX

Oceanic crust is accreted at a range of spreading rates, anywhere from ultraslow rates of < 20 mm/yr to fast rates of > 75 mm/yr full-rate. The nature of oceanic crust produced at spreading centers changes with spreading rate, a trend known for almost three decades. While faster spreading centers produce fairly heterogeneous, igneous crust through mainly magmatic processes, slower spreading centers produce more heterogeneous crust, both in thickness, lithology, and morphology. The transition from slow to ultraslow spreading rates was previously thought to be abrupt, but recent, larger global compilations of seismic crustal thickness contain a more gradual change in crustal thickness with spreading rate in addition to an increase in variability with decreasing spreading rate. In order to understand the processes that control this trend, we investigated the oceanic crust at the Mid-Cayman Spreading Center (MCSC), one of the slowest spreading centers in the world. Previous seismic tomography modeling of the central MCSC region imaged very heterogeneous seismic structure, and many areas had ambiguous lithological interpretations. In order to uncover the magmatic processes that lead to the observed seismic variability, the lithological interpretations of seismic structure need to differentiate between serpentinized mantle and igneous crust. Consequently, we use multiple methods and data together to reduce non-uniqueness in interpretation. Three profiles in the central MCSC region were analyzed using P-wave travel-time tomography, forward seismic amplitude modeling, and forward gravity modeling. Lithology was then interpreted considering the results from these three methods in addition to seafloor rocks from previous studies in order to differentiate between exhumed serpentinized mantle and igneous crust. We find that much of the < 6 Ma oceanic crust at the MCSC is a mixture of gabbroic bodies within serpentinized peridotite, with some amount of basaltic cover. The average magmatic crustal thickness is ~ 3 km, but ranges from 0-6 km, which is ~2 km less than the seismic crustal thickness estimates. The greatest magmatic crustal thickness occurs at oceanic core complexes (OCCs), while the minimum occurs where there is exhumed mantle towards segments ends. The variability observed in seismic crustal thickness trends can be explained by fluctuations in magmatism, both along-axis and across-axis in time, and does not require a sharp shift in crustal accretion processes but allows for a continuum of melting processes that vary with spreading rate.

Keywords: oceanic crust, seismology, tectonics, ultraslow-spreading centers

MG
LCPHD

Extraordinary preservation of a deepwater channel-levee system in Green Canyon 955, Northern Gulf of Mexico

Patrick Meazell
Meazell, K., Department of Geological Sciences, The University of Texas at Austin
Flemings, P., Department of Geological Sciences, The University of Texas at Austin
Santra, M., Institute for Geophysics, The University of Texas at Austin

Pressure cores of hydrate-bearing turbidite deposits in Green Canyon block 955 (GC 955), deepwater Gulf of Mexico, record extraordinary preservation of sedimentary structures that allow for a detailed sedimentological study of deepwater channel-levee deposits. The levees of the deepwater channel in GC 955 are composed of alternating sandy silt and clayey silt layers. Gas hydrate is concentrated within the sandy silts, with little to no hydrate is present within the clayey silts. The greatest amount of sandy silt is found near the base of the system, which fines upwards. Bed thickness follows a similar pattern, with a break that may record a gravitational failure of the levee. We propose a depositional model to explain the architectural elements of a deepwater channel system. This study provides insight into important deepwater hydrocarbon reservoirs.

Keywords: deepwater channel-levee systems, gas hydrate, Gulf of Mexico

LCPHD-15

MG
LCPHD

Heterogeneous Upper Plate Extension in South Central Chile and Implications for Megathrust Fault Development

Kelly Olsen
Olsen, K., Institstute for Geophysics, The University of Texas at Austin, Austin, TX
Bangs, N., Institstute for Geophysics, The University of Texas at Austin, Austin, TX
Trehu, A., College of Earth, Ocean, and Atmospheric Sciences, Oregon State, Corvallis, OR
Contrerars-Reyes, E., Departamento de Geofísica, Universidad de Chile, Satiago, Chile

In early 2017, we collected ~5,000 km of multichannel seismic data in south central Chile using a 15.1 km long streamer and 6,600 in^3 airgun source. Prestack depth migrated images of these data show extensive normal faulting within the slope and shelf sediment that we have used to infer variations in the shallow stress along the margin. In the 2010 Mw8.8 Maule rupture area (34-39°S), normal faulting begins within the upper 1/3 of the slope (>25km from the trench), and typically extends landward across the shelf to the end of the seismic line, 80-100 km from the trench. Listric faults with ~0.5-1 km spacing and offsets up to 500 m tend to form in the upper slope, while low offset (~10 m), high angle (55-65°) normal faults form across the shelf. In the 1960 Mw9.5 Valdivia rupture area (39-44°S), normal faulting begins ~15 km landward of the trench, much closer to the toe than in the Maule area. Again, listric faults form across the slope and high-angle normal faults form across the shelf. In both regions, normal faults extend through the entire slope/shelf sediment section, but offsets in the underlying middle prism basement (paleoaccretionary complex) are below seismic resolution.

Convergent margins typically undergo compressional stress, but can develop extensional structures due to uplift and oversteepening related to subduction of large topographic features, shortening from faults and folds, and underplating. Other processes such as subduction erosion or gravitational collapse caused by lowering of basal shear stress also result in extension. Due to the subduction of a thick (1-2 km) sediment packet, and the lack of large (>1 km) seamounts or ridges on the incoming Nazca plate at the scale of these observations, it is unlikely that ridge subduction, tectonic erosion, or major changes in megathrust stress conditions are currently factors in upper plate extension. Seismic images in both areas show extensive trench sediment subducting beneath the toe. Consequently, some or all of these underthrust sediments are likely underplated, which could cause the upper plate extension. On the basis of normal fault patterns, sediment may be underplated closer to the toe within the Valdivia region than in the Maule region, leading to important differences in conditions along the plate boundary fault between these two great earthquake slip regions.

Keywords: subduction zones, earthquakes, seismic reflection imaging, Chile, fault-mapping

PS
LCPHD

Fracture orientations of granitoid peak ring rocks in the Chicxulub impact crater

Naoma McCall
McCall, N., Institute for Geophysics, Jackson School of Geosciences, University of Texas at Austin, Austin, TX
Gulick, S., Institute for Geophysics, Jackson School of Geosciences, University of Texas at Austin, Austin, TX
Hall, B., Enthought, Inc, Austin, TX
Riller, U., Institut für Geologie, Universität Hamburg, Bundesstrasse 55, Hamburg, 20146, Germany
Poelchau, M., University of Freiburg, Geology, Albertstraße 23b, Freiburg, 79104, Germany
Rae, A., Department of Earth Science and Engineering, Imperial College London, SW7 2AZ, UK
Morgan, J., Department of Earth Science and Engineering, Imperial College London, SW7 2AZ, UK
Lofi, J., Géosciences Montpellier, Université de Montpellier, France

In 2016 IODP/ICDP Expedition 364 drilled the peak ring of the Chicxulub impact structure, and recovered core from depths of 505 meters below sea floor (mbsf) to 1334 mbsf. The bottom 590 meters of core is largely composed of uplifted, heavily fractured and deformed granitic rocks. The core was scanned using x-ray computer tomography (CT), resulting in a three-dimensional model of the core imaged at 0.3mm resolution. Using orientation measurements of planar fractures in the granitic core and crosscutting relationships within CT-defined fracture facies, we seek to confirm the direction and relative timing of rock displacement and elucidate current models of crater formation.

Using CT data, we grouped the fractures into four initial facies: open fractures; filled fractures; discrete fine fractures, and pervasive fine fractures. Filled fractures are filled with cataclasites, ultra-cataclasites and hydrothermal minerals. After orienting the core by matching the CT images to acoustic images of the borehole wall, we used CT images to measure the dip and dip direction of over 2,000 open, filled and discrete fine planar fractures. We verified the fracture facies before measurement by comparing the CT data with acoustic wellbore images and high-resolution linescan images of the split core. Pervasively fractured intervals proved too deformed to accurately measure individual fracture planes.

We observe that fractures filled with ultra-cataclasite and cataclasite have the strongest preferred orientations, with the highest density of ultra-cataclasite and cataclasite fractures dipping towards the southwest and east respectively.

Keywords: Chicxulub, Crater, K-Pg, Fractures, Computer Tomography

PS
LCPHD

Helium Diffusion Kinetics of Shocked Zircon from the Chicxulub Impact Crater

Catherine Ross
Ross, C., Department of Geological Sciences, University of Texas at Austin
Stockli, D., Department of Geological Sciences, University of Texas at Austin
Rasmussen, C., Institute of Geophysics, University of Texas at Austin
Gulick, S., Institute of Geophysics, University of Texas at Austin

Less than 10% of Earth's impact craters are accurately or precisely dated. (U-Th)/He dating of impactites is a promising application of low-T thermochronometry and has been employed to directly date the timing of shock heating and post-impact hydrothermal circulation. To evaluate the accuracy of obtained (U-Th)/He impact ages, and possible effects of post-impact hydrothermal fluid flow, a quantitative understanding of He diffusion kinetics in shock-damaged minerals is indispensable. Others have investigated the effects of radiation damage on He diffusion kinetics and He retentivity in apatite and zircon, but no systematic studies exist on the effects of impact-induced shock microstructures and damage. In zircon, high dosages of radiation damage, leading to metamictization, appears to systematically lower He retentivity due to damage interconnectivity, while in apatite low damage levels tend to lead to increased He retentivity due to trapping.

The IODP-ICDP Expedition 364 drill core from the Chicxulub crater enables us to study the effects of impact-induced shock microstructures in zircon on He diffusion kinetics. For this purpose, variably shocked zircon crystals, ranging from brittle cracking to planar deformation features to granular (polycrystalline) textures to amorphization were imaged using scanning electron microscopy. Cycled fractional-loss in-vacuo helium diffusion experiments were heated from 300-600°C for 1-3 hours to determine the diffusion kinetics as a function of shock-induced damage. We found that at lower shock levels, zircon is characterized by activation energies and He retentivities comparable to undamaged zircon, while exhibiting typical damage annealing behavior during prograde heating. At higher shock levels (i.e., planar deformation and granular grains), zircon displays a drastic decrease in the activation energy during low-T prograding heating steps (<420°C), making the zircon effectively unretentive. We attribute this sudden decrease in retentivity to thermal fragmentation during prograde heating. Quantitative constraints on He diffusion kinetics as a function of impact microstructure are critical to our understanding of the robustness and reliability of He dating of impact events and the thermal sensitivity to post-impact hydrothermal processes and burial.

Keywords: helium diffusion, zircon, Chicxulub crater, shock metamorphism

SETP
LCPHD

Cordillera evolution along the southern Central Andean margin recorded by detrital zircon U-Pb and Hf isotopes

Tomas Capaldi
Capaldi, T., Department of Geological Sciences, The University of Texas at Austin, Austin, TX
Horton, B., Department of Geological Sciences, The University of Texas at Austin, Austin, TX
McKenzie, R., Department of Earth Sciences, University of Hong Kong, Hong Kong, China
Mackaman-Lofland, C., Department of Geological Sciences, The University of Texas at Austin, Austin, TX
Stockli, D., Department of Geological Sciences, The University of Texas at Austin, Austin, TX

Detrital zircons from ancient to modern sediments provide an integrated view of long-lived Cordilleran processes that involve orogenic growth and collapse, arc magmatism, terrane accretion, and slab dynamics along the Andean margin of South America. Combined U-Pb geochronology and Hf isotope analyses of detrital zircon represents a powerful method for evaluating regional geologic patterns and the processes of crustal addition, removal, and recycling. Whereas zircons with positive εHf values similar to the depleted mantle originated from juvenile crust, zircons with negative εHf values crystallized from melts derived from old recycled crust. In considering the Phanerozoic magmatic and tectonic history of the continental margin along Chile-Argentina (28-33°S), our study highlights six key elements of the Cordilleran system. (1) Cambrian-Ordovician Pampean and Famatinian arc magmatism during subduction and accretion of the Cuyania terrane, involving evolved crustal-derived magmatism (mean ?Hf -5.24). (2) Silurian-Early Carboniferous passive margin characterized by waning arc magmatism with Late Devonian evolved magmatism (mean ?Hf -6.75) overprinting early Paleozoic arcs. (3) Late Carboniferous-Permian initiation of the Gondwanan arc and associated crustal orogenesis producing distinctively low values (mean ?Hf -6.31). (4) Permian-Triassic orogenic collapse and emplacement of the Choiyoi igneous complex, recording juvenile magmatic influx with more positive ?Hf values averaging -0.35. (5) Jurassic-Paleogene Andean arc magmatism highlighted by cyclical, ~20-30 Myr phases of juvenile, mantle-derived magmatism (highly positive mean ?Hf +6.49). (6) Neogene flat-slab subduction during Andean shortening and induced magmatic crustal recycling of thickened continental crust (mean ?Hf -0.29). This study highlights how Cordilleran arc systems (a) produce evolved magmas during initial subduction-accretion events and orogenesis, (b) transition from crustal to more juvenile magmas generated during orogenic collapse, (c) show persistent juvenile mantle-derived magmas during cyclical Andean-style arc magmatism, and (d) trend toward more evolved magma production during crustal shortening and phases of flat-slab subduction.

Keywords: Andes, magmatism, geodynamics, sediment record

SETP
LCPHD

Tectonometamorphic evolution of the Southern and Central Menderes Massif, western Turkey

Thomas Etzel
Etzel, T., Department of Geological Sciences, University of Texas at Austin
Catlos, E., Department of Geological Sciences, University of Texas at Austin
Kelly, E., Department of Geological Sciences, University of Texas at Austin
Atakturk, K., GeoEngineers, Seattle, WA
Cemen, I., University of Alabama
Lovera, O., University of California, Los Angeles

Geologic history of the Menderes Massif (MM), western Turkey is difficult to discern, partly due to a series of collisional and extensional events, each imparting a deformation fabric and, in some cases, producing recrystallization of prograde metamorphic minerals. To avoid recrystallization effects, we focused on garnet crystals, which commonly retain prograde chemical zoning, and constructed thermodynamic models of chemical zoning from cores to rims, yielding estimates of pressure (P) and temperature (T) changes during prograde growth.

Models from Selimiye nappe rocks in the Southern Menderes Massif (SMM) show an almost linear P-T path from 555-570^{o}C and 5.9-6.0 kbar to 582-586^{o}C and 7.3-7.7 kbar. Models from Çine nappe rocks in the SMM show "N-shaped" P-T paths where core growth initiates at 510-551^{o}C and 5.1-5.9 kbar and rim growth terminates at 568-583^{o}C and 6.1-7.0 kbar, with observed mid-path P decreases of up to 1.0 kbar. In the Central Menderes Massif (CMM), in Bozdag and Bayindir nappe rocks, only two paths were successfully modeled (from adjacent outcrops in the same structural block in the Bayindir nappe). The first starts at 565^{o}C and 6.4 kbar and increases to 592^{o}C and 7.5 kbar, and the second is isobaric from 531^{o}C and 7.1 kbar to 571^{o}C and 7.3 kbar. Additional P-T estimates of garnet core growth in the CMM rocks, applied to highest spessartine concentrations near garnet geometric centers and made by isopleth thermobarometry, give 530-625^{o}C and 6.0-7.0 kbar.

If intracrystalline diffusion affected CMM core chemical zoning, growth conditions may be overestimated. Further, given the inconsistency between Bayindir paths, we propose CMM garnets experienced thermal conditions different from SMM samples. The simple SMM paths suggest Selimiye nappe garnets grew during continuous burial whereas complex Çine nappe paths are consistent with repeated burial. Overlap between the Selimiye path and the second Çine pressure increase may imply contemporaneous growth during a second burial event, possibly from overthrusting of Cyclades-Menderes Thrust hanging wall following closure of the Izmir-Ankara Ocean during the Alpine Orogeny.

Keywords: Menderes Massif, Garnet, Thermobarometry

SETP
LCPHD

Triassic and Jurassic Rift Basin Records of Continental Breakup along the Eastern North American Margin, U.S.A.

Zachary Foster-Baril
Foster-Baril, Z., Department of Geological Sciences, The University of Texas at Austin, Austin, TX
Stockli, D., Department of Geological Sciences, The University of Texas at Austin, Austin, TX
Bailey, C., Department of Geology, College of William & Mary, Williamsburg, VA
Wilk, K., Department of Geology, College of William & Mary, Williamsburg, VA
Duke, H., Department of Geology, College of William & Mary, Williamsburg, VA

The Triassic and Jurassic syn-rift basin fill along the Eastern North American Margin (ENAM) provides insights into the initial rifting, crustal necking and lithospheric attenuation, and the interplay between crustal thinning and the transition to magmatic break-up. These proximal ENAM rift basins, from New Hampshire to South Carolina, record the early tectonostratigraphic and 3-D geometric evolution of continental rifting characterized by ~30 Myr of deposition prior to CAMP magmatism and continental break-up. The alluvial, fluvial, and lacustrine lithofacies of the Newark Supergroup comprise the proximal rift strata of several individual basins. Carnian to Sinemurian deposits occur in a series of half grabens with predominately east-dipping basin bounding faults that formed along preexisting Appalachian-Variscan transpressive fault boundaries. While previous studies focused on individual basin structures and stratigraphy, no integrated regional tectonic, stratigraphic, or provenance studies of rift basin evolution framed by modern models exist for the ENAM basins.

Sedimentation patterns and border fault exhumation histories provide constraints on the style of rifting and mechanics responsible for continental extension and thinning pre- and post-CAMP. This study presents extensive new regional DZ U-Pb-He provenance data integrated with detailed stratigraphy and bedrock thermochronology to elucidate 1) the evolution of 3D sediment dispersal pathways during progressive rifting, 2) the timing and geometric evolution of crustal extension, and 3) the timing of magmatism and its consequence for the evolution of ENAM rifting and syn-rift stratigraphy. Preliminary DZ U-Pb results and field observations from the Culpeper Basin, located in Virginia and Maryland, show that Carnian deposition was proximally sourced from the adjacent basin bounding footwall, but Norian and Rhaetian strata were primarily sourced from the east with a dramatic reduction of footwall input. The syn-magmatic (CAMP) sedimentary rocks show source terranes that include the adjacent footwall and hanging wall. These results suggest two major paleodrainage reconfigurations during progressive rifting with the first in the Carnian and the second during CAMP magmatism.

Keywords: Rifting, Triassic, Jurassic, ENAM

LCPHD-21

SETP
LCPHD

Drainage networks in the early-northern Andes Mountains: Paleogene depositional and paleo-environmental record of the Quingeo Basin, Ecuador

Sarah George
George, S., Department of Geological Sciences, The University of Texas at Austin, Austin, TX
Horton, B., Department of Geological Sciences and Institute for Geophysics, The University of Texas at Austin, Austin, TX
Vallejo, C., Departamento de Geología, Escuela Politécnica Nacional, Quito, Ecuador

The Paleogene Quingeo Basin sits at ~2700 m elevation between the Eastern and Western Cordilleras of Ecuador and preserves one of the only hinterland Paleogene sedimentary records in this portion of the Andes. The original basin position (forearc, hinterland, or foreland) is unknown, yet is key to reconstructing early Andean drainage networks and topographic growth of the Eastern and Western Cordilleras. Using measured sections, clast counts, paleocurrent measurements, and detrital zircon U-Pb geochronology, we address the age and source of sedimentary basin fill of the Quingeo Basin, the depositional systems present, and implications for large-scale sediment routing patterns during early Andean uplift. Together these data sets suggest that the Quingeo Basin formed in the early Paleogene and rapidly filled with sediments derived from the Eastern Cordillera. Provenance and maximum depositional ages suggest early emergence of the Eastern Cordillera, and seem to suggest that the Western Cordillera in southern Ecuador did not form until after the cessation of deposition in Quingeo Basin.

Keywords: Andes, Ecuador, basin analysis, U-Pb detrital zircon geochronology, sediment routing

SETP
LCPHD

Provenance and Pathways of the Cretaceous-Paleogene Paleo-Rio Grande River: Deciphering Signals from Complex Source Terranes Using Detrital Zircon Geo-Thermochronology

Cullen Kortyna
Kortyna, C., The Department of Geological Sciences, The University of Texas at Austin, Austin, TX
Stockli, D., The Department of Geological Sciences, The University of Texas at Austin, Austin, TX
Sharman, G., Department of Geosciences, The University of Arkansas, Fayetteville, AR
Covault, J., Bureau of Economic Geology, The University of Texas at Austin, Austin, TX

Depth-profile detrital zircon (DZ) U-Pb geochronology provides opportunities for new insights into source-to-sink systems that drain complex, highly variable source terranes. Numerous studies have employed DZ U-Pb geochronology to reconstruct how Paleogene fluvial sediments were routed through the W U.S. and Mexico Cordillera to fluvial-deltaic strata along the Gulf of Mexico. However, there is still considerable uncertainty surrounding sediment sources and sediment dispersal pathways for the Late Cretaceous and Paleogene Paleo-Rio Grande river system. Competing interpretations disagree on whether the Paleo-Rio Grande predominantly drained source terranes in W Mexico or the SW U.S. As a consequence, paleo-Rio Grande deltaic deposits along the south Texas coast are not well linked to up-dip sediment sources and tectonic regimes. This study combines depth-profile LA-ICP-MS DZ U-Pb data from nearshore fluvial-deltaic strata in S and SW Texas with depth-profile data from continental fluvial strata 100's of km's up-dip in W Texas to determine likely sediment source terranes and delineate sediment dispersal pathways. Selecting zircons dated by U-Pb for (U-Th)/He double dating will provide insight into the exhumation history of specific source terranes within the S Texas sediment-routing system.

DZ U-Pb age spectra (~7200 ages from 52 samples) from Cretaceous-Paleogene fluvial-deltaic sediments in south Texas and the Tornillo Basin of west Texas are characterized by dominant Paleogene-Late Cretaceous age modes, subordinate Jurassic, 1.4, and 1.7 Ga and minor Permo-Triassic, Silurian-Ordovician, Neoproterozoic, and 1.1 Ga age modes, and a scarcity of Early Cretaceous DZ ages, typical of sources from the Western U.S. but not from western Mexico. DZ core and rim age relationships show six main clusters: Jurassic cores with Late Cretaceous rims, 1.1 Ga cores with Ediacaran-Ordovician rims, 1.4-1.7 Ga cores with Late Cretaceous-Paleocene rims, 1.4-1.7 Ga cores with Permian rims, 1.4 Ga cores with 1.1 Ga rims, and 1.7 Ga cores with 1.4 Ga rims. Detrital zircon U-Pb ages, including core and rim relationships, suggest that the paleo-Rio Grande river system received sediment from a mixture of recycled sedimentary, volcanic, and basement source terranes in southeastern Arizona/New Mexico, northeastern Mexico (Chihuahua Trough and Sabinas Uplift) and southern Colorado/New Mexico (e.g., Colorado Mineral Belt). This interpreted catchment area is extensive, incorporating large portions of the southwestern U.S. and northeastern Mexico where it drained a tectonically active hinterland characterized by first-cycle magmatic input and sedimentary recycling of Laramide inversion structures. Furthermore, this dataset provides robust constraints on the sediment sources and pathways of the paleo-Rio Grande river system to the Gulf of Mexico and offers a predictable set of DZ signals to compare against offshore datasets in order to evaluate sediment mixing and routing in shelfal and deepwater GOM systems. Lag-time diagrams from (U-Th)/He double dates will give first order approximations of hinterland erosion and sediment input to provide better constraints on the sediment budget of the Gulf of Mexico.

Keywords: Provenance, Texas, Sediment-Routing, Detrital Zircon Geochronology, Rio Grande

SETP
LCPHD

Andean deformation and foreland basin evolution during Neogene changes in subduction zone geometry (32-33°S)

Chelsea Mackaman-Lofland
Mackaman-Lofland, C., University of Texas at Austin, Austin, TX
Horton, B., University of Texas at Austin, Austin, TX
Fuentes, F., YPF, Buenos Aires, Argentina
Constenius, K., University of Arizona, Tucson, AZ
Ammirati, J., Universidad de Chile, Santiago, Chile
Stockli, D., University of Texas at Austin, Austin, TX
Capaldi, T., University of Texas at Austin, Austin, TX
Orozco, P., Universidad Nacional de San Juan, San Juan, Argentina
Alvarado, P., Universidad Nacional de San Juan, San Juan, Argentina

The southern Central Andes recorded retroarc shortening, basin evolution, and magmatic arc migration during Neogene changes in subduction. Above the modern flat-slab segment at 32-33°S, spatial and temporal linkages between thin- and thick-skinned foreland shortening, basement-involved exhumation of the main cordillera, and lower-crustal hinterland thickening remain poorly resolved. We integrate new geochronological and thermochronological data for bedrock and Neogene foreland basin fill with structural, sedimentological, and broadband seismic results to reconstruct the exhumation history and evaluate potential geometric linkages across several structural domains. $^{40}Ar/^{39}Ar$ volcanic ages and zircon U-Pb maximum depositional ages for synorogenic clastic deposits in the Manantiales Basin constrain the timing of synorogenic sedimentation to ~22-12 Ma. Detrital zircon age distributions record sequential unroofing of thin-skinned thrust sheets in the main cordillera until ~15 Ma, followed by shutoff of the main cordillera provenance signal and a shift from fluvial to alluvial fan deposition. Apatite (U-Th)/He cooling ages confirm rapid exhumation of basement-involved structural blocks along the basin margins from at least ~15-5 Ma, consistent with the timing of the Manantiales facies and provenance shifts and a coeval (~12-10 Ma) pulse of thin-skinned shortening and exhumation previously identified in the eastern foreland. We compare thermochronometry results with forward modeled low-temperature cooling ages to explore whether the regional episode of middle to late Miocene exhumation was accommodated by (a) geometrically disconnected but contemporaneous basement-involved and thin-skinned shortening, or (b) a regionally connected thin- and thick-skinned decollement system. Finally, late Miocene–Pliocene (~5-2 Ma) cooling ages in the hinterland reflect passive uplift above a major footwall ramp during the latest stage of Andean orogenesis.

Keywords: Andes, Argentina, flat-slab subduction, fold-thrust belt, foreland basin, provenance, U-Pb geochronology, (U-Th)/He thermochronology

SETP
LCPHD

Inner core hemispherical differences inferred from waveform modeling of stacked dense array data

Peter Nelson
Nelson, P., Jackson School of Geosciences, The University of Texas at Austin, Austin, TX
Grand, S., Jackson School of Geosciences, The University of Texas at Austin, Austin, TX

Knowledge of the velocity and attenuation structure at the base of the outer core and top of the inner core is crucial to understanding core dynamics. Here we stack data recorded by the dense HiNet(Okada et al., 2004) and CEA Arrays at epicentral distances of 130-142o and 148-160o to create low noise PKP AB, DF, CD and BC waveforms sampling the two hemispheres of the inner core (Creager, 1999) over a large distance range. The data sampling the western hemisphere is poorly fit by AK135 (Kennett et al., 1995) while the data sampling the eastern hemisphere is fit slightly better. We invert for ICB depth in addition to the velocity and attenuation at the bottom 400 km of the outer core and top 600 km of the inner core using the reflectivity method along with very fast simulated annealing (VFSA) (Muller,1985; Sen and Stoffa 1991). We find to fit the timing and relative amplitude of the PKP phases there must be a broad low velocity zone in the western hemisphere and a thin high velocity zone in the eastern hemisphere right below the ICB.

Keywords: Core Seismology

SETP
LCPHD

Reconstructing middle to lower crustal thermal and tectonic histories from apatite U-Pb thermochronometry by laser-ablation depth-profile ICP-MS analysis

Margaret Odlum
Odlum, M., UT Austin
Stockli, D., UT Austin

Apatite U-Pb dating by TIMS and ICP-MS using whole or polished grains has been used to investigate thermal processes and exhumation histories of middle and lower crustal rocks. However, these bulk ages generally do not reveal continuous thermal history information and do not allow distinguishing between rapid or slow monotonic cooling, more complex thermal histories, such protracted residence in the partial retention zone or reheating, or complex growth or recrystallization (crack and seal) during metamorphism or deformation, critical for accurate geologic and tectonic interpretations. Detailed apatite depth profiling LA-ICP-MS U-Pb analysis presents the opportunity to recover radial age profiles and evaluate the topology of in terms of diffusive loss or non-Fickian processes with sub-micron resolution and recover quantitative thermal history information, while also constraining the intra-grain Pb common (Pbc) composition and being able to correct for it. This study presents a detailed workflow for apatite U-Pb depth-profile LA-ICP-MS analysis to understand U-Pb age topology, intra-grain complexities, and data interpretation. First, unpolished apatite grains were mounted on adhesive tape, depth-profiles analyzed with an excimer laser using a 40µm spot at 4mJ for 30sec, and data corrected for depth-dependent and elemental fractionation. Integrated bulk samples ages were used to constrain both upper and lower intercept in Tera-Wasserburg concordia space to determine bulk age and Pbc composition. Subsequently, U-Pb ages were calculated for individual 3-sec (~2µm) depth intervals from single grain analyses, employing a Pbc correction based on the bulk Pbc composition. Depth-profiled Pbc-corrected 2µm increment ages were plotted as apatite U-Pb age spectra (age vs. depth) for each analyzed apatite grain and qualitatively categorized according to spectrum topologies and qualitatively interpreted in terms of cooling rate for diffusive U-Pb profiles or non-Fickian profile behavior. Selected apatite grains with representative U-Pb age profiles were flipped 90° on the adhesive tape, embedded in epoxy, polished to expose a grain-internal cross-section of the ablation pit, and imaged with a scanning electron microscope (SEM) to reveal possible zoning, deformation, or growth/recrystallization. This methodology was applied and tested on mid- to lower-crustal basement rocks in the North Pyrenean Zone which represent crustal sections exhumed during Early Cretaceous hyperextension. The high-grade, amphibolite to granulite, gneisses yielded Aptian-Albian apatite U-Pb ages with mostly plateau-like, flat U-Pb age spectra, arguing for very rapid cooling below 450°C during crustal thinning and hyperextension. Upper crustal granites yielded Carboniferous apatite U-Pb ages, overlapping with zircon U-Pb ages, and flat apatite U-Pb age spectra, suggesting rapid post-magmatic cooling after shallow-crustal granites emplacement. In contrast, apatite from a shear zone separating upper and lower-crustal rocks, exhibited variable U-Pb age with non-monotonic age spectra topologies, falling between Carboniferous and Early Cretaceous. SEM imaging of these apatite revealed complex intra-grain growth and recrystallization, interpreted to represent retrograde growth crack-and-seal recrystallization during progressive ductile to brittle shearing during Early Cretaceous rifting, resulting in Carboniferous and Early Cretaceous age domains within single grains. This new methodology allows for qualitative and quantitative interpretation of high-resolution apatite U-Pb ages and recovery of mid- to lower-crustal thermal and tectonic histories.

Keywords: thermochronology, lower crust, rifting

SETP
LCPHD

From Rifting to Subduction: Evidence for the Role of Past Tectonics Influencing Subduction Initiation at the Puysegur Trench, New Zealand

Brandon Shuck
Shuck, B., The University of Texas Institute for Geophysics
Gulick, S., The University of Texas Institute for Geophysics
Van Avendonk, H., The University of Texas Institute for Geophysics
Gurnis, M., Caltech
Stock, J., Caltech
Sutherland, R., Victoria University of Wellington
Hightower, E., Caltech
Patel, J., Victoria University of Wellington
Saustrup, S., The University of Texas Institute for Geophysics

The critical ingredients and conditions to initiate a new subduction zone are widely debated. However, there is a general agreement that subduction initiation likely takes advantage of previously weakened lithosphere. To evaluate how pre-existing lithospheric structures may facilitate underthrusting and lead to a mature subduction zone, we present an analysis of the Puysegur margin, a young deep-sea trench with a diverse tectonic history. The Puysegur margin exhibits several characteristics of a subduction zone, including ongoing plate convergence, an active Benioff zone, and adakitic volcanism. Plate reconstructions show that the margin has experienced a complicated tectonic transformation from rifting to seafloor spreading, to strike-slip motion, and most recently to incipient subduction, all in the last ~45 million years.

Here we present new seismic images from the South Island Subduction Initiation Experiment (SISIE) which surveyed the Puysegur region in February-March, 2018. SISIE acquired 1252 km of deep-penetrating multichannel seismic (MCS) data on 8 lines, including 2 critical dip lines which extend from the incoming Australian plate to across the forearc Solander Basin.

Our preliminary MCS profiles reveal several important findings within the Solander Basin: (1) The crust is extended and tilted on large normal faults. We infer that the basement here is thinned continental Campbell Plateau crust formed during Eocene rifting. (2) In the south, we see thinner continental crust stretched over a wider distance and evidence of numerous volcanic sills, which suggests that there is a north-south transition in crustal structure, possibly related to a temporal evolution in rifting processes. (3) The basin contains up to 3 km of sediment including distinguishable packages of pre-, syn-, and post-rift sedimentary sequences. (4) We find fault zones deforming of all these sequences, suggesting some of the normal faults inverted upon compression likely related to subduction initiation.

These early, yet convincing images suggest subduction at the Puysegur Trench was assisted by inherited buoyancy and reactivation of structural weaknesses that were imprinted into the lithosphere during an earlier phase of continental rifting which aided plate failure and subduction nucleation ~30 million years later.

Keywords: Subduction Initiation, Rifting, Tectonics, Subduction Zone Dynamics, Zealandia

SETP
LCPHD

Upper Mantle Seismic Anisotropy as a Constraint for Mantle Flow and Continental Dynamics of the North American Plate

Wanying Wang
Wang, W., Institute for Geophysics and Department of Geological Sciences, The University of Texas at Austin, Austin, TX
Becker, T., Institute for Geophysics and Department of Geological Sciences, The University of Texas at Austin, Austin, TX

Seismic anisotropy is a constraint for the tectonics of continental plates and asthenospheric convection. Dense shear wave splitting (SWS) measurements from the USArray promise to advance our understanding of North American plate dynamics. Here, we evaluate a range of contributions to the observed azimuthal anisotropy. Comparing the fast polarization plane orientations ("fast axes") from SWS with absolute plate motions (APM), we confirm that the overall angular misfit is small. This suggests that upper mantle anisotropy is mainly affected by plate motion induced shear, leading to lattice preferred orientation (LPO) of olivine. However, some regions show large misfits, perhaps due to small scale convection, upper mantle viscosity variations, or frozen in lithospheric anisotropy. We therefore conduct a wide range of global mantle flow computations to explore the role of lateral viscosity variations (LVVs) and density driven flow. We consider LVVs due to plate boundaries, continental lithosphere, cratonic roots and sub-oceanic asthenosphere. Compared to APM models, mantle flow models show large misfit between LPO models and SWS, but LVVs improve the fit throughout the study area. This improvement is mainly due to a relatively weak oceanic asthenosphere. Density-driven flow derived from seismic tomography further improves the predicted anisotropy compared to pure plate induced shear. Varying the shape of cratonic roots causes distinct changes in predicted LPO, and both density and LVVs affect regional misfits. However, while misfits are diagnostic of regional mantle flow, our tests indicate that there is no straightforward, plate-wide scenario that would provide an explanation of SWS based on asthenospheric flow alone. When considering frozen-in structure in the lithosphere, it is possible to fit SWS measurements with a coherent, 50-100 km thick lithospheric complement to the asthenosphere. Regionally, the lithospheric complement agrees with the orientations of crustal azimuthal anisotropy and might indicate past tectonic event signatures in the lithospheric anisotropy. Our results suggest the importance of density driven flow and viscosity variations on LPO formation. However, there are still questions concerning the link between seismic anisotropy, mantle flow, and continental dynamics.

Keywords: Lithosphere, Seismic anisotropy, Upper mantle

SHP
LCPHD

Anatomy of an exhumed river-channel belt

Benjamin Cardenas
Cardenas, B., UT Austin
Mohrig, D., UT Austin
Goudge, T., UT Austin

Physical and numerical experiments, as well as theory suggests that the clastic sedimentary rock record is primarily composed of a scour-and-fill architecture, where the deposits most likely to be preserved are those filling the deepest scours to move through a particular location. To test this hypothesis for fluvial channel belts, we use a rich dataset collected from the Cretaceous Cedar Mountain Formation, Utah, USA. Unmanned Aerial Vehicles were used to produce overhead photomosaics and structure-from-motion digital-elevation models. Sets of dune (n = 1,071) and bar (n = 107) strata exposed on the top surface of an exhumed channel belt were mapped onto its photomosaics, as were their measured transport directions. This data was complimented by fifty-nine stratigraphic sections and thirty-one lateral sections that were collected along the vertical exposures defining the channel belt margins. Together the vertical sections and planform mapping show that the studied belt is a compound structure composed of the stacked deposits of multiple, individual channel belts and representing 5 to 6 channel reoccupations. Lateral sections reveal bar strata made up of sets of dune cross-beds recording the frozen-in-place kinematics of bar forms. Locally, the paleo-topography of Cretaceous-age bar forms even define the upper surface of the outcrop. Comparison of the channel-belt centerline to local paleotransport directions indicate channel planform was preserved through multiple re-occupations. The preservation of these channel elements is not consistent with the null hypothesis of a scour-and-fill dominated stratigraphy. We interpret this departure to be a product of the kinematics of the depositional system. Rapid avulsions could preserve the final state of the active channel bed and its individual bar elements. Frequent avulsions with respect to lateral migration rates would also minimize lateral channel amalgamation, as we observe. A frequently avulsing river system would also favor multiple channel reoccupations, as the time available to completely fill and bury unoccupied channels with flood plain sediment would be minimized; this is consistent with the 5 to 6 stacked channel belts observed. This dune-to-bar-to-channel scale preservation of belt elements falsifies the scour-and-fill hypothesis and provides a foundation for future studies connecting properties of fluvial systems to the generation of channel-belt strata.

Keywords: fluvial, sedimentology, channel belt, dune, stratigraphy

SHP
LCPHD

Detrital Zircon Transport Lag in Fluvial Bedload

Max Daniller-Varghese
Daniller-Varghese, M., Department of Geosciences, The University of Texas at Austin, Austin, TX

The difference in transport rates and times of different density particles, such as detrital zircons in quartz sand, is critically important to accurately assessing sediment provenance. Because zircons are typically twice as dense as their surrounding sediment, and because transport rate scales with grain density, zircon transport rate as bedload will be smaller than that of quartz sand. Moreover, intermittent transport conditions, sediment segregation into floodplains, or preferential sequestration in deep pools can add substantial time lag.
We experimentally modeled fluvial bedload containing detrital zircons using a 5m x 0.6 m domain in a flume. Using magnetite sand as a proxy---it has a similar density as zircons---we developed mature, three-dimensional bedforms with variable scour depths that transported multiple bedform lengths. We measured magnetic particle concentration by separating them from bed samples with a magnet and then related change in concentration directly to transport rate. Our experimental results suggest that detrital zircon transport is substantially slower than bulk sediment transport because denser particles segregated to bedform troughs. The ratio of transport rates will be integrated into a simple hydrodynamic transport model, in order to constrain a minimum transport lag for dense particles from source to sink.

Keywords: Experimental Sedimentology, Source to Sink, Detrital Zircons, Fluvial Transport

SHP
LCPHD

Linear-sourced slope channel systems in high sediment supply basin margin clinoforms

Yuqian Gan
Gan, Y., Jackson School of Geosciences, The University of Texas at Austin, Austin, TX
Olariu, C., Jackson School of Geosciences, The University of Texas at Austin, Austin, TX
Steel, R., Jackson School of Geosciences, The University of Texas at Austin, Austin, TX

Current research on deepwater slope channels tends to focus on single channel or channel belt that are fed by a point source on the continental shelf, and data are biased towards large systems of continental margin-scale (>1km) clinoforms. However, there is good evidence for linear-sourced slope channel systems on the slopes of moderately deepwater clinoforms (<1km) that are common for petroleum prolific back-arc, foreland, and lacustrine basins. These basins are characterised by a progradation-dominant shelf edge trajectory, with multiple contemporaneously active slope channels and thick basin floor fans. How shelf-edge trajectory influences slope channel systems and deep water sand deposition, we map slope channel distribution of Late Cretaceous Fox Hill-Lewis clinoforms in Washakie basin, and compare the results from the aggradational early clinoforms vs. the progradational late clinoforms. The mapped slope-channel distribution strongly suggests that the basin-floor fan complexes are fed by multiple slope channels confined within well-defined high frequency (fourth and fifth-order) sequences. Channels on the deepwater slope merge with basin floor fans as aprons on the lower slope to toe-of-slope. Incisions near the shelf edge, cross-cutting multiple fifth-order sequences, directly link shelf edge deltas to slope channels and fans, especially for the progradation-dominant clinoforms.. Channel log motifs are not evenly distributed through the height of any clinoform but tend to cluster, suggesting channel elements within a larger slope channel complex. Channel thickness varies from few meters for each channel element, to fifty meters for the stacked channel complex. The width of channel complexes is mostly within 3-5 km. Local net to gross in the channels can be more than fifty percent. We also evaluate whether the progradation rate of the shelf-edge influences the density of slope channels immediately in front of the shelf. Further testing will clarify if the spacing of the slope channels can be related to the density of small rivers, thus controlled by climate and Laramide tectonic uplift rate. Overall the study explores the under-evaluated role of linear sourced slope channels in source to sink systems.

Keywords: deep water slope channel, Western Interior Seaway, Laramide Orogeny.

SHP
LCPHD

Toward a mechanistic understanding of Li isotope transfer within landscapes

Evan Ramos
Ramos, E., Department of Geological Sciences, The University of Texas at Austin
Breecker, D., Department of Geological Sciences, The University of Texas at Austin

The quantitative reconstruction of paleoenvironments is paramount in benchmarking the resilience of past ecosystems to climate change. Since ecosystems influence the balance between physical and chemical weathering in a landscape (known as its weathering regime and notated as W/D), the quantification of physical and chemical weathering rates from ancient landscapes should elucidate ecosystem responses to abrupt changes in climate. The advancement of thermochronometric techniques and cosmogenic radionuclide dating have led to high-fidelity data sets of erosion rates from ancient landscapes. Current methods for quantifying chemical weathering rates from ancient landscapes are contrarily limited to well-controlled environments. Luckily, lithium (Li) isotopes are prevailing as a primary geochemical tool for quantifying chemical weathering rates of silicate minerals in ancient continental settings.

Due to the strongly preferential uptake of the light stable isotope of Li, ^{6}Li, over the heavy stable isotope, ^{7}Li, by secondary minerals during weathering, the δ^{7}Li values (the ^{7}Li/^{6}Li ratio of a sample normalized to a standard) of water and sediments in weathering environments unambiguously reflect the degree of secondary mineral formation. Unlike other geochemical proxies for weathering, Li isotopes are not preferentially incorporated into the terrestrial biomass, which further enhances its utility in extracting information from weathering environments. Recent studies have empirically demonstrated relationships between weathering regimes and the δ^{7}Li values of both river water and secondary minerals in catchments. These data come from rivers draining a vast range of rock types and existing in different climates, giving credence to the strength of these relationships holding true in the geologic past. Despite the preponderance of evidence, the physiochemical mechanisms that underpin these relationships are poorly resolved. Through numerical modeling, our study thus seeks to characterize the geologic conditions that can generate the relationships between Li isotopes and weathering regimes.

In our study, we update a previously developed model for soil formation to include porous media fluid flow, thermodynamically-consistent rate laws for mineral dissolution and precipitation reactions, and lithium isotope transport. Further, we impose our model over a variety of geologic conditions, which include bedrock lithology, precipitation rates, erosion rates, and atmospheric temperature, to determine which range of conditions that can reproduce these empirical relationships. Over the range of conditions that we query, our preliminary results poorly agree with the empirical relationship at moderate W/D values but agree well at high and low W/D values. Erosion and precipitation rates are primarily responsible for the areas of good agreement. Contrarily, the model's inability to reproduce δ^{7}Li values at moderate W/D values suggests that other processes need to be incorporated into the model, including sorption/desorption reactions on mineral-fluid interfaces. Altogether, our study underscores the importance of physical weathering and fluid availability during Li isotope transport in landscapes.

Keywords: lithium isotopes, weathering, Earth system science, carbon cycle, critical zone, modeling

CCG
U

A new description and analysis of the extinct lobster genus [i]Uncina.[/i]

Brooke Bogan
Bogan, B., The University of Texas at Austin, Austin, TX
Martindale, R., The University of Texas at Austin, Austin, TX

Lagerstätten are fossil assemblages exhibiting exceptional preservation, often including soft parts. A new Lagerstätte was recently discovered in Canada; this assemblage contains a wealth of fossils from the Early Jurassic, including icthyosaurs, fish, crinoids,cephalopods and crustaceans. Many of the crustacean fossils found represent the extinct lobster genus *Uncina*. In the past, only a handful of these animals have been published on and their range was very small- mostly found in Europe. This study expands the range of previously described species *U. pacifica, U. posidoniae* and *U. ollerenshawi* as well as describes new species. In this study, we will analyze the morphology of new Uncinid lobster specimens to determine their similarity to previously described species as well as name new species. As most specimens contained measurable claws, a variety of claw measurements were taken in order to establish a standard method for identifying these animals. At least one new species has been named using this method. Previously unknown information about these animals can be determined from this analysis including the discovery of new information about previously named specimens. This study has expanded the range of previously known species, identified new species and given new insight into the lives of these animals, thus enhancing our understanding of the biodiversity of the past.

Keywords: paleontology, Lagerstätten, Lagerstätte, Martindale, lobster, Jurassic, geobiology, morphology

CCG
U

A new long wavelength airborne sounding radar for temperate glacier thickness measurement with a case study on the Hubbard Glacier, Alaska, USA

Michael Christoffersen
Christoffersen, M., Jackson School of Geosciences, The University of Texas at Austin, Austin, TX
Holt, J., Lunar and Planetary Laboratory and Department of Geosciences, University of Arizona, Tucson, AZ
Truffer, M., Geophysical Institute, University of Alaska at Fairbanks, Fairbanks, AK
Larsen, C., Geophysical Institute, University of Alaska at Fairbanks, Fairbanks, AK

Radar sounding of temperate glaciers to determine ice thickness is a persistently difficult problem. Strong attenuation and scattering of radio frequency signals caused by warm ice necessitates transmitting high power, long wavelength signals to achieve the necessary depth penetration. Additionally, many temperate glaciers inhabit relatively narrow valleys, which can cause extreme ambiguity when interpreting radar products. Reflections from valley walls or other off-nadir features can very often appear to be the base of a glacier, leading to incorrect interpretation if this issue is not acknowledged and dealt with. A final issue common to all fast flowing glaciers are zones of heavy crevassing making ground based radar infeasible. In this scenario airborne radar becomes necessary to quickly and safely acquire thickness measurements over the crevassed areas. Airborne radar presents a unique set of benefits and challenges when compared to ground based radar. We present a newly developed sounding radar system suitable for airborne use. The radar transmits a two kilowatt peak power linear chirp with a center frequency of either 2.5 or 5 MHz, enabling detection of a basal reflection at depths of 900 meters or more. In conjunction with the radar hardware we have developed a surface clutter simulator, software that can predict the locations of off-nadir returns that frequently occur when radar sounding in narrow valleys. This allows for significantly increased confidence when interpreting radar products. As a part of NASA's operation IceBridge, radar data was acquired over the Hubbard Glacier with the new sounder in May 2018. Hubbard descends from the St. Elias Mountains into Disenchantment Bay, which opens into the Gulf of Alaska. We chose Hubbard as a case study site for this radar because there are few reliable thickness measurements, even though Hubbard is the largest tidewater glacier in North America. The radar successfully penetrated to the base of the glacier, measuring thicknesses greater than 600 meters. This new data is combined with previously acquired thickness measurements and historical bathymetric data to create a raster map of the bed below Hubbard. This bed map shows a large trough underneath the convergence of Hubbard and the Valerie Glacier that reaches depths of over 400 meters below sea level. There is a finger from the main trough extending up Hubbard. These bed troughs are conduits for subglacial water and sediment movement, and therefore are an important control on the evolution of the morainal bank which in turn is a major player in tidewater glacier terminus dynamics. Increasing knowledge of bed topography through radar sounding will enable more accurate modeling of the Hubbard Glacier and systems like it.

Keywords: Radar, Cryosphere, Alaska, Glaciers

CCG
U

Strontium Isotope Profile from a Lower Jurassic Shallow Water Carbonate Platform in the Dinarides, Slovenia: A High-Resolution Picture of the Toarcian Oceanic Anoxic Event

Sean Kacur
Kacur, S., Jackson School of Geosciences, The University of Texas at Austin, TX
Martindale, R., Jackson School of Geosciences, The University of Texas at Austin, TX
Ettinger, N., Jackson School of Geosciences, The University of Texas at Austin, TX
Loewy, S., Jackson School of Geosciences, The University of Texas at Austin, TX
Banner, J., Jackson School of Geosciences, The University of Texas at Austin, TX
Košir, A., Research Center of the Slovenian Academy of Arts and Sciences, Ivan Rakovec Institute of Palaeontology

Oceanic Anoxic Events (OAEs) such as the Toarcian Oceanic Anoxic Event (T-OAE) are associated with some of the most significant climatic and paleoceanographic changes in the Phanerozoic. Traditional approaches to studying OAEs examine the relationships between volcanism, geochemical changes, anoxia, and black shale deposition in deep-water settings. Nevertheless, OAEs are also intervals of significant shallow-water biotic turnover. Despite their importance, shallow-water OAE records are difficult to characterize; the dearth of pelagic fossils (e.g., ammonites and belemnites) means there is often poor biostratigraphic control and necessitates bulk-rock analysis for high-resolution studies. Strontium isotope ($^{87}Sr/^{86}Sr$) curves can be used to tie loosely constrained strata to better-dated Jurassic sections, thereby enhancing temporal controls. More importantly, $^{87}Sr/^{86}Sr$ and carbon isotopes ($\delta^{13}C$) are linked through the global weathering cycle. For the T-OAE, paired $^{87}Sr/^{86}Sr$ and $\delta^{13}C$ measurements can be used to test the hypothesis that an increase in global weathering was a contributing factor to the Toarcian biotic crisis.

Here we present $^{87}Sr/^{86}Sr$ data from a section of the Adriatic Carbonate Platform on the Trnovski Gozd Plateau in Slovenia. Our data show the negative carbon isotope excursion that demarcates the onset of the T-OAE is followed by a positive Sr excursion. We interpret the paired isotope excursion as the release of light volcanogenic CO_2, followed by an increase in crustal weathering due to climatic warming. Thus, an increase in shallow-water nutrient levels may have been a co-driver for biotic turnover. Additionally, we use supplementary stable isotope and trace element data from carbonates to evaluate the reliability of the $^{87}Sr/^{86}Sr$ curve generated from bulk-rock. This study demonstrates a multi-proxy approach to quantifying the shallow-water geochemical signature of OAEs and the consequent transitions in life.

Keywords: Geochemistry, Earth-life transitions, Isotopes, Carbonates

CCG
U

Reconstructing paleo-ENSO variability during the Holocene using geochemical proxies from corals

Brooke Kopecky
Kopecky, B., University of Texas Institute for Geophysics, Jackson School of Geosciences, The University of Texas at Austin, Austin, TX
Lawman, A., University of Texas Institute for Geophysics, Jackson School of Geosciences, The University of Texas at Austin, Austin, TX
Partin, J., University of Texas Institute for Geophysics, Jackson School of Geosciences, The University of Texas at Austin, Austin, TX
Quinn, T., University of Texas Institute for Geophysics, Jackson School of Geosciences, The University of Texas at Austin, Austin, TX
Taylor, F., University of Texas Institute for Geophysics, Jackson School of Geosciences, The University of Texas at Austin, Austin, TX
Lawrence, R., Department of Earth Sciences, University of Minnesota, Minneapolis, MN
Cheng, H., Xi'an Jiaotong University, Xi'an China, University of Minnesota, Minneapolis, MN
Shen, C., Department of Geosciences, National Taiwan University, Taipei, Taiwan

The El Niño Southern Oscillation (ENSO) is the leading mode of interannual variability in the tropical ocean and has pronounced impacts on the global climate. Additionally, understanding ENSO variability is increasingly important in order to make predictions about how ENSO will change in a warming climate. Instrumental sea surface temperature (SST) records from the tropical Pacific provide a means for understanding variability in the ENSO system. However, the observational record of temperature is not long enough to understand constrain our understanding of natural ENSO variability. Coral geochemical proxy records allow for an extension of the SST record prior to the instrumental record. We use paired coral Sr/Ca and oxygen isotope ($\delta^{18}O$) measurements to construct paleo-SST records during the Holocene from four *Porites lutea* fossilized corals from the southwest tropical Pacific. Three of these corals are from Tetapare, Solomon Islands (8.7°S, 157.5°E) and one is from Port Havannah, Vanuatu (17.6°S, 168.2°E). U/Th absolute ages indicate that the four corals were alive 6017 ± 23, 7170 ± 44, 7255 ± 50, and 11014 ± 49 years ago. Tropical SST data from these periods through the Holocene are important constraints for validating climate models run under past conditions, such that the comparison of past conditions will help constrain and improve model projections for the future.

Keywords: El Niño, ENSO, Climate, Corals

EG
U

Modeling Episodic Fluid Migration in Salt Basins

Preston Fussee-Durham
Fussee-Durham, P., Jackson School of Geosciences, The University of Texas at Austin, Austin, TX
Hesse, M., Jackson School of Geosciences, The University of Texas at Austin, Austin, TX

Previous studies have documented the presence of migrated hydrocarbons in rock salt suggesting these stratigraphic traps have lost some of their sealing capacity; however, the mechanism for their emplacement is poorly understood. Typically, salt is assumed to undergo a form of visco-elasto-plastic deformation. On geologic timescales, however, salt is expected to behave as a highly viscous non-Newtonian fluid. An important consequence of this viscous nature is the compaction and decompaction in response to differences between pore fluid and solid pressures. These deformations induce significant porosity changes that cannot be neglected and lead to new non-linear phenomena unknown in rigid or elastic porous media. To understand the conditions under which pore fluids can enter salt on geologic timescales, a numerical model for flow in ductile porous media is developed. Specifically, the model is composed of a viscous salt layer sandwiched between overlying and underlying elastic sandstone reservoirs. The entire domain is subjected to overlying sedimentation and the resulting compaction of the elastic reservoirs generates elevated pore fluid pressures. Model results suggest there may be an initial hydrodynamic component to the ability of a salt layer to arrest fluid migration.

Keywords: Salt Traps, Fluid Flow in Ductile Porous Media

EG
U

Quantitative Uncertainty Assessment of Reservoir Facies Estimates from Inverted Impedances and Rock-Physics Modeling

David Wiggs
Wiggs, D., Jackson School of Geosciences, The University of Texas at Austin, Austin, TX
Spikes, K., Jackson School of Geosciences, The University of Texas at Austin, Austin, TX

Quantitative seismic interpretation is the process to obtain facies and/or rock properties from inverted seismic impedances. This study quantifies three sources of uncertainty (error) in facies estimates to allow for a better understanding of risk assessment and prospect evaluation. Data used in this study include a pre-stack 3-D seismic volume and wireline logs from one vertical well within the Marco Polo Field in the Green Canyon, Gulf of Mexico. Four primary steps comprise this workflow: well log analyses and facies identification, pre-stack seismic impedance inversion, rock-physics modeling, and facies classification. Elastic properties from well-log data along with a rock-physics model establish the relationship between reservoir properties (porosity, fluid saturation, and lithology) and elastic properties (P- and S-impedances). The inversion of pre-stack seismic data provides the elastic properties at every location within the 3-D seismic volume. A rock-physics model translates these impedance values to reservoir properties. This process generates a 3-D volume that contains the most probable facies at each point. Three limitations are inherent in this technique. First, the resolution of the rock properties depends upon the resolution of the seismic data. Second, the relationship between impedances and reservoir properties is non-unique, in which different combinations of reservoir properties can lead to an impedance value. Third, the facies estimates have errors in them due to errors in the rock-physics model, errors in the inverted data, and errors in the match between the data and the model.

Keywords: Rock Physics, Elastic Properties, Error Quantification

MG
U

Benthic Foraminiferal Paleoenvironmental Analysis of the Trinity River Paleovalley on Cores Collected Offshore Galveston Bay, Gulf of Mexico

Patricia Standring
Standring, P., Institute for Geophysics, The University of Texas at Austin, Austin, TX
Gulick, S., Institute for Geophysics, The University of Texas at Austin, Austin, TX
Swartz, J., Institute for Geophysics, The University of Texas at Austin, Austin, TX
Goff, J., Institute for Geophysics, The University of Texas at Austin, Austin, TX
Lowery, C., Institute for Geophysics, The University of Texas at Austin, Austin, TX

Sediment infilling the Trinity River paleovalley records the transgressive depositional environment of the Texas coast since the last glacial maximum 20 kyr B.P. Of particular interest are the location and volume of fluvial sand deposits (e.g., point bars) within the channel of the Trinity paleoriver, a crucial resource on the sand-poor Texas shelf which may be used for potential beach nourishment and other coastal rejuvenation projects. To date, the Bureau of Ocean and Energy Management-funded Trinity River Paleovalley Project (TRiPP) has mapped the valley-fill fluvial, estuarine and marine sediments using geophysical data. Our purpose is to analyze sediment piston cores from the Trinity River paleovalley to provide a more complete paleoenvironmental reconstruction of the river channel, carbon date macrofauna found in the sediment cores to provide exact timing on the sea level rise, and place these in context of the geophysical images to understand the evolution of the Texas continental shelf during the last marine transgression. Here, we use four piston cores taken within the paleovalley during the Marine Geology and Geophysics Field Course in May 2018 to add sedimentological, paleoenvironmental, and age constraints to the seismic data. We present biostratigraphic analysis of these sediment cores, from which we tie paleoenvironmental reconstructions to an extensive seismic dataset. Preliminary sedimentary and benthic foraminifera analysis of piston cores PC-2 and PC-3 reveal an overall rise in sea level and a change in the paleoenvironment from fluvial to estuarine over a period of several thousand years. Our research includes quantitative foraminiferal population counts, percentages on diversity of foraminifera genera, grain size analysis, and integration with existing seismic data in the region. High percentages of *Ammonia* and *Elphidium* genera, and low levels of diversity in other foraminifera genera, within the sediment core samples, indicate the paleonvironment was predominantly estuarine, showing fluctuations in sea level and shifting depositional environments from central bay to bay mouth.

Keywords: Foraminifera, Galveston Bay, Holocene, Sea Level Change

PS
U

Semi-Automatic Glacier Terminus Recognition Through Landsat Image Processing

Mauricio Exiga
Goliber, S., University of Texas Institute for Geophysics, The University of Texas at Austin, Austin, TX
Exiga, M., The University of Texas at Austin, Austin, TX

Glacier terminus variability through seasonal advances and retreats allow insights into changes in the climate, ocean, atmosphere, and sedimentary environments. More specifically, the Greenland ice sheet (GrIS) has seen dramatic changes and ice loss over the past two decades as upstream thinning and acceleration increase, creating a positive feedback loop where this ice loss is continuing to be seen. Through manual tracking and vectorization of Landsat satellite images, the terminus position and shape of these marine terminating glaciers can be recorded over an extended period of time. These vectors can serve as primary sources of data for researchers to process GrIS changes, but due to how slow the hand-picked vectors are able to be created there is a limit on the number of individual glaciers that can be measured and cataloged. With dozens of glaciers remaining to be processed for this time series data over years of satellite data, a need has arisen for automatization. In this project we focus on using image processing techniques on Landsat 8 files such as anisotropic diffusion and automatic edge detection to obtain these vectors. Due to difficulties in distinguishing glacier mass from ice mélange and heavy shadows, the semi-automatic picked glacier vectors are only accurate in favorable conditions. We are currently in the process of exploring more advanced techniques in image processing to be able to overcome these challenges such as creating a neural network trained from previous hand-picked vectors.

Keywords: Greenland, GrIS, Glacier, MATLAB

SETP
U

Insights to copper porphyry deposits from magmatic apatites in the Grasberg-Ertsberg mining district of Papua, Indonesia

Hannah Anderson
Anderson, H., Jackson School of Geosciences, The University of Texas at Austin, Austin, TX

This study uses magmatic apatites from the Ertsberg-Grasberg Cu-Au mining district in Papua, Indonesia to quantify critical magma chamber volatiles (Cl, S) of copper porphyry deposits. Volatiles which transport and precipitate metals are proposed to concentrate through bubbles sourced from the magma to form economic deposits. Chlorine preferentially partitions into apatite from the magma. Chlorine is highly diffusive and is commonly remobilized in the apatite crystal structure. Sulfur is a trace element that can enter and remain in the apatite crystal structure via coupled substitution. The chlorine and sulfur contents of the magma can change over time through degassing and magma chamber recharge which are recorded in sulfur zoning. Conservation of mass can be used to determine the concentration of chlorine and sulfur for the original magma using measured concentration. In this study, quantitative and semi-quantitative x-ray map electron microprobe analyses are used to determine the concentration of chlorine and sulfur apatites from five intrusions: Karume and Kali (non-mineralized with respect to copper), Dalam (0.5 wt% Cu), Ertsberg (associated with skarn-related copper mineralization), and the MGI (1 wt % Cu). The results show a spread of chlorine values for each igneous body, with Dalam and MGI having the largest reported chlorine range (around 0.1 mols Cl per 12 O). Each intrusion, except Dalam and MGI, have a distinct range in chlorine concentration values. All five intrusions have approximately the same sulfur concentration range (0-0.045 mols of S per 12 O). Apatite x-ray maps indicate homogenous chlorine concentrations for all intrusions. Sulfur zonation varies per intrusion; but, on average, Ertsberg apatites have three zones with more sulfur concentrated cores, Dalam have four zones with both sulfur-rich and poor cores, Kali have four zones, and MGI apatites do not show distinct zoning. The one sample of Karume shows interesting resorption textures for the four crystals mapped.

Keywords: porphyry, apatites, volatiles

SETP
U

Stockwork vein zone in the Grasberg porphyry Cu-Au deposit, Papua, Indonesia: Structural and chemical implications

Eytan Bos Orent
Bos Orent, E., Department of Geological Sciences, The University of Texas at Austin, Austin, TX

The Grasberg Igneous Complex is the largest (2+ billion tonnes) ore deposit in the Ertsberg-Grasberg mining district of Papua, Indonesia. With an average ore grade of roughly 1 wt. % copper and 1 gram/tonne gold, the ore deposit is a supergiant that has been producing approximately 5% of the world's new copper supply for more than the past two decades. The ore is associated with a hydrothermal system beneath it that was active at ~3 Ma. The system consists of two distinct mineralization events following the emplacement of the first two magmatic phases, the Dalam and the Main Grasberg Intrusion (MGI). The center of the MGI is host to the stockwork zone, a region of abundant quartz and magnetite veins that was dilated in three dimensions. This was followed by another pulse of hydrothermal alteration that is responsible for most of the copper mineralization in the complex. A sample suite of 85 slabs was prepared from seven horizontal drill cores at the 3,700-meter elevation in the stockwork zone, 40 of which were also prepared into thin sections. Crosscutting veins provide temporal constraints. Mineralization can be subdivided into five categories. Early veins (stages 1-3) are predominantly quartz and magnetite, while later veins (stages 4-5) deposited much of the copper minerals chalcopyrite and bornite. Bornite is localized to an area about 200 meters across, suggesting a center of mineralization in the northwest quadrant of the MGI. This location is consistent with previous mapping of the pervasive hydrothermal alteration within the Grasberg Igneous Complex. The difference in vein petrology over time provides insight into fluid temperature. Quartz oversaturates in solution at temperatures roughly 300°C higher than that of chalcopyrite in solution. This knowledge constrains relative temperatures near the cupola of the stock extruding from the underlying magma chamber.

Keywords: economic geology, ore deposits

SETP
U

The Effect of H2O on the Anomalous Velocities and Compressibilities of Rhyolitic Glasses up to 3 GPa

Jesse Gu
Gu, J., Department of Geological Sciences, Jackson School of Geosciences, The University of Texas at Austin, Austin, TX
Fu, S., Department of Geological Sciences, Jackson School of Geosciences, The University of Texas at Austin, Austin, TX
Yamashita, S., Institute for Planetary Materials, Okayama University, Misasa, Tottori, Japan
Okuchi, T., Institute for Planetary Materials, Okayama University, Misasa, Tottori, Japan
Gardner, J., Department of Geological Sciences, Jackson School of Geosciences, The University of Texas at Austin, Austin, TX
Lin, J., Department of Geological Sciences, Jackson School of Geosciences, The University of Texas at Austin, Austin, TX

Rhyolitic eruptions are some of the largest and most devastating. Therefore, understanding the physical properties (e.g. sound velocity, density, and compressibility) of representative melts is important for interpreting melt distribution, migration, and evolution in the Earth's crust. Previous studies have shown that sound velocities and elastic moduli in silicate glasses and melts anomalously decrease with increasing pressure up to 1.5-2 GPa. At pressures higher than 2 GPa, sound velocities and elastic moduli increase with pressure. This softening in sound velocities and elastic moduli have been attributed to the polymerization and anomalous densification of the silicate network. Incorporation of water as hydroxyl groups or dissolved molecular water into such melts has also been shown to decrease sound velocities and elastic moduli of melts near ambient pressures. However, the influence of water on these properties is still unknown at higher pressures. In this study, we use glass as an analogue to crustal melts in addition to Brillouin Light Scattering and FTIR Spectroscopy to measure the sound velocities, compressibilities, and speciation of water in three rhyolitic glasses with varying water contents up to 3 GPa. We observe a decrease in sound velocities and compressibilities with increasing water content at ambient conditions. However, at higher pressures, the incorporation of water increases sound velocities and elastic moduli. From FTIR measurements, we show how the different species of water, hydroxyl groups and dissolved molecular water, alter the physical properties of the glass at different pressures. These observations are then be linked to the buoyancy and stability of hydrous melts in the Earth's crust.

Keywords: rhyolite, glass, melt, elasticity

SETP
U

Origin of Cockade Textures in the Multi-Stage Vein System of the Rozália Mine, Banská Hodruša, Slovakia

Thomas Quintero
Quintero, T., The University of Texas at Austin, Austin, TX
Kyle, R., The University of Texas at Austin, Austin, TX

Numerous epithermal base and precious metal-rich veins are hosted by the Middle Miocene Štiavnica stratovolcano within the Central Slovakia Volcanic Field in the western Carpathian arc. These deposits have been mined since the Middle Ages and have historically produced 4,000 t Ag, 80 t Au, 55,000 t Pb, 70,000 t Zn, and 8,000 t Cu up to 1992. Today Rozália is the only working gold mine in central Europe, producing ore averaging between 7-10 g/t Au. Three main mineralization stages have been defined for the Rozália ore deposit. Most of the gold was introduced into the system during the second stage which is characterized by quartz, rhodonite, carbonates, pyrite, sphalerite, galena, chalcopyrite, petzite, hessite, and high fineness gold (80.6-87.8%). Cockade and other breccias formed during the second stage of this deposit and provide evidence for syntectonic controls of mineralization. Fluid inclusion studies of quartz and sphalerite from the Karolina vein system, which hosts the cockade textures, indicate precipitation from 250-300 °C from aqueous solutions with a salinity of 1-5 weight % NaCl eq. Cockade textures are unusual features within brecciated fault zones that are characterized by discontinuous concentric mineral zones around nuclei of volcanic fragments, with multiple generations of mineral cement forming more than 50% of the cockade texture. The two major hypotheses for the formation of cockade textures are the partial inward metasomatic replacement or alteration of clasts, as well as the repeated rotation of clasts and accretion of mineral cements. This study utilizes high resolution X-ray computed tomography to define 3D textural relationships which provide evidence for the formation of cockade textures and other breccias in similar vein systems worldwide.

Keywords: cockade, textures, breccia, gold, sulfide, hydrothermal, Slovakia, Rozalia, Neogene

SHP
U

Effects of Grain Interlocking on the Threshold of Motion in Gravel-Bed Rivers

John Franey
Franey, J., Department of Geological Sciences, The University of Texas At Austin, Austin, TX
Johnson, J., Department of Geological Sciences, The University of Texas At Austin, Austin, TX

When simulating fluvial systems, sediment transport is an integral factor to having an accurate and useful model. The variable ????$_{c^*}$, which quantifies the threshold of motion for non-negligible transport of grains, describes the shear stress the fluid must overcome to entrain and transport sediment. When the shear stress of the flow is above this threshold there will be a net erosion of material from the bedload. Many factors affect ????$_{c^*}$, ranging from grain size, shape, and density, the size distribution of surrounding grains, the history of net deposition or erosion, bed slope, imbrication and overlapping of grains, and pocket geometry. This project will focus on isolating the effect that grain interlocking has on the ????$_{c^*}$ variable, and produce a quantitative assessment of how the interlocking of grains effect thresholds of motion for sediment transportation. Laboratory flume experiments will be used to calibrate model parameters. This will be accomplished by using a 4 meter by 10 centimeter flume and a mixture of grains ranging from 1 millimeter to 24 millimeters in diameter, which will scale up to coarse gravel in natural rivers. The mixture will be placed in the flume and screened flat. The bed load will then be allowed to stabilize under flowing water. Once the bed load has reached equilibrium, flow will cease, and the interlocking of surface grains will be disrupted using a fine-tipped instrument while negligibly changing the surface topography. When flow resumes, the resulting transient increase in transport rate and related bed surface changes from the subtle disrupting of interlocking grains will be measured. Overall, the transport rate and eroded size distribution, and bed surface topography and spatial size distribution will be measured to isolate the effects of grain interlocking has on ????$_{c^*}$. The results of changing the interlocking of grains could range from extremely local topology changes to a large mass of grains becoming entrained and a total reworking of the system. The outcome of this experiment will allow for a better constraint on the ????$_{c^*}$ variable, which in turn will produce more accurate sediment transport models for future, related experiments.

Keywords: sediment transport,threshold of motion,fluvial system

SHP
U

Geomorphic Influence on Canopy Structure in Eldorado Valley, Nevada

James Gearon
Gearon, J., Department of Geological Sciences, The University of Texas, Austin, TX
Young, M., Bureau of Economic Geology, The University of Texas, Austin, TX

The influencing role of geomorphology on vegetation assemblage and structure has been studied in regional and small-scale environments. Rarely are the basin-scale connections between geomorphological constraints and vegetation characteristics studied. This scale of inquiry could inform future research into habitats, desert ecology, and soil identification, mainly due to the ability to infer geomorphological and subsurface characteristics of a region using vegetation data. In this study, we seek to better understand how landscape position and local-scale geomorphic features in an alluvial fan complex influences canopy structure. The project takes advantage of previously collected airborne LiDAR data (5-7 pts/m 2) and high-resolution imagery (4 bands, 0.15 m resolution) from a 2016 study to investigate causal relationships between vegetation and geomorphology in the Mojave Desert, supplementing a recently completed study by Young et al., 2017. The site for this research is within the Boulder City Conservation Easement in Eldorado Valley, Nevada, USA. Here we posit that discrete, observable basin-scale geomorphic attributes constrain plant characteristics and distribution in arid environments. The data collected in the study area led to the identification of more than 66 million individual plants spread across 35,500 hectares. The large spatial extent and heterogeneity of this study area made comprehensive geostatistical analysis a technical challenge requiring nested, iterative methods to catalog, sort, and eventually analyze the data. The presence of closely-spaced, active, dendritic drainages influenced vegetation assemblages, but somewhat masked the underlying relationship between geomorphology and canopy structure. However, tentative findings indicate a strong relationship between canopy characteristics (height, canopy size, volume, and spatial distribution) and lateral distance from adjacent drainages, confirming our hypothesis.

Keywords: Arid Environments, Ecohydrology, Desert Shrubs, Spatial Variability, Soil Variability, Big Data, GIS, Water-Stressed Environments, Soil Science, Geomorphology

SHP
U

Refining Sediment Transport Models

Kate Grobowsky
Grobowsky, K., Jackson School of Geosciences, The University of Texas At Austin, Austin, TX

Tsunamis and storm surges have cost coastal settlements loss of infrastructure and human lives, but human observations are insufficient and must be complimented by geologic deposit interpretations. Sediment transport inverse models have been proposed to characterize hydrodynamic features of paleo-tsunamis and storm surges. A simple advection-settling model has been shown to perform competently and has been refined according to laboratory data, but lacks completeness. We have developed additions to model to include the resuspension of transported grains wherein settled grains are assigned a probability of deposition and reintroduced to the turbulent flow. Depositional probabilities, number of grains transported, and multiple resuspensions have been found to influence a deposit's grain size distribution (GSD). Rugosity of sediment paths and advection lengths between multiple resuspensions are visualized. Differences in deposit GSD due to the manipulation of resuspension necessitate a continuation of this work

Keywords: tsunami, sediment transport, inverse model

SHP
U

The Fate of the Mississippi River Sediment During the Last Glacio-eustatic Cycle: A Volumetric Quantification

Ryan Herring
Herring, R., Department of Geological Sciences, The University of Texas at Austin, Austin, TX
Olariu, C., Department of Geological Sciences, The University of Texas at Austin, Austin, TX

Paralic sedimentary deposits contain almost 40% of the Earth's known hydrocarbon reservoirs and continue to be important for the industry, and even more so by its key link in understanding sediment fate into a source-to-sink perspective. In order to achieve a greater understanding of sediment dispersal during transgression and regression associated with river deltas, the last such cycle of the Mississippi River delta is studied herein. Previously published sediment thickness maps and borehole data of the Mississippi valley, delta, and shelf deposits have been compiled to discover how the Mississippi locus of deposition fluctuated since the Last Glacial Maximum (LGM). This investigation also compared calculated river derived sediment volumes during the last 20ky to deduce the volume and rate of sediment that bypassed the shelf onto the slope.

At the LGM (19ka) when the sea level was 120 metres below present, the Mississippi River lay entrenched into the shelf and it built its deltas on the shelf margin. As the base level rose rapidly subsequent to the LGM, the river filled its valleys with sediment in the ensuing retrogradation and formed depocentres outside the valley. As the sea levelled, the river's deltas prograded back outside of its valleys. Digitizing and employing previously published data showed that shelf depocentres migrated widely from the outer to the inner shelf following sea level rise and had thicknesses varying between 5–500 metres. This investigation seeks to test the various hypotheses concerning the locus of deposition during each of the stages of sea level rise. To this end, the sediment deposited in the valley and delta has been mapped and the volume quantified for each of these stages.

Recently calculated values for the Mississippi River water discharge since the LGM, estimated to have fluctuated to as much as eight times (160,000 m^3s^{-1}) that of the present, allowed for the enumeration of sediment discharge through time. Using the rate of sea level rise to plot the location of the shoreline with the inferred past river mouth and the delta through time, the rate of volumetric change of the mapped on shelf deposits was calculated with respect to time. By deducting this rate of volumetric change of mapped on shelf deposits from the computed sediment discharge through time, the rate and volume of off shelf deposition since the Last Glacial Maximum was quantified, displaying a higher rate of deposition before the retreat of the shelf margin deltas.

Keywords: Mississippi, shelf, delta, river, volume, glacial-eustatic cycle, Last Glacial Maximum (LGM), sediment dispersal, source to sink, sediment fate, well logging

SHP
U

Sediment mixing in modern eolian environments with detrital zircon U-Pb geochronology and detrital feldspar REE geochemistry: Example from the Andean broken foreland basin of Argentina

Jaime Hirtz
Hirtz, J., Department of Geological Sciences, The University of Texas at Austin, Austin, TX
Capaldi, T., Department of Geological Sciences, The University of Texas at Austin, Austin, TX
George, S., Department of Geological Sciences, The University of Texas at Austin, Austin, TX
Horton, B., Department of Geological Sciences, The University of Texas at Austin, Austin, TX
Stockli, D., Department of Geological Sciences, The University of Texas at Austin, Austin, TX
Mohrig, D., Department of Geological Sciences, The University of Texas at Austin, Austin, TX

The tectonic configuration of the South-Central Andes (~30-33°S) in west-central Argentina is characterized by foreland uplifts related to flat slab subduction of the Nazca plate beneath the South American plate. Erosional denudation of these basement-involved foreland uplifts results in the deposition of terrigenous sediments in adjacent broken foreland basins. Consequently, we expect to find evidence of these orogenic events by analyzing their drainage basin systems. However, existing sediment provenance analyses with ancient eolian sandstones from these partitioned basins assume that sediments are well mixed. For this reason, we intend to alleviate assumptions about sediment mixing by combining detrital feldspar (DF) rare earth element (REE) geochemistry with detrital zircon (DZ) uranium-lead (U-Pb) geochronology in a modern eolian setting. We hypothesize that eolian sediments mix in equal proportions, where samples collected throughout the dune contain an equal proportion of sediments from each source. Since previous work on modern rivers suggest that sediment provenance is currently indistinguishable due to overlapping DZ U-Pb age distributions, the incorporation of feldspar (KAlSi3O8 – NaAlSi3O8 – CaAl2Si2O8) REE geochemistry indicates that fluvial signals are unique, and that sediment mixing can be quantified. To test this hypothesis, twelve unconsolidated sand samples were collected from the Medanos Grande and Medanos Telteca sand dunes and the Rio San Juan, Rio Mendoza, and Rio Bermejo rivers in west-central Argentina. Zircon U-Pb geochronology was determined by analyzing the ratio of $^{207}Pb/^{235}U$ and $^{206}Pb/^{238}U$. Meanwhile, the detrital feldspar REE concentrations in polished thin sections (~30μm) involved a mass scan table of ^{139}La, ^{140}Ce, ^{141}Pr, ^{146}Nd, ^{147}Sm, ^{153}Eu, ^{157}Gd, ^{159}Tb, ^{163}Dy, ^{166}Er, ^{169}Tm, ^{172}Yb, and ^{175}Lu, as well as ^{23}Na, ^{27}Al, ^{29}Si, ^{39}K, and ^{43}Ca. These analyses were performed using a Laser Ablation-Inductively Coupled Plasma-Mass Spectrometer at the Jackson School of Geosciences. Results from dual phase sediment provenance indicate that fluvial sediments are unique, where sediments from each river can be distinguished from each other, and that eolian sediments are well mixed. This analysis is important due to the combination of zircon and feldspar which provides a formidable data set to reduce assumptions about sediment mixing which is beneficial for future investigations of modern and ancient eolian sediments.

Keywords: Andes, Argentina, Eolian, Surface Processes, Zircon Geochronology, Feldspar Geochemistry.

SHP
U

Controls on the sedimentation and morphology of an oxbow lake along the Trinity River, Texas, USA

Matthew Nix
Nix, M., Jackson School of Geosciences, The University of Texas at Austin, Austin, TX
Hassenruck-Gudipati, H., Jackson School of Geosciences, The University of Texas at Austin, Austin, TX
Swartz, J., Insitute for Geophysics, The University of Texas at Austin, Austin, TX
Sylvester, Z., Bureau of Economic Geology, The University of Texas at Austin, Austin, TX
Kim, W., Jackson School of Geosciences, The University of Texas at Austin, Austin, TX
Mohrig, D., Jackson School of Geosciences, The University of Texas at Austin, Austin, TX

Oxbow lakes and their subsequent filling by sediment play an important role in the dynamics of channel self-confinement and in the evolution of meander belts. In spite of this, research lacks in characterizing the rates and spatial changes in sediment deposition and bed aggradation along the limbs of oxbow lakes. The aim of this study is to understand the effect that floods have on oxbow sedimentation. Here we document the filling history of an oxbow lake along the Trinity River that has been cut off for 23 years. We observe significant flooding events on the river through analysis of aerial photographs and river hydrographs for the years after the oxbow cutoff, which occurred in 1995. Between 2011 and 2015, there were 76 days of major flooding spread out over 5 events, one of which lasted >55 days. Between 2015 and 2017, there were another 6 events totaling 146 days of flooding. Using time-lapse airborne lidar collected in 2011, 2015, and 2017, we observed varying amounts of aggradation within the downstream plug; thus allowing us to quantify the effects of different magnitudes of floods. The downstream plug shows 0.14 km^3 of aggradation from 2011 to 2015, and 0.16 km^3 of aggradation from 2015 to 2017. Meanwhile, only very small amounts of aggradation were observed at the upper limb, which had already been filled with sediment. Trenches dug into the downstream plug reveal 2-m high foresets that dip into the lake. This sediment accumulation is primarily composed of climbing-ripple stratification interpreted as suspension deposits that have been reworked by low rates of bedload transport. Grain size samples from the trenches document a well-sorted distribution of very fine-to fine sand with an average D50 of 120 μm. Chirp seismic lines were collected along the entire oxbow length to resolve sedimentation patterns within the lake. These transects reveal low-angle inclined strata prograding into the lake from both the upper and lower oxbow limbs. Our data set is intended to quantitatively describe the range of filling styles in oxbow lakes and the effect of floods on their filling histories.

Keywords: Sediment transport, Sedimentology, river geomorphology, seismic analysis

SHP
U

EVOLUTION OF RETURN-FLOW CHANNELS CUT INTO SAN JOSE ISLAND, TEXAS, CAUSED BY HURRICANE HARVEY

Arisa Ruangsirikulchai
Ruangsirikulchai, A., The University of Texas at Austin, Austin, TX
Wilson, K., The University of Texas at Austin, Austin, TX
Hassenruck-Gudipati, H., The University of Texas at Austin, Austin, TX
Lapotre, M., Harvard University, Cambridge, MA
Mohrig, D., The University of Texas at Austin, Austin, TX

Coastline resilience relies on predicting storm impacts on beach morphologies. However, return-flow channels, a morphodynamic consequence of storm surge ebb, have not been well-studied. Our study investigates the erosional evolution of return-flow channels on San Jose Island in Texas as a result from Hurricane Harvey in 2017. These channels are up to 300 m in length and have multiple upstream heads with single, elongated downstream necks. Depth measurements along and across four channels show the deepest parts of most channels being near their upstream heads and associated knickpoints. Channel-bottom elevations here ranged from 0.78 - 1.95 m below mean sea level. These deep spots resemble plunge pools of horseshoe waterfalls, implying a similar set of developmental mechanisms associated with flow focusing. Subaqueous channel margins can be stepped, indicating a lithologic control on the pattern and amount of erosion. A rack line of debris was observed ~ 5 m above mean sea-level on the landward side of the island. Four large barges drifted across the island during return-flow, coming to rest at the landward edge of the coastal dune complex without producing drag marks on the surface. We interpreted the rack line, the barges, and the 'bathtub rings' within some of the channels as indicators of a high and slowly draining water level during channel cutting. Scours preserved on the landward side of dunes document a seaward flow direction; there was no evidence of washover deposits. Vegetation density appears to have controlled erosion rates as sediment samples collected at seaward and landward points along the channels show a similar grain-size distribution. A pre-hurricane airborne lidar survey collected by the U.S. Army Corps of Engineers in 2016 and a post-hurricane survey flown by the Bureau of Economic Geology at UT-Austin in 2017 are used to quantify beach morphological change associated with channel formation, including the volume of eroded material, and channel dimensions and density. Channels are shown to take advantage of pre-existing low topography between dune ridge lines. The field data and lidar analyses will guide the construction of a return-flow channel-evolution model using ANUGA, a morphodynamic modeling suite.

Keywords: coastal geomorphology, LiDAR, numerical modelling, storms

SHP
U

Stratigraphic Evaluation of Trinity Aquifers in Hays and Western Travis County and Implications for Groundwater Availability

Nicholas Soto-Kerans
Soto-Kerans, N., University of Texas at Austin

Trinity Aquifers are very important groundwater resources in central Texas. However, they show signs of hydrologic stress and depletion in some areas. This study focused on detailed stratigraphic evaluations to better understand hydrologic variations in the Trinity Aquifer system. The study consisted of seven wells located throughout the Western Travis and Northern Hays County area spanning XX miles. All the wells had cuttings and geophysical logs. Two of the wells are multiport monitor wells providing detailed hydrologic data. Geophysical logs, cuttings, thin sections (where available), and outcrop descriptions were compiled, integrated and correlated. Stratigraphic cross sections were constructed and hydrologic data for the wells were plotted and compared to geologic data.

Results suggest that there are stratigraphic variations in the Middle and Lower Trinity units that may influence groundwater availability. From stratigraphic top to bottom, the Upper Glen Rose is a regionally consistent carbonate interval. The Middle Trinity Aquifer is composed of the Lower Glen Rose, Hensel and Cow Creek limestone. The discontinuous nature of the biostrome/reef intervals in the Lower Glen Rose appears to correlate to poor water quality and poor yield where the reef is absent. The Hensel, which transitions from a predominantely clastic and water bearing interval in the updip areas, to a thinner silty, dolomitic aquitard internval downdip. The underlying Cow Creek indicates a facies transition from an updip grainstone to dolomite in the downdip areas with higher yields. The underlying Hammett is a regionally consistent clay and aquitard unit for the Middle Trinity.

In addition to high levels of pumping, groundwater availability appears to be influenced by facies changes within the Middle Trinity units of the study area. Understanding the detailed straigraphy will provide insights into these important groundwater resources.

Keywords: depositional facies analysis, hydrostratigraphic analysis, carbonate stratigraphy

SHP
U

Grainflow Thickness: Surface Process to Subsurface Record

Xiafei Zhao
Zhao, X., The University of Texas at Austin, Austin,TX
Cardenas, B., The University of Texas at Austin, Austin,TX
Kim, W., The University of Texas at Austin, Austin,TX

Grainflows, or sand avalanches, on the slipfaces of aeolian dunes form via the relaxing of oversteepened lee slopes. Grainflows transport sediment from the upper slipface to the lower slipface of the dune. Prior work has focused on understanding grainflow geometry across the slipface. However, the stratigraphic record favors preservation of the bottommost lee face. Relationships between the geometry of the bottommost grainflow deposit, which is most likely to be preserved in ancient cross-sets, and its formative dune are not fully understood. Here, we explore how dune height controls the thickness of the bottommost grainflow deposits. Using LIDAR data from White Sands, New Mexico, USA, lee slope angles of 300 dunes were measured to obtain a range of lee face slopes for a mass balanced model. The model calculates bottommost grainflow thickness for a range of dune heights by relaxing the maximum slipface slope to the minimum slope. Slope relaxation is modeled as scour above a bypass point on the slipface, and equal deposition below the bypass point. Slopes range from 28° to 35° with a mean of 30° and a standard deviation of 1°. Additionally, multiple growing sand pile experiments as high as 5-6 cm showed grainflow-constructed lee slopes range from 30° to 35°. Results from both LIDAR data and the sand pile experiment show slopes fluctuate independently from slipface height, indicating a linear increase in grainflow mass with dune height. Future work involves trenching recent deposits at White Sands to constrain the modeled relationship between dune height, which will be known, and preserved grainflow base thickness. Slipface positions where grainflows transition from net-erosional to depositional will also be measured. When informed by experiments, modern observations, and recent deposits, the mathematical model will be useful in estimating dune heights from ancient aeolian cross-strata and lead to a better overall interpretation of the aeolian rock record.

Keywords: aeolian, stratigraphy, sedimentary processes

THANK YOU

to our sponsors, volunteers, and participants!

TEXAS Geosciences
The University of Texas at Austin
Jackson School of Geosciences

ConocoPhillips

Graduate Student Executive Committee
GSEC